

03095



**UNIVERSIDAD NACIONAL AUTÓNOMA DE MÉXICO**

**INSTITUTO DE GEOFÍSICA  
POSGRADO EN CIENCIAS DE LA TIERRA**

**ESTUDIO DE LAS FUENTES SÍSMICAS E INTERACCIÓN DE  
ESFUERZOS DURANTE ALGUNOS GRANDES SISMOS RECIENTES EN  
LA ZONA DE SUBDUCCIÓN DEL PACÍFICO MEXICANO.**

**TESIS**

QUE PARA OBTENER EL GRADO DE

**DOCTOR EN CIENCIAS  
(SISMOLOGÍA)**

PRESENTA

**MIGUEL ÁNGEL SANTOYO GARCÍA GALIANO**

DIRECTOR

**DR. TAKESHI MIKUMO**

Agosto, 2005

m 346536



Universidad Nacional  
Autónoma de México



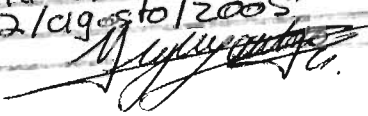
**UNAM – Dirección General de Bibliotecas**  
**Tesis Digitales**  
**Restricciones de uso**

**DERECHOS RESERVADOS ©**  
**PROHIBIDA SU REPRODUCCIÓN TOTAL O PARCIAL**

Todo el material contenido en esta tesis esta protegido por la Ley Federal del Derecho de Autor (LFDA) de los Estados Unidos Mexicanos (México).

El uso de imágenes, fragmentos de videos, y demás material que sea objeto de protección de los derechos de autor, será exclusivamente para fines educativos e informativos y deberá citar la fuente donde la obtuvo mencionando el autor o autores. Cualquier uso distinto como el lucro, reproducción, edición o modificación, será perseguido y sancionado por el respectivo titular de los Derechos de Autor.

*A mi querida esposa Julieta.  
A mis padres Miguel y Rosa.  
A la memoria de mis abuelos.*

Autoriza a la Dirección General de Bibliotecas de la UNAM a difundir en formato electrónico e impreso el contenido de mi trabajo recepcional.  
NOMBRE: Miguel Angel Sancho  
García Galiano  
FECHA: 2/ agosto/ 2005  
FIRMA: 

***All religions, arts and sciences are branches of the same tree. All these aspirations are directed toward ennobling man's life, lifting it from the sphere of mere physical existence and leading the individual towards freedom.***

***Todas las religiones, artes y ciencias son ramas de un mismo árbol. Estas aspiraciones están dirigidas a ennoblecer la vida del hombre, elevándolo de la esfera de la mera existencia física, y conduciendo al individuo hacia la libertad.***

**A. Einstein**

# ÍNDICE

<b>RESUMEN</b> .....	2
<b>ABSTRACT</b> .....	4
<b>INTRODUCCIÓN</b> .....	6
<b>CAPÍTULO I.</b> Agrupamiento espacio-temporal de grandes sismos interplaca a lo largo de la zona de subducción en México: una evidencia de interacción de esfuerzos de la fuente.....	18
<b>CAPÍTULO II.</b> Posible interacción lateral de esfuerzos en una secuencia de grandes sismos de interplaca en las placas subducentes de Cocos y Rivera.....	45
<b>CAPÍTULO III.</b> Proceso de falla y su cambio de esfuerzos cosísmicos asociado durante el sismo interplaca del 30 de enero de 1973, Colima, México ( $M_w=7.6$ ).....	65
<b>CAPÍTULO IV.</b> Proceso de ruptura y cambio de esfuerzos asociado con el sismo intraplaca del 11 de enero de 1997 ( $M_w=7.1$ ), en Michoacán, México.....	92
<b>CAPÍTULO V.</b> Posible interacción de esfuerzos entre un gran sismo de subducción y un sismo de fallamiento normal en la zona de subducción Mexicana.....	123
<b>CAPÍTULO VI.</b> Ruptura dinámica y cambio de esfuerzos en un sismo de falla normal en la placa de Cocos subducente.....	134
<b>CONCLUSIONES</b> .....	145
<b>CONCLUSIONS</b> .....	149
<b>REFERENCIAS ADICIONALES</b> .....	153
<b>AGRADECIMIENTOS</b> .....	158

## RESUMEN

En esta tesis se presenta un estudio sobre las fuentes sísmicas y la interacción de esfuerzos durante algunos grandes sismos recientes en la zona de subducción del pacífico mexicano. En el primer trabajo (Capítulo I) se prueba la hipótesis de que agrupamientos espacio-temporales de grandes sismos, pueden ser causados por la transferencia de esfuerzos a lo largo de la interfaz tectónica en la zona de subducción mexicana. Aquí, se propone un método novedoso para el análisis de los tiempos de interocurrencia entre eventos, tomando en cuenta la extensión espacial de los cambios en los esfuerzos de Coulomb cosísmicos. En el segundo trabajo (Capítulo II) se estudia con mayor profundidad y detalle, la posibilidad de interacción lateral de esfuerzos en una secuencia de eventos recientes de subducción ocurridos en la interfaz Rivera-Norteamérica y en la porción noroccidental de la interfaz Cocos-Norteamérica. En el tercer trabajo (Capítulo III), se revisan los parámetros de fuente puntual del sismo de Colima del 31/01/1973 y se calcula mediante la inversión cinemática de formas de onda, la distribución de deslizamientos sobre el plano de falla. Con base en estos resultados se calculan los esfuerzos de Coulomb cosísmicos asociados sobre el plano de falla extendido y se discuten sus implicaciones tectónicas. En el Capítulo IV se realiza un análisis de las propiedades focales del sismo de falla normal del 11/01/1997 en las costas de Michoacán, y se calcula mediante la inversión de formas de onda la distribución de los deslizamientos cosísmicos sobre el plano de falla. Con base en estos, se calculan los esfuerzos de Coulomb cosísmicos en dos planos diferentes con el fin de estimar la transferencia de esfuerzos al volumen circundante y el posible disparo de la sismicidad posterior localizada en las inmediaciones del evento principal. En el Capítulo V se estudia con detalle la posible interacción de esfuerzos entre el sismo de falla normal del 11/01/1997 y el macrosismo del 19/09/1985. Se calculan los cambios de esfuerzos dinámicos dentro y fuera del área de ruptura del sismo de 1985 y se comparan con la posición espacial relativa entre éste y el evento de falla normal. Así mismo se discuten los posibles efectos producidos por los cambios en los esfuerzos postsísmicos y la posibilidad de que estos cambios sean realizados por deslizamientos asísmicos en el área del sismo de 1985. En el Capítulo VI se estudian las propiedades dinámicas de la ruptura y de transferencia de esfuerzos del sismo del 11 de enero de 1997.

Se concluye en la tesis, primeramente, que la transferencia de esfuerzos debido a grandes sismos interplaca en la zona de subducción del Pacífico en México, puede efectivamente conducir a agrupamientos en el espacio-tiempo, y que en el futuro será necesario tomar en cuenta estos resultados en el cálculo de pronóstico y peligro sísmico. Así mismo, se determinó que las interacciones laterales de esfuerzos de Coulomb entre grandes sismos de interplaca a lo largo de la zona de subducción, juegan un papel importante en el disparo o aceleración del tiempo de ocurrencia de los grandes sismos subsecuentes. Se observa por otra parte, que las distribuciones de deslizamientos en sismos tanto interplaca como intraplaca son bastante heterogéneas, evidenciando la existencia de variaciones espaciales en los valores de esfuerzos tectónicos y en las resistencias en la interfaz. Se observa también que el disparo por transferencia de esfuerzos, puede ser extendido a la interacción entre eventos con diferentes planos de falla y mecanismos sismogénicos. Finalmente, las caídas de esfuerzos obtenidas de la inversión dinámica del sismo intraplaca de falla normal del 11/1/97, sugieren la existencia de estados de esfuerzos mayores dentro de la placa subducente que los obtenidos en la interfaz con la placa continental durante el sismo del 19/09/85. Las funciones de tiempo de la fuente generadas dinámicamente durante este sismo de falla normal, resultaron relativamente de corta duración (0.5-2.0 seg), lo cual podría atribuirse a que las heterogeneidades encontradas en las caídas de esfuerzos son esencialmente de pequeña escala.

## **ABSTRACT**

In this thesis we study the seismic sources and the stress interaction during some great recent earthquakes in the Mexican subduction zone. In Chapter I we test the hypothesis that the coseismic stress transfer can lead to the clustering of large and great thrust earthquakes along the tectonic interface in the Mexican subduction zone. Here, we propose a new method for the analysis of inter-occurrence times, taking into account the spatial extent of the coseismic Coulomb stress changes. In Chapter II we explore in detail the possible lateral stress interaction among a sequence of seven great recent subduction earthquakes, occurred in the Rivera-North America and the northwestern portion of the Cocos-North America interfaces. In Chapter III we re-examine the point source characteristics of the 31/1/1973 Colima earthquake and compute a kinematic waveform inversion for the slip distribution over the fault plane. Based on these results we compute the associated Coulomb Failure stress changes over the extended fault plane and discuss its tectonic implications. In Chapter IV we analyze the main point source properties of the 11/01/1997 Michoacan normal faulting earthquake, and compute the slip distribution over the fault plane by a linear kinematic waveform inversion. Based on these results, we calculate the Coulomb Failure stress function over two different planes, in order to estimate the amount of stress transferred to the neighbouring volume and the possible triggering of post-event seismicity. In Chapter V we carefully study the possible stress interaction between the 11/01/1997 normal faulting event and the 19/09/1985 great Michoacan subduction earthquake. We compute the dynamic stress changes inside and outside the rupture area of the 1985 earthquake and compare the stress changes in its vicinity with the spatial location of the normal event. We discuss here the possible effects of these changes on the post-seismic state of stress, and the possibility that these changes could be enhanced by aseismic slips in the rupture area of the 1985 mainshock. In Chapter VI we perform a study of the dynamic properties of the rupture and the stress changes due to the 11/01/1997 normal faulting Michoacan earthquake, based on its kinematic distribution of slips.

We conclude in the thesis that the stress transfer produced by large and great earthquakes in the Mexican subduction zone, can effectively lead to a space-time clustering behaviour of events, and that in the future it will be necessary to take into account these results when performing earthquake forecasts and seismic hazard estimations in Mexico. We also determine



that the lateral coseismic Coulomb stress interactions among great thrust earthquakes in the Mexican subduction zone, plays an important role in the seismic triggering and time acceleration of the subsequent seismicity. On the other hand, it can be observed that the slip distributions of interplate and intraplate earthquakes in the Mexican subduction zone are quite heterogeneous, making evident the existence of spatial variations in the tectonic stresses and strengths. We also show that the stress triggering can be extended to the interaction among earthquakes with different fault planes and mechanisms. Finally, the stress drops computed from the dynamic inversion of the intraplate event of 11/01/97, suggests the existence of higher stresses within the subducting slab than those observed on the 19/09/85 earthquake on the upper interface. The dynamically generated slip-velocity source time functions for this event were found to have short slip durations, which can be attributed to the short scale-length of stress-drop heterogeneities.

## INTRODUCCIÓN

Un sismo ocurre cuando los esfuerzos en una falla exceden la resistencia de fricción en la interfaz. A nivel tectónico, tanto los esfuerzos como la resistencia son valores que en general dependen de la posición espacial y del tiempo. Un reflejo de esto son las heterogeneidades que presentan las distribuciones de deslizamientos sísmicos (e.g. *Archuleta, 1984; Mendoza y Hartzell, 1988, 1989 y 1999; Mendoza, 1993 y 1995; Yagi et al., 2004, etc*), así como las irregularidades espacio-temporales observadas en algunos ciclos sísmicos de zonas tectónicamente activas (e.g. *Goes, 1996*).

Dadas las implicaciones que el conocimiento sobre estos ciclos tiene en la estimación del peligro y el riesgo sísmico, diversas líneas de investigación han sido encaminadas a estudiar, con profundidad, tanto los procesos de ruptura como las posibles relaciones de esfuerzos entre sismos en una región, a todos los niveles de magnitud.

En el análisis de la interacción de esfuerzos, una de las técnicas más utilizadas y exitosas es la evaluación de los esfuerzos de Coulomb cosísmicos ( $\Delta CFS$ ). Se ha observado por ejemplo que existe una clara preferencia de las réplicas y de la microsismicidad posterior a un sismo, a ocurrir en las regiones donde existen incrementos en los  $\Delta CFS$  (e.g. *Das y Scholz, 1981; Reasenberg y Simpson, 1992; Stein et al., 1992 y 1994; Deng y Sykes, 1997a; Toda et al., 1998, etc.*). Así mismo, hay evidencia de que eventos medianos y grandes pueden llegar a ser disparados por sismos adyacentes previos de magnitudes semejantes, si éstos están ubicados en las regiones donde los esfuerzos de Coulomb son también positivos (e.g. *Hudnut, et al., 1989; Harris y Simpson, 1992; Jaumé y Sykes, 1992; King et al., 1994; Deng y Sykes, 1997b; Hardebeck et al., 1998, etc.*). Cabe mencionar sin embargo, que en las regiones donde los  $\Delta CFS$  son negativos, se ha visto que la sismicidad no necesariamente desaparece o se reduce. *Harris y Simpson, 1996 y 1998* han encontrado que en estas zonas, llamadas también “*sombras de esfuerzos*”, en algunas ocasiones se reduce la tasa de sismicidad pero sin llegar esto a ser observado de forma regular.

Entre los efectos espacio-temporales que este tipo de transferencia de esfuerzos suele provocar, se encuentra la ocurrencia en cascada ó el agrupamiento (*Clustering*) de grandes

sismos. La secuencia de eventos observada en la falla del Norte de Anatolia en Turquía, el siglo pasado, es un ejemplo de ello. Allí, diversos autores (e.g. *Stein et al., 1997, Nablant et al., 1998 y Hubert-Ferrari et al., 2000, entre otros*) han mostrado evidencias sobre la influencia que tienen los cambios de los esfuerzos de Coulomb cosísmicos en la generación sucesiva de grandes eventos. Así mismo, trabajos paralelos han probado la importancia de conocer los cambios en el estado de esfuerzos dentro de la zona de falla de grandes sismos, con base en el conocimiento en detalle de los procesos de ruptura (e.g. *Mikumo y Miyatake, 1993 y 1995; Bouchon, 1997; Toda et al, 1998; Perfettini et al, 1999, etc.*).

En México, el agrupamiento espacio-temporal de réplicas es un fenómeno ampliamente observado y bien reconocido (e.g. *Kelleher et al, 1973; Reyes, et al., 1979; Singh et al 1979; Astiz y Kanamori, 1984; UNAM Seismology Group 1986; Nishenko and Singh, 1987; Valdés et al, 199x; Courboux et al., 1997, etc.*). Sin embargo, estudios previos han sugerido también la existencia de agrupamientos espacio-temporales de grandes sismos interplaca en la zona de subducción del Pacífico mexicano (e.g. *Singh et al., 1981; Nishenko and Singh, 1987; Ward, 1991*), así como algunas posibles relaciones espacio-temporales entre éstos y sismos intraplaca localizados en la placa oceánica subducente (e.g. *Singh, et al., 1985 y 2000; Pardo y Suárez, 1995; Cocco, et al., 1997, Mikumo, et al., 2002*). Se han obtenido también resultados sobre el posible disparo de sismicidad en el Valle de México provocado por algunos grandes sismos lejanos (e.g. *Singh, et al. 1998*), y sobre las posibles implicaciones que tienen los cambios de esfuerzos dinámicos dentro del área de ruptura, durante algunos grandes sismos interplaca en la zona de subducción (*Mikumo, et al., 1998*). Así también, existe un número significativo de estudios sobre la distribución de dislocaciones cinemáticas de algunos grandes sismos mexicanos entre otras propiedades de la fuente.

Sin embargo debido a que la sismicidad en el país exhibe poca regularidad, a que permanece una carencia de estudios sobre los posibles efectos de los cambios de esfuerzos en regiones adyacentes, y a que el registro sísmico instrumental existente es relativamente corto, el ciclo sísmico en esta zona de subducción permanece aún poco comprendido.

Esta tesis se encuentra enfocada en dos temas principales:

- I. En el estudio de las propiedades cinemáticas y dinámicas de la fuente sísmica de algunos grandes sismos importantes en la zona de subducción mexicana, que aún no han sido estudiados desde este punto de vista, y
- II. En el estudio de los cambios de esfuerzos durante grandes eventos inversos de subducción y normales dentro de la placa subducente, sus posibles relaciones debido a la transferencia de esfuerzos, sus efectos espacio-temporales y finalmente las posibles implicaciones de estas anteriores en el ciclo sísmico.

#### *Marco tectónico.*

La sismicidad en el pacífico sur de México está dominada principalmente por la subducción de las placas oceánicas de Rivera y Cocos bajo la placa continental de Norte América, a lo largo de la trinchera mesoamericana.

La placa de Rivera es relativamente pequeña y joven, entre 11.0-13.0 Ma (e.g. *Klitgord y Mammerickx, 1982; Kostoglodov y Bandy, 1995*), con tasas de convergencia relativas a Norte América que varían de entre 2.0 y 3.3 cm/año (e.g. *DeMets y Stein, 1990*) hasta 5.0 cm/año (e.g. *Kostoglodov y Bandy, 1995*), recorriendo la costa desde el norte del estado de Jalisco hasta el estado de Colima. El borde suroriental de esta placa es incierto, sin embargo diversos autores coinciden que está limitada por la unión triple entre las placas de Rivera, Cocos y Norte América, cerca del Graben El Gordo (EGG por sus siglas en inglés). La placa de Cocos por su parte, comienza su convergencia al noroeste en el estado de Colima, y continúa hacia el sureste hasta el estado Chiapas y la frontera con Guatemala. Ésta tiene tasas de convergencia respecto a Norteamérica que van desde los 5.0 cm/año cerca del borde nororiental (EGG), hasta los 8.0 cm/año a la altura del Istmo de Tehuantepec (*DeMets y Stein, 1990; Kostoglodov and Bandy, 1995*).

La subducción de estas dos placas es generadora de la mayor parte de la sismicidad en la zona de convergencia del sur de México, compuesta por diversos tipos de sismos. Entre estos se encuentran los producidos en las interfaces entre las placas, o sismos interplaca, y los

que son generados en el interior de la placa oceánica subducente, que en esta tesis llamaremos sismos intraplaca.

*Agrupamiento espacio-temporal de grandes sismos interplaca a lo largo de la zona de subducción en México: una evidencia de interacción de esfuerzos de la fuente.*

Como ya se mencionó anteriormente, en trabajos previos se ha sugerido la existencia de agrupamientos espacio-temporales de grandes sismos en México. En el artículo *Space-time clustering of large thrust earthquakes along the Mexican subduction zone: An evidence of source stress interaction* (Capítulo I), se prueba la hipótesis de que dichos agrupamientos pueden ser causados por la transferencia de esfuerzos a lo largo de la interfaz en la zona de subducción mexicana. Aquí, se propone un método novedoso para el análisis de los tiempos de interocurrencia entre eventos, tomando en cuenta la extensión espacial de los cambios producidos en los esfuerzos de Coulomb cosísmicos.

Los resultados muestran que para el periodo en estudio (1900-2003), existen al menos dos grupos de intervalos de tiempo donde las frecuencias observadas son mucho mayores que las esperadas por un proceso de Poisson. En el primer grupo, entre 0 y 5 años a partir del acontecimiento de un gran sismo, estas frecuencias resultan ser de cerca del doble que las esperadas, con una probabilidad de ocurrencia del orden de 30%. Este marcado agrupamiento en el espacio-tiempo, muy probablemente es debido a la interacción de esfuerzos de Coulomb cosísmicos, ya que después de realizar la misma prueba estadística directamente al catálogo, los tiempos de interocurrencia de los eventos estudiados se ajustan a un modelo de Poisson.

En el segundo grupo, para intervalos entre los 30 y 50 años posteriores a la ocurrencia de un gran sismo, las frecuencias observadas alcanzan hasta 1.7 veces las esperadas. Este segundo modo podría asociarse, a diferencia del anterior, con los esfuerzos debidos a la recarga tectónica existente en el régimen convergente de la zona. Estos periodos resultan ser también consistentes con los intervalos de recurrencia de largo plazo observados previamente por diversos autores para este tipo de sismos en México (e.g. *Singh et al., 1981; Singh et al., 1984; Nishenko y Singh, 1987, etc.*). Por las implicaciones que tienen estos resultados en el

análisis de los ciclos sísmicos en México, es importante tomarlos en cuenta en las futuras estimaciones de pronóstico y peligro sísmico.

*Posible interacción lateral de esfuerzos en una secuencia de grandes sismos de interplaca en las placas subducentes de Cocos y Rivera.*

En el estudio anterior, la extensión del área de influencia de los esfuerzos sobre las regiones adyacentes a la ruptura, es calculada con base en una distribución de deslizamientos teórica sobre el plano de falla. En sismos reales, las distribuciones de deslizamientos tienen en general mayores heterogeneidades. Así, resulta importante considerar que siempre que los datos lo permitan, será deseable el uso de distribuciones de deslizamientos más realistas en los estudios de transmisión e interacción de esfuerzos.

Con base en esto, y con el fin de detallar la transferencia de esfuerzos y la posible interacción de grandes eventos en la zona de subducción mexicana, se estudió con mayor profundidad una secuencia de eventos recientes de subducción ocurridos en la interfaz Rivera-Norteamérica y en la porción noroccidental de la interfaz Cocos-Norteamérica. Las características cinemáticas de seis eventos de esta secuencia han sido ya estudiadas en trabajos previos por otros autores (*Petatlán del 14/03/1979,  $M_w=7.6$ ; Playa Azul del 25/10/1981,  $M_w=7.4$ ; Michoacán del 19/09/1985,  $M_w=8.1$ ; Zihuatanejo del 21/09/1985,  $M_w=7.6$ ; Colima-Jalisco del 09/10/1995,  $M_w=8.0$  y Tecomán del 22/01/2003,  $M_w=7.5$ ).*

Un evento más, el de *Colima del 31/01/1973 ( $M_w=7.6$ )* que forma parte de este grupo y que completa la serie, es estudiado en sus características cinemáticas y distribución de deslizamientos más adelante en la presente tesis, en el Capítulo III.

Así, con base en la distribución espacial de deslizamientos de estos siete sismos, en el artículo titulado *Possible lateral stress interactions in a sequence of large interplate thrust earthquakes on the subducting Cocos and Rivera plates* (Capítulo II), se estudian con detalle los cambios en los esfuerzos de Coulomb cosísmicos debidos a cada sismo, y se discuten sus posibles interacciones y los posibles efectos de la relajación postsísmica viscoelástica en el estado de esfuerzos general. Para el análisis, se calcularon estos esfuerzos de Coulomb sobre

la interfaz tectónica, superponiéndolos en el espacio en función de sus tiempos de ocurrencia, y suponiendo que en ninguno de los segmentos de la interfaz tectónica ocurren deslizamientos postsísmicos silenciosos ni existen efectos por causas de la recarga tectónica.

Debido a las incertidumbres en la tectónica de la región cercana a la unión triple Rivera-Cocos-Norteamérica, el estudio se dividió en dos partes: una para los eventos que ocurrieron en la interfaz Cocos-Norte América y la otra para los que ocurrieron en la interfaz Rivera-Norte América.

De los resultados, se observa que el estado de esfuerzos presenta grandes variaciones en el interior de la ruptura de dichos eventos, y que estas heterogeneidades pueden ser debidas tanto a irregularidades en la carga tectónica regional como a los cambios cosísmicos y postsísmicos provocados por los temblores previos. Por otro lado se comenta en este trabajo que las heterogeneidades en las resistencias también pueden ser atribuidas, entre otras, a pequeñas variaciones de la temperatura, la presión de poro, la humedad, y otros efectos equivalentes como la corrosión de esfuerzos observada en laboratorios.

Tomando en cuenta que la resolución en las distribuciones de deslizamientos, así como los probables errores en la localización pueden conducir a ligeras inexactitudes en el análisis de interacción, se observó que en 6 de los 7 eventos estudiados, dado un sismo el punto de inicio de la ruptura del sismo subsecuente está localizado en su zona de incrementos en los esfuerzos de Coulomb cosísmicos. Esto sugiere la existencia de un efecto de disparo (*triggering*) del evento subsecuente por causa del anterior, adelantando así su tiempo de ocurrencia. Este comportamiento ha sido también reportado para otras secuencias de eventos en diversas fallas de transcurrencia (*strike slip*) en el mundo (e.g. en Turquía, *Nablant et al., 1998*; en Japón, *Toda et al, 1998*, en California, *Stein 1999*, etc).

*Proceso de falla y su cambio de esfuerzos cosísmicos asociados durante el sismo interplaca del 30 de enero de 1973, Colima, México (M<sub>w</sub>=7.6).*

Entre los eventos recientes que aun no han sido investigados en sus características de falla finita, destaca el sismo de Colima del 31 de enero de 1973 (M<sub>s</sub>=7.6). Este temblor tiene una

importancia relevante debido a que, por su magnitud y por encontrarse en una región con un alto potencial sísmico, puede tener una influencia significativa, como ya se describió anteriormente, en el estado de esfuerzos de la región particularmente en las interfaces Cocos-Norte América y Rivera-Norte América.

El sismo del 31 de enero de 1973, se encuentra localizado en el límite noroccidental de la zona de convergencia de la placa de Cocos, cerca de la unión triple Cocos-Rivera-NorteAmérica. Éste ha sido ya estudiado en sus características de fuente puntual por varios autores (e.g *Lomnitz, 1977; Reyes et al., 1979; Chael y Stewart, 1982; Singh y Mortera, 1991*), sin embargo, en ninguno de estos trabajos se han analizado específicamente las características de fuente finita y de cambio de esfuerzos asociados a la ruptura.

Por una parte, los estudios previos coinciden en que éste es un sismo somero de falla inversa con bajo ángulo de incidencia, pero difieren en las estimaciones de profundidad del hipocentro así como en su mecanismo focal. En el artículo *Faulting process and its associated coseismic stress change during the 30 January, 1973, Colima, Mexico interplate earthquake (M<sub>w</sub>=7.6)* (Capítulo III), se estudia la distribución de deslizamientos sobre el plano de falla de este temblor mediante la inversión cinemática de formas de onda, se calculan los esfuerzos de Coulomb cosísmicos asociados a esta distribución, y se discuten sus implicaciones tectónicas.

Así, primeramente se recalcularon los valores de profundidad y del mecanismo focal. Los resultados muestran un evento de falla inversa ( $St=285^\circ$ ,  $Dip=16^\circ$ ,  $Ra=85^\circ$ ) con una profundidad del hipocentro de 16 km, valores que ahora son más consistentes con el entorno tectónico de la región (*Pardo y Suárez, 1995*). La inversión cinemática indica una ruptura irregular con dos asperezas principales y una función de tiempo de la fuente de 26 segundos, similar en duración a los resultados de *Quintanar (1991)* y *Singh y Mortera (1991)*. Los cambios en los esfuerzos de Coulomb asociados, muestran dentro del área de ruptura, algunos “*parches*” con caídas de esfuerzos máximos de 40 bar, así como algunos otros con incrementos en los esfuerzos de hasta 25 bar, evidenciando la existencia de heterogeneidades espaciales tanto en la resistencia como en los esfuerzos en la zona de falla.



Fuera del área de ruptura, se observa una región circundante con claros incrementos en los esfuerzos sobre el plano de falla extendido. Si se considera que un incremento de 0.5 bar en los esfuerzos de Coulomb, sería suficiente para tener una influencia efectiva en eventos subsecuentes en las regiones adyacentes a la fuente (e.g. *Stein, 1999*), este sismo podría llegar a tener influencias significativas en sismos posteriores adyacentes, hasta distancias de 1.5 veces la longitud de su ruptura a lo largo de la zona de subducción.

*Proceso de ruptura y cambio de esfuerzos asociado con el sismo intraplaca del 11 de enero de 1997 ( $M_w=7.1$ ), en Michoacán, México.*

Hasta ahora, se han estudiado las características de fuente finita y las posibles relaciones de esfuerzos entre sismos interplaca de falla inversa. Sin embargo, las posibles relaciones espacio-temporales entre sismos intraplaca y sus respectivas réplicas en México, es un tema que cuenta hasta el momento con menos resultados al respecto.

El sismo del 11 de enero de 1997, es un evento de profundidad intermedia y falla normal localizado dentro de la placa subducente. Los primeros estudios realizados por otros autores, mostraron que es un evento de falla prácticamente vertical con un mecanismo consistente con el régimen extensional esperado para la zona y una magnitud  $M_w=7.1$ .

Si bien este tipo de eventos tiene por lo general un deficiente número de réplicas comparado con los sismos de subducción en México (e.g. *Singh et al, 1985, 1999 y 2000*), en este caso fue posible localizar 19 réplicas y obtener en 16 de ellas sus mecanismos focales. En el artículo *Source process and stress change associated with the 11 January, 1997 ( $M_w=7.1$ ) Michoacan, Mexico, inslab earthquake* (Capítulo IV) se realiza un análisis de sus propiedades focales suponiendo una fuente puntual, y se calcula mediante la inversión de formas de onda, la distribución de los desplazamientos cosísmicos sobre el plano de falla. Con base en estos, se calculan los esfuerzos de Coulomb cosísmicos en dos planos diferentes: uno sobre el plano de falla mismo, y otro a lo largo de una sección perpendicular al plano de falla, este último con el fin de estimar la transferencia de esfuerzos al volumen circundante y el posible disparo de la sismicidad posterior localizada en las inmediaciones del evento principal.

Los resultados de la inversión cinemática muestran una distribución heterogénea de deslizamientos, con la ruptura de una gran aspereza al sureste del epicentro y confinada entre los 20 y los 35 km de profundidad. Este confinamiento puede haber sido uno de los factores responsables de la fuerte directividad observada en varias estaciones tanto locales como telesísmicas. Así mismo, el cambio en el estado de esfuerzos cosísmicos muestra heterogeneidades espaciales que evidencian de nuevo, aun en este tipo de sismos, irregularidades espaciales tanto en los valores de esfuerzos como en los de las resistencias de fricción.

Por otra parte, se observa que las réplicas de este evento en realidad no están definiendo el plano de ruptura como en otros casos similares, ya que prácticamente todas estas se encuentran ubicadas al norte, fuera del plano de falla del evento principal. Al comparar su distribución espacial con la de los cambios en los esfuerzos de Coulomb cosísmicos, se ve que la mayoría de ellas ocurre en las regiones calculadas con incrementos en los  $\Delta CFS$ . Esto sugiere que el sismo principal, más bien puede haber disparado la sismicidad sobre planos de debilidad adyacentes en el interior de la placa subducida. Esto reasalta, entre otras cosas, la necesidad de tener prudencia al asumir que la distribución de réplicas marca en general la posición espacial del plano de ruptura del sismo principal.

#### *Posible interacción de esfuerzos entre un gran sismo de subducción y un sismo de fallamiento normal en la zona de subducción Mexicana*

Como se ha mencionado anteriormente, diversos autores han encontrado posibles relaciones entre sismos someros de subducción con sismos de falla normal y profundidad intermedia (e.g. Singh, et al., 1985 y 2000; Pardo y Suárez, 1995; Cocco, et al., 1997, Mikumo, et al., 2002). Los sismos intraplaca ocurren por lo general bajo un régimen extensional. De acuerdo con algunos estudios previos, éstos tienden a localizarse ya sea cerca de la trinchera oceánica o en la zona de desdoblamiento donde la placa oceánica se subduce subhorizontalmente (e.g. Pardo y Suarez., 1995; Singh et al., 1985, Singh et al., 1999 y 2000, etc.).

El sismo del 11 de enero de 1997 es un evento de profundidad intermedia y falla normal localizado en una zona poco esperada, ya que ocurrió justo bajo del área de ruptura del macrosismo de 1985. Por el corto periodo de tiempo transcurrido entre ellos, diversos autores han sugerido una posible relación causal, al igual que entre algunos otros sismos de subducción y sismos de falla normales intraplaca (e.g. *Singh, et al., 1985 y 2000; Pardo y Suárez, 1995; Cocco, et al., 1997, Mikumo, et al., 2002, etc*). En el artículo *A possible stress interaction between large thrust and normal faulting earthquakes in the Mexican subduction zone* (Capítulo V), se estudia la posible interacción de esfuerzos entre el sismo del 11 de enero de 1997 y el sismo del 19 de septiembre de 1985. Se calculan los cambios de esfuerzos dinámicos dentro y fuera del área de ruptura del sismo de 1985 y se comparan estos cambios con la posición espacial relativa entre éste y el evento de falla normal. Así mismo se discuten los posibles efectos de los cambios en los esfuerzos postsísmicos y la posibilidad de que estos cambios sean realizados por deslizamientos asísmicos en el área del sismo de 1985.

Con base en la distribución de deslizamientos del sismo de 1985 obtenida por *Mendoza y Hartzell (1989)*, se observa que el evento de 1997 ocurrió en la zona de máximos incrementos en los esfuerzos de Coulomb cosísmicos dentro de la placa subducente. También se observa que los cambios en el estado de esfuerzos debido al evento de 1985, evaluados sobre el plano de falla del sismo de 1997, coinciden con el patrón de deslizamientos de éste último. Esto da lugar a especular que, incluso, dicho patrón puede haber sido influenciado por el evento previo.

En el trabajo de *Mikumo et al 2002*, se estudia también la posible interacción entre otros dos sismos en una situación similar; el sismo de subducción del 29 de noviembre de 1978 y el sismo del 30 de septiembre de 1999, en Oaxaca, México. En ese trabajo, se observa de que el sismo de falla normal intraplaca ocurre al igual que en Michoacán, en la zona de máximos incrementos en los esfuerzos de Coulomb cosísmicos, evidenciando así una posible relación causal. En ese trabajo se estudian también los efectos de la relajación viscoelástica en los cambios de esfuerzos postsísmicos, que al final resultan no ser suficientes para cancelar los efectos de los esfuerzos de Coulomb cosísmicos.

Estos dos ejemplos parecen sugerir que este tipo de relación entre eventos con diferentes mecanismos sismogénicos puede ser más común de lo que previamente se pensaba.

*Ruptura dinámica y cambio de esfuerzos en un sismo de falla normal en la placa de Cocos subducente.*

En los trabajos anteriores, se ha descrito la conveniencia de estudiar la ruptura sísmica desde diversos puntos de vista, y se ha visto que tanto los cambios de esfuerzos estáticos como los dinámicos proporcionan información útil para el análisis de la posible interacción de esfuerzos cosísmicos dentro, fuera y entre sismos en una determinada región.

El estudio de los procesos dinámicos dentro del área de ruptura, a diferencia del caso estático, proporciona información relevante sobre el progreso de la liberación de momento sísmico durante la ruptura misma. Los detalles espacio-temporales que este análisis proporciona son importantes en la caracterización de la ruptura, pues evalúa factores como la variación espacial de la duración de las funciones de tiempo de la fuente (STF) o Rise Time, los cambios de esfuerzos durante el sismo y el exceso de resistencia remanente al final del evento.

En el artículo *Dynamic rupture and stress change in a normal faulting earthquake in the subducting Cocos plate* (Capítulo VI), se estudian las propiedades dinámicas de la ruptura del sismo del 11 de enero de 1997. A diferencia del estudio realizado en el capítulo IV, en este caso se obtienen los cambios en los esfuerzos dinámicamente consistentes con las formas de onda observadas en estaciones cercanas a la fuente, con base en las distribuciones de deslizamientos previamente calculadas. En el estudio se realizan dos modelos dinámicos, uno basado en una velocidad de ruptura y rise-time constantes y el otro incorporando las funciones de tiempo dinámicamente consistentes obtenidas en el primer modelo.

Los resultados de ambos modelos muestran que la ruptura se confina aún más que en el caso cinemático (capítulo IV), entre los 30 y los 45 km de profundidad, y que las funciones de tiempo de la fuente son de corta duración, con variaciones en amplitud y en duración dependiendo de su posición en la ruptura, siendo estas mayores en el área de la aspereza

principal. La distribución de los cambios de esfuerzos muestra una mayor heterogeneidad que en el caso estático obtenido en el capítulo IV. Esta distribución sin embargo, parece ser más consistente que la obtenida en el análisis estático, con el patrón de esfuerzos transferidos por el sismo de 1985 al sismo de 1997.

# Capítulo I

AGRUPAMIENTO ESPACIO-TEMPORAL DE GRANDES SISMOS INTERPLACA A LO LARGO DE LA ZONA DE SUBDUCCIÓN EN MÉXICO: UNA EVIDENCIA DE INTERACCIÓN DE ESFUERZOS DE LA FUENTE.

## Space-Time Clustering of Large Thrust Earthquakes along the Mexican Subduction Zone: an Evidence of Source Stress Interaction

*By Miguel A. Santoyo, Shri K. Singh, Takeshi Mikumo and Mario Ordaz*

### **Abstract**

The spatio-temporal plot of epicenters of large ( $M_s \geq 6.9$ ) subduction earthquakes in Mexico (1900 to present day) suggests that these earthquakes cluster in space and time. In this work we test the hypothesis that the coseismic stress transfer may lead to this clustering. For the analysis we estimate the spatial extent of the coseismic Coulomb stress change for these large events, and then perform a statistical analysis using the  $\chi^2$  goodness of fit test for the inter-event time intervals. We find that there are, at least, two groups of time intervals where the observed frequencies are much higher than that expected from a Poisson model, indicating a bimodal pattern. For the first mode, the observed frequencies for the 0-5 years interval becomes about 2.1 times the expectation, with a probability of occurrence of about 30%. These results show that large thrust Mexican earthquakes between 1900 and 2003, are clustered in space and time probably due to stress interactions among them. The second mode includes the time interval of 30-50 years. In the interval 30-40 years, the observed frequencies become about 1.7 times the expectation and about 1.2 times the expectation for the 40-50 years interval. This second mode could be associated with a re-loading interval of tectonic stress due to the plate convergence, and appears consistent with the long-term recurrence periods of large thrust earthquakes in the Mexican subduction zone.

### **1. Introduction.**

A glance at the spatio-temporal plot of epicenters of large subduction earthquakes in Mexico, which occurred during the last 103 years on the Pacific coast, suggests that these events are clustered in space and time (e.g. Singh et al., 1981; Nishenko and Singh, 1987a; Ward, 1991). Several authors have reported a positive correlation between the coseismic stress changes on the neighborhood of the source region, and the occurrence in clusters of subsequent

earthquakes with different magnitudes in the same area (e.g. King *et al.*, 1994; Stein *et al.*, 1994; Toda *et al.*, 1998; Deng and Sykes, 1997; Harris, 1998; Gomberg *et al.*, 1998; Freed and Lin, 1998; Stein 1999). Here, the term stress transfer or earthquake interaction implies that given an earthquake, the time of occurrence of the following large events in its close neighborhood is accelerated in time due to its coseismic stress increase outside the main slip region.

In this study, we test the hypothesis that the coseismic stress transfer leads to clustering of large thrust earthquakes in the Mexican subduction zone. For this purpose, we define a criterion to obtain the inter-occurrence times, taking into account the spatial extent of the changes of the Coulomb failure stress due to the coseismic slips of each earthquake. The analysis is performed with the aid of the Pearson  $\chi^2$  statistical test, with reference to a Poisson model of earthquake occurrence as our null hypothesis. For this purpose, we analyze the Mexican earthquake catalog from 1900 to 2003.

## **2. Earthquake Data**

The Mexican earthquake catalog is complete from 1900 to the present for events with magnitudes  $M_s \geq 6.5$  (Singh *et al.*, 1984; Kostoglodov and Pacheco, 1999). As our method is based on the spatial relationship between large earthquakes, we only consider rupture areas greater than  $625 \text{ km}^2$  ( $25 \text{ km} \times 25 \text{ km}$ ), which is equivalent to events with  $M_s \geq 6.9$ . The catalog for this period and magnitudes comprises 46 shallow thrust earthquakes (Table 1).

## **3. Method of analysis**

### **3.1. Rupture areas**

The rupture areas for each earthquake are estimated from their aftershock areas when they are known. The aftershock areas have been mapped for only 24 out of the 46 events (Figure 1 and Table 1). For the remaining events, we estimate the rupture area from an empirical relation:  $\log(S) = M_s - 4.1$  (e.g. Utsu and Seki, 1954; Purcaru and Berckhemer, 1978; Wells and Coopersmith, 1994), where  $S$  is the source area in  $\text{km}^2$ , and  $M_s$  is the surface-wave magnitude. During the period considered here, there are four earthquakes of magnitude  $M_w = 6.9$  with known aftershock areas. All of them show an aspect ratio of about  $L = W$  (see



Figure 1), where  $L$  is the length along the strike direction and  $W$  is the width along the dip direction,  $L$  being the horizontal distance of the estimated source area  $S$ . From this observation, we assume that the remaining 6.9 earthquakes on the catalog behave approximately in the same way. For the events with magnitudes over 7.0 with known aftershock areas, they show aspect ratios between  $1.5 < L/W < 3.0$  (Figure 1), so we assume an aspect ratio of  $L=2W$  for them.

### 3.2. Inter-event times

It is critical to establish the rule by which the inter-occurrence times between earthquakes will be determined. One possibility is to take the earthquake catalog in a region and a minimum threshold magnitude, and to calculate the time difference between subsequent events as they appear in the catalog. Since this method does not take into account the spatial distance between the events, one could be accounting for the time interval between two earthquakes that could be several hundreds of kilometers apart from each other.

Our criterion to obtain the inter-event times specifically consists of the following: We first select, from the catalog, the earthquake that occurred first in time, and estimate the possible extent of the zones of coseismic increase in the Coulomb failure stress ( $\Delta CFS$ ) from the rupture area, as described in the next section. Second, from all the rupture areas for subsequent events, we look for the first event in time that spatially overlaps the zone of stress increase due to the specified earthquake, and then take the time interval between them if they actually overlap. Third, because this spatial overlapping could be only partial, we check if the zone of stress increase is completely overlapped by the fault area of the second event. If not, we take the remaining non-overlapped region, and continue searching for the next consecutive earthquake whose fault area spatially overlaps the remaining region. Then, we take again the inter-event time between the first-specified and third events. In this way, the procedure is repeated until the entire region of stress increase due to the specified earthquake is fully overlapped. We consider in this procedure that an earthquake can produce a stress influence to more than one earthquake in the future, and also that a given earthquake can be influenced by more than one event in the past. We also assume that all the stress accumulated due to an earthquake in the overlapped zone will be released by the next events.

The above method is recursively applied to the time for each earthquake in the catalog, until the entire time period of the catalog is analyzed. This procedure provides a set of inter-event times between earthquakes that are now related in the spatial domain. In a later section we show a detailed example of this procedure.

After this is done, the inter-event times are analyzed by the aid of the  $\chi^2$  statistical test, with reference to a Poisson model of occurrence. We analyze two sets of inter-event times: the set “A”, obtained by the method proposed above, which takes into account the stress interaction between earthquakes, and another set “B”, obtained from the time difference between subsequent events directly as they appear in the catalog.

### 3.3. Coulomb failure stress

For the computation of the Coulomb failure stress change, we used the relation  $\Delta\text{CFS} = \Delta\tau + \mu' \Delta\sigma_n$  (e.g. Harris, 1998), where  $\Delta\tau$  is the shear stress change in the direction of the fault slip,  $\Delta\sigma_n$  is the change in the tensional stress normal to the fault plane, and  $\mu'$  is an apparent coefficient of friction  $\mu' = \mu (1-p)$ , where  $\mu$  is the static coefficient of friction and  $p$  is the pore pressure in the source volume. In this study, we used the formulations given by Okada (1985, 1992) to compute the coseismic  $\Delta\text{CFS}$  in a 3-D tensorial way. In the computations, we used a shear modulus of  $\mu = 3.5 \times 10^{11}$  (dyn/cm<sup>2</sup>), with a Poisson ratio of  $\nu = 0.25$ . For the tectonic apparent coefficient of friction, we used the value of  $\mu' = 0.4$  adopted by Mikumo *et al.*, (1999; 2002) for the Mexican subduction zone.

As all the thrust earthquakes considered in this study occur on the upper plate interface between the North-America Plate and the Rivera or Cocos Plates (see Figure 1), the  $\Delta\text{CFS}$  function is computed on this fault interface with the average direction of faulting motion. For the Mexican subduction zone, we used the average parameters:  $\delta = 15^\circ$  (dip), and  $\lambda = 90^\circ$  (slip). The strike is assigned depending on the subducting plate. In the case of the Rivera plate, we used a strike of  $\theta_r = 300^\circ$ , and for the Cocos plate we used  $\theta_c = 290^\circ$ .

To define the spatial extent of coseismic stress increase that would affect future earthquakes, we tentatively take the area whose  $\Delta\text{CFS}$  brings the adjacent region at least 1.0 bar (0.1 MPa) closer to the failure. Values of this order have been recognized by different authors to have effective influence on the neighborhood seismicity around the fault area (e.g. King *et al.*, 1994; Harris, 1998; Hardebeck *et al.*, 1998; Stein, 1999).

Earthquakes have a heterogeneous slip distribution over the fault plane. Unfortunately, this information is available only for some recent Mexican earthquakes. Due to this limitation, we assumed an elliptical distribution of slip over the fault, tapered with a cosine function of 15% for all events (Figure 2a), which is expected from a nearly uniform stress drop. As we will discuss in a next paragraph, this assumption does not significantly affect the estimation of the  $\Delta\text{CFS}$  on the extended plane.

Using this model for earthquakes with magnitudes between  $M=7.0$  and  $M=8.0$  and a mean depth of 20 km, the area with  $\Delta\text{CFS} \geq +1.0$  bar is found to be about four to five times the original fault area. This means that the length of this area along the trench is about twice the fault length (see Figures 2b and 2c). In this study we call this length as the distance of effective influence (DEI). Note that the values of  $\Delta\text{CFS}$  outside the ruptured fault area are positive when computed over the extended fault plane, and non-uniform negative values inside the fault area. In general, actual earthquakes have also some positive  $\Delta\text{CFS}$  zones inside the fault area due to heterogeneous slip distribution. Due to this, in our analysis we consider the fault rupture length as a portion of the DEI.

Figure 3 shows the space-time plot of all the selected earthquakes for this study. The “x” axis (abscissa) is the distance along the trench, taken along the line ABC shown in Figure 1, which is approximately parallel to the trench. The “y” axis (ordinate) represents time in years, beginning in 1900. The earthquake fault zones are projected onto the line ABC, and are shown as horizontal lines where their ordinate value is the date of their occurrence. Thick solid lines represent the fault extent of each earthquake in the direction parallel to the trench, and thin lines denote the spatial extent of their stress influence (the DEI length) projected onto line ABC.

In Figure 4 we show an example of the method to obtain the inter-event times from the space-time plot in Figure 3. Here, we take a sub-catalog of 8 earthquakes that occurred between 1900 and 1945, and between 400 and 700 km along the projection line A-B-C. We begin with the DEI of earthquake A (27/3/1908), as it is the first to appear in the sub-catalog (Figure 4a). The next earthquake to appear in time on the catalog is event B (13/10/1908), but its rupture area does not overlap the DEI of event A, so the time interval between them is not taken into account. The next earthquake to appear in time is event C (31/10/1909). In this case, its rupture area partially overlaps the DEI of event A, so the time interval  $\Delta_1$  between them is taken into account. However, since event C does not overlap the entire DEI length of A, we continue searching for the next consecutive earthquake whose fault area spatially overlaps the remaining region. Here event D (7/6/1911) does not overlap the DEI of A, but event E (16/12/1911) does it so we take the time  $\Delta_2$  between A and E. Event F (8/5/1933) again overlaps a small part of the remaining region, so we take the time interval  $\Delta_3$ . In the same sense, only event H (22/2/1943) and not event G (15/4/1941), overlaps the remaining region of A, so we take only  $\Delta_4$  between A and H. Now the DEI of A is completely overlapped by the four events. We repeat the procedure with the DEI of the next event B. Here, event D is the only one to overlap the DEI of B, so in this case we only take the time interval  $\Delta_5$  (Figure 4b). Following the same procedure, in Figure 4c, we find that only events E, F and H overlap the DEI of C, so we take the times  $\Delta_6$ ,  $\Delta_7$  and  $\Delta_8$  respectively. Figure 4d shows that for event D, only G and H overlap its DEI so we take the time intervals  $\Delta_9$  and  $\Delta_{10}$ . In this example we can observe that one earthquake can influence more than one event in the future, and that a given earthquake can be influenced by more than one event in the past.

A more detailed analysis using actual slip distributions over the fault plane will not necessarily produce a significant difference on the DEI obtained by our method. The Coulomb stress changes outside the rupture fault area are not very sensitive to the slip distribution inside the fault area. Variations of the slip are significant only inside the source area, in the sense that as one goes away from the main slip zone, the  $\Delta\text{CFS}$  represents the result due to the sum of the mean slip variations. In order to check this assumption, we performed tests to compare the variations in the  $\Delta\text{CFS}$  outside the main fault area, assuming an elliptical slip distribution, with

those from the slip distributions obtained by kinematic waveform inversion of three earthquakes: the 19/09/1985 Ms=8.1, Michoacan (Mendoza and Hartzell, 1989), the 14/09/1995 Ms=7.3 Copala (Courboulex, et al 1999), and the 25/04/1989 Ms=6.9, San Marcos (Santoyo, 1989 and Zuñiga et al, 1993) earthquakes. The results on DEI differ only by 15%. Further tests described in appendix show that these variations in the DEI do not significantly affect the final results.

There is a possibility, however, that the absolute value of  $\Delta\text{CFS}$  would become somewhat larger if some difference in elastic properties between the crust overriding the subducting plate and those inside the plate is taken into account, and hence that the DEI would become slightly larger. In a more detailed analysis, it would also be necessary to incorporate postseismic stress variations due to plate convergence and viscoelastic relaxation process (e.g. Mikumo *et al.*, 2002).

#### **4. Results from statistical analysis and discussion**

Following the method outlined earlier, we obtained 113 inter-event times for the set of 46 earthquakes. A statistical analysis of these inter-event times is now performed by the aid of the  $\chi^2$  test for the goodness of fit (e.g. Benjamin and Cornell, 1970; pp 457). Our working hypothesis is that the inter-event times (A) obtained by our method would differ significantly from a Poisson process, showing a clustering behavior.

To ensure that our results are due to earthquake interactions and not simply to the time distribution of the earthquakes in the catalog, we also analyzed the set of inter-event times (B) taken simply from the time difference between subsequent events as they appear in the catalog. In this case, the  $\chi^2$  test is expected to favor the null hypothesis, showing a Poisson behavior.

The inter-event time intervals (A) obtained by our method are grouped into two class intervals (5.0 and 10.0 years) taking care of having no less than 5 elements in each interval, and the data are analyzed for the 99% and 99.9% significance levels (Benjamin and Cornell, 1970). The results are summarized in Table 2. For the two different selections of class intervals, the

results do not allow us to reject the working hypothesis of earthquake clustering, on the ground that the test results are greater than both of the 1.0% and 0.1%  $\chi^2$  distribution percentage points (Abramowitz and Stegun, 1972), as seen in Table 2. To assure that our method would not identify an unclustered dataset as a clustered one, we performed the test which is explained in detail in the appendix. Also in the appendix we performed another test of the effects of changing 15% the length of the DEI.

In Figure 5a it can be observed that once an earthquake has occurred, approximately 30% of the subsequent events occur in the next 5 years, possibly due to the stress interactions.

The next set of time intervals (B) taken directly from the catalog, was grouped into the class interval of 5 years taking the same procedure as for the previous set A. The results from the  $\chi^2$  test for this case are summarized in Table 2. Here the results do not allow us to reject the null hypothesis, showing that these inter-event times follow a much more random behavior.

In Figures 5b and 5c it can be observed that there are two groups of time intervals where the observed frequencies of occurrence are much higher than those expected from the Poisson model, indicating a bimodal pattern. This behavior could be divided into a short-term mode of clustering of events, and a long-term mode for recurrence-type period for large earthquakes.

The first group of intervals, or the first mode, falls between 0 and 5 years, where the observed frequencies are approximately two times higher than that expected from the Poisson model. The second group of intervals, or the second mode, falls between 30 and 50 years, and the observations are about two times the Poisson's expectation.

These results imply that just after the first year of the occurrence of a large earthquake, the probability of occurrence of another large event in the same region is much higher than that expected from a random process, and that in the interval "0-5" years, the probability of occurrence due to the interaction between large earthquakes is near 35%.

The second mode (30-50 years) could be associated with the re-loading interval of tectonic stress due to the plate convergence. In fact, these results do not appear inconsistent with the analysis of recurrence times based on the seismic gap hypothesis. Nishenko and Singh (1987a) found that in the Mexican subduction zone, the long-term recurrence time for earthquakes with magnitudes  $M_s \geq 7.5$  varies from 28 to 54 years, with a mean of about 40 years. Using a different method than Nishenko and Singh, Zuñiga and Wyss (2001) also observed recurrence times of these orders (20-40 years) in the southern portion of the Mexican subduction zone. The second mode of our results indicates that the lobe in the frequencies of occurrence between 30 to 50 years could be associated with the long-term recurrence periods found by Nishenko and Singh, and Zuñiga and Wyss, among others.

Even though these results are not inconsistent with the analyses by the seismic gap theory for long-term recurrence periods, there is an important group of large events that occur soon after the occurrence of large earthquakes. Thus, special care should be taken in relation to the time periods after a large earthquake have occurred, especially for seismic hazard analyses for large subduction earthquakes in Mexico.

Recently on January 22, 2003, a large earthquake with magnitude  $M_w = 7.6$  occurred in front of the coast of the Mexican state of Colima, at the southeast end of the 09/10/1995,  $M_w = 8.0$ , Jalisco earthquake fault (Singh et al., 2003; Yagi et al, 2004) (Table 1). This earthquake occurred just in the area of the effective stress influence from the 1995 Jalisco earthquake, 8 years after its occurrence, and also from the 1973 earthquake, almost 30 years after the event (Figure 3). In agreement with our results and the results by other authors, this could be an indication that the last event has influenced the occurrence of a next event with a positive  $\Delta CFS$ , incrementing the rate of seismicity in its adjacent zones. Under our scheme, given the 1995 earthquake, the probability of occurrence of the 2003 event in its area of positive effective stress influence, was about 36% after 8 years as shown in Figure 5a. This value is about twice that expected from the Poisson model.

## 5. Conclusions

Several studies have shown that the clustering of earthquakes is not restricted to aftershock or foreshock sequences, but also occurs for large and great earthquakes (e.g. Kagan and Knopoff, 1976; Kagan and Jackson, 1991). Our study shows that the probable stress interaction in a group of large thrust earthquakes ( $M_w \geq 6.9$ ) in the Mexican subduction zone, is leading to their clustering behavior in space and time. It also shows that this behavior is not simply due to the temporal distribution of the large earthquakes itself on the catalog.

We find that given a large earthquake ( $M_w \geq 6.9$ ), the probability of occurrence of another large event in the same region is much higher than that expected from a random process. In the interval of 0 to 5 years, the probability of occurrence of another large earthquake in the neighboring region is about 30%, about twice that expected from a Poisson model. The results of our analysis should be taken into account in earthquake forecast and seismic hazard estimation in Mexico.

On the other hand, it is necessary to perform a more detailed analysis in a three dimensional scheme to account for the inter-event times due to the stress interaction between shallow-thrust and in-slab normal faulting earthquakes in this subduction zone.

## ACKNOWLEDGEMENTS

The authors wish to acknowledge fruitful discussions with Javier Pacheco. The Coulomb failure stress computations were performed using the code DIS3D. We thank two anonymous reviewers and Stefan Wiemer for their critical comments. This work was partially supported by DGAPA, UNAM project No. IN111601 and CONACYT project No. 41209-F.

## REFERENCES

Abramowitz, M, and I. A. Stegun (1972). Handbook of mathematical functions with formulas, graphs and mathematical tables. *Dover Publications Inc. NewYork*



Anderson J.G., S.K. Singh, J.M. Espíndola, and J. Yamamoto (1989). Seismic strain release in the Mexican Subduction thrust, *Phys. Earth Planet. Interiors* **58**, 307-322.

Astiz, L. and H. Kanamori (1984). An earthquake doublet in Ometepe, Guerrero, Mexico, *Phys. Earth Planet. Interiors* **34**, 24-45.

Benjamin, Jack R. and C. Allin Cornell, (1970). Probability, statistics and decision for civil engineers, *McGraw Hill, Spanish edition, Mexico*.

Courboux, F., M.A. Santoyo, J. Pacheco, and S.K. Singh (1997). The 14 September 1995 (M=7.3) Copala, México earthquake : A Source study using teleseismic, regional, and local data, *Bull. Seism. Soc. Am.* **87**, pp. 999-101.

Deng J, and L.R. Sykes (1997). Evolution of the stress field in southern California and triggering of moderate-size earthquakes: A 200-year perspective, *J. Geophys. Res.* **102**, 9859-9886.

Freed, A.M. and J. Lin (1998). Time dependent changes in failure stress following thrust earthquakes, *J. Geophys. Res.* **103**, 24393-24409.

Gomberg, J., N.M. Beeler, M.L. Blanpied and P. Bodin (1998). Earthquake triggering by transient and static deformations, *J. Geophys. Res.* **103**, 24411-24416.

Hardebeck, J., J. Nazareth, and E. Hauksson (1998). The static stress change triggering model: Constraints from two southern California aftershock sequences, *J. Geophys. Res.* **103**, 24,427-24,437.

Harris, R. (1998). Introduction to special section: stress triggers, stress shadows, and implications for seismic hazards, *J. Geophys. Res.* **103**, 24347-24358.

Havskov, J., S.K. Singh, E. Nava, T. Domínguez and M. Rodríguez (1983). Playa Azul, Michoacan, Mexico earthquake of 25 October ( $M_s = 7.3$ ), 1981, *Bull. Seism. Soc. Am.*, **73**, 449-457.

Kagan, Y. and L. Knopoff (1976). Statistical search for non-random features of the seismicity of strong earthquakes, *Phys. Earth Planet. Interiors* **12**, 291-318.

Kagan, Y. and D.D. Jackson (1991). Long-term earthquake clustering, *Geophys. J. Int.* **104**, 117-133.

King, G.C.P., R.S. Stein, and J.Lin (1994). Static stress changes and the triggering of earthquakes, *Bull. Seism. Soc. Am.* **84**, 935-953.

Kostoglodov, V. and J. Pacheco (1999). Cien años de sismicidad en México. *Instituto de Geofísica, UNAM*; Poster.

Mikumo T., S. K. Singh, and M.A. Santoyo (1999). A possible stress interaction between large thrust and normal faulting earthquakes in the Mexican subduction zone, *Bull. Seism. Soc. Am.* **89**, 1418-1427.

Mikumo, T., Y. Yagi, S.K. Singh, and M.A. Santoyo (2002). Coseismic and postseismic stress changes in a subducting plate: Possible stress interactions between large interplate thrust and intraplate normal faulting earthquakes, *J. Geophys. Res.*, **107**, B1, ESE5-1-ESE5-12.

Nishenko, S.P. and S.K. Singh (1987a). Conditional probabilities for the recurrence of large and great interplate earthquakes along the Mexican subduction zone, *Bull. Seism. Soc. Am.* **77**, 2095-2114.

Nishenko, S.P. and S.K. Singh (1987b). The Acapulco-Ometepec, Mexico, earthquakes of 1907-1982: Evidence for a variable recurrence history, *Bull. Seism. Soc. Am.* **77**, 1359-1367.

Ortiz, M., S.K. Singh, V. Kostoglodov, and J. Pacheco (2000). Source areas of the Acapulco-San Marcos, Mexico earthquakes of 1962 (M 7.1; 7.0) and 1957 (M 7.7), as constrained by Tsunami and uplift records. *Geofísica Internacional* **39**, No. 4, 337-348.

Okada, Y. (1985). Surface deformation due to shear and tensile faults in a half space, *Bull. Seism. Soc. Am.* **75**, 1135-1154.

Okada, Y. (1992). Internal deformation due to shear and tensile faults in a half space, *Bull. Seism. Soc. Am.* **82**, 1018-1040.

Pacheco, J., S. K. Singh, J. Dominguez, A. Hurtado, L. Quintanar, Z. Jimenez, J. Yamamoto, C. Gutierrez, M.A. Santoyo, W. Bandy, M. Guzman and V. Kostoglodov (1997). The October 9, 1995 Colima-Jalisco, Mexico, earthquake (Mw 8): An aftershock study and a comparison of this earthquake with those of 1932, *Geophys. Res. Lett.*, **24**, 2223-2226.

Purcaru, G. and H. Berckhemer (1978). Quantitative relations of seismic source parameters and a classification of earthquakes, *Tectonophysics* **84**, 57-128.

Reyes, A., J.N. Brune, and C. Lomnitz (1979). Source mechanism and aftershock study of the Colima, Mexico earthquake of January 10, 1973, *Bull. Seism. Soc. Am.*, **69**, 1819-1840.

Santoyo M.A. (1994). Estudio del proceso de ruptura del sismo del 25 de abril de 1989 usando registros de movimientos fuertes y telesísmicos. *Master Thesis. UACPyP-C.C.H.*, UNAM.

Singh, S.K, Havskov, K. McNally, L. Ponce, T. Hearn, and M. Vassiliou (1980). The Oaxaca Mexico earthquake of 29 november 1978: A preliminary report on aftershocks. *Science* **207**, 1211-1213.

Singh, S.K., L. Astiz, and J. Havskov (1981). Seismic gaps and recurrence periods of large earthquake along the Mexican subduction zone: a reexamination, *Bull. Seism. Soc. Am.* **71**, 827-843.

Singh, S.K., M. Rodríguez, and J.M. Espíndola (1984). A catalog of shallow earthquakes of Mexico from 1900 to 1981, *Bull. Seism. Soc. Am.* **74**, 267-279.

Singh, S.K., L. Ponce and S. P. Nishenko (1985). The great Jalisco, Mexico, earthquakes of 1932: Subduction of the rivera plate, *Bull. Seism. Soc. Am.* **75**, 1301-1313.

Singh, S. K. and F. Mortera (1991), Source-time functions of large Mexican subduction earthquakes, morphology of the Benioff zone, and the extent of the Guerrero gap, *J. Geophys. Res.* **96**, 21487-21502.

Singh, S.K., J.F. Pacheco, L. Alcantara, G. Reyes, M. Ordaz, A. Iglesias, S.M. Alcocer, C. Gutierrez, C. Valdés, V. Kostoglodov, C. Reyes, T. Mikumo, R. Quaas, and J.G. Anderson (2003). A preliminary report on the Tecomán, México, earthquake of 22 January 2003 (Mw 7.4) and its effects. *Seism. Res. Lett.*, **74**, 279-289.

Stein, S. (1999). The role of stress transfer in earthquake occurrence, *Nature*, **402**, 605-609.

Stein, R.S., G.C.P. King, and J. Lin (1994). Stress triggering of the 1994 M=6.7 Northridge, California earthquake by its predecessors, *Science*, **265**, 1432-1435.

Toda S., R. S. Stein, P. A. Reasenberg, J. H. Dieterich, and A. Yoshida (1998). Stress transferred by the 1995 Mw=6.9 Kobe, Japan, shock: Effect on aftershocks and future earthquake probabilities, *J. Geophys. Res.* **103**, 24543-24565.

UNAM Seismology Group (1986). The september 1985 Michoacan earthquakes: Aftershock distribution and history of rupture, *Geophys. Res. Lett.* **13**, 573-576.

Utsu , T. and A. Seki (1954). A relation between the area of aftershock region and the energy of mainshock. *J. Seism. Soc. Jap.*, **7**, 233-240.

Valdés, C. and D. Novelo (1998). The western Guerrero, Mexico, seismogenic zone from the microseismicity associated to the 1979, Petatlán and 1985, Zihuatanejo earthquakes, *Tectonophysics*, **287**, 271-277.

Ward S.N. (1992) An application of synthetic seismicity calculations in earthquake statistics: The middle America trench, *J.Geophys.Res.*, **97**,6675-6682.

Wells, D. L., and K. J. Coppersmith, (1994). New empirical relationships among magnitude, rupture length, rupture width, rupture area, and surface displacement, *Bull. Seismol. Soc. Am.*, **84**, 974-1002.

Yagi, Y., T. Mikumo, J. Pacheco and G. Reyes (2004). Source rupture process of the Tecomán, Colima, Mexico earthquake of 22 January 2003, determined by joint inversion of teleseismic body-wave and near-source data. *Bull. Seism. Soc. Am.*, **94**, 1795-1807.

Zúñiga F.R., Gutierrez, C., Nava E., Lermo, J., Rodriguez, M., Coyoli, R. (1993). Aftershocks of the San Marcos, earthquake, of april 25, 1989 and its implications for the potential of the Acapulco-San Marcos region. *Pure and Applied Geophysics*, special issue on Subduction Zone Earthquakes., **140**, 287-300,.

Zuñiga, F.R., and M. Wyss (2001). Most- and least-likely locations of large to great earthquakes along the pacific coast of Mexico estimated from local recurrence times based on b-values. *Bull. Seism. Soc. Am.* **91**, 1717-1728.

## APPENDIX

To ensure that our method would not identify an unclustered dataset as a clustered one, we performed the following test: we generated a large number of synthetic catalogs with the same magnitude exceedence rate characteristics (expected number of earthquakes per unit time) of the actual one, but with a known Poissonian behavior in time, and applied our method to them. We then, checked how many synthetic catalogs produced a possible non-Poissonian behavior, according to our algorithm. To do this we generated 10,000 catalogs, where for each catalog we assigned the following characteristics:

I. Following a Poissonian model, the inter-event times (termed as inter-arrival times by Benjamin and Cornell, 1970), were assigned an exponential distribution, with the same value of  $\lambda=46/103=0.447$  (event/year) as the actual catalog. To simulate the inter-event times we used

$$\tau_i = -\left(\frac{1}{\lambda}\right) \ln(u_i)$$

where  $\tau_i$  = inter-event time,  $u_i$  is a uniformly distributed random number between 0 and 1, and

$$T_i = \sum_{k=1}^i \tau_k$$

is the time of occurrence of each earthquake in the synthetic catalog.

II. The spatial location along the trench of each earthquake was set following a uniform distribution  $x_i = 1350 u_i$ , where  $u_i$  is again a uniformly distributed random number between 0 and 1.

III. For the magnitude distribution of events in the catalog, we assigned a truncated Gaussian distribution with  $E_m = 7.03$  and  $\sigma = 0.84$  which are the mean and standard deviation values for this distribution, obtained from the actual catalog. Then,  $M_i = E_m + \sigma y_i$ ,  $6.8 \leq M_i \leq 8.2$ , where  $M_i$  is the magnitude assigned to each event, and  $y_i$  is a random number with standard normal distribution. Then, the DEI for each event was assigned according to the relation  $\log(S) = M - 4.1$  and  $L = 2W$ . Finally, we applied the method to each synthetic catalog.

From this test, our method concluded that only 512 out of the 10,000 synthetic catalogs (5.12%), behaved as non-Poissonian and 94.88% of the cases behaved as Poissonian, indicating that our method is working with a good confidence level, and that it is very unlikely that an unclustered dataset could be identified as clustered by our algorithm.

Another test performed was to assure that a change of 15% in the length of the DEI length due to the different distribution of slips, would not significantly affect the results of the statistical analysis. Here we changed this length in three different ways: I. First we increased by 15% the values of DEI of all the earthquakes on the catalog, and applied our method; II. We reduced by 15% the DEI values of all earthquakes on the catalog, and again applied the method, and III. We generated a random 15% increase or decrease of the DEI for each earthquake on the catalog, and applied the method in 100 different runs. In all cases (100%), the tests yielded no evidence to favor the Poisson hypothesis of earthquake occurrence.

#### **Authors Affiliation**

Instituto de Geofísica  
Universidad Nacional Autónoma de México (UNAM)  
Circuito Institutos s/n, Ciudad Universitaria  
Coyoacán, 04510  
México, D.F., México.  
(M.A.S., S.K.S, T.M.)

Instituto de Ingeniería  
Universidad Nacional Autónoma de México (UNAM)  
Circuito Institutos s/n, Ciudad Universitaria  
Coyoacán, 04510  
México, D.F., México.  
(M.O.)

Table 1  
Catalog of Shallow, Thrust Mexican Earthquakes with Magnitudes  $M_s \geq 6.9$  (1900-2003).

No. Event	Date	Location*		M*	L <sup>§</sup>	No. Event	Date	Location*		M*	L <sup>§</sup>
		Lat.	Lon.					Lat.	Lon.		
1	1900/1/20	20.0	-105.0 <sup>1</sup>	(7.6) <sup>2</sup>	79.5 <sup>3</sup>	24	1941/4/15	18.85	-102.94 <sup>1</sup>	(7.9) <sup>1</sup>	112.3 <sup>3</sup>
2	1900/5/16	20.0	-105.0 <sup>1</sup>	(7.1) <sup>2</sup>	44.7 <sup>3</sup>	25	1943/2/22	17.62	-101.15 <sup>1</sup>	(7.7) <sup>1</sup>	89.2 <sup>3</sup>
3	1907/4/15	[16.62]	[-99.2] <sup>4</sup>	7.9 <sup>4</sup>	150.6 <sup>4</sup>	26	1950/12/14	{16.61}	[-98.82] <sup>4</sup>	7.3 <sup>7</sup>	58.2 <sup>4</sup>
4	1908/3/26	16.7	-99.2 <sup>5</sup>	(7.8) <sup>2</sup>	100.1 <sup>3</sup>	27	1957/7/28	[16.59]	[-99.41] <sup>4</sup>	7.8 <sup>7</sup>	92.0 <sup>4</sup>
5	1908/3/27	17.0	-101.0 <sup>5</sup>	(7.2) <sup>2</sup>	50.2 <sup>3</sup>	28	1962/5/11	[16.93]	[-99.99] <sup>9</sup>	7.1 <sup>9</sup>	40.0 <sup>9</sup>
6	1908/10/13	18	-102 <sup>5</sup>	(6.9) <sup>5</sup>	35.5 <sup>3</sup>	29	1962/5/19	[16.85]	[-99.92] <sup>9</sup>	7.0 <sup>9</sup>	35.0 <sup>9</sup>
7	1909/7/30	16.8	-99.9 <sup>1</sup>	(7.5) <sup>2</sup>	70.9 <sup>3</sup>	30	1965/8/23	[15.58]	[-96.02] <sup>10</sup>	7.5 <sup>7</sup>	108.5 <sup>10</sup>
8	1909/7/31	16.62	-99.45 <sup>1</sup>	(7.1) <sup>2</sup>	44.7 <sup>3</sup>	31	1968/8/2	[16.01]	[-98.01] <sup>10</sup>	7.3 <sup>7</sup>	70.0 <sup>10</sup>
9	1909/10/31	17.1	-101.1 <sup>1</sup>	(6.9) <sup>2</sup>	35.5 <sup>3</sup>	32	1973/1/30	[18.29]	[-103.41] <sup>11</sup>	7.7 <sup>11</sup>	90.0 <sup>11</sup>
10	1911/6/7	17.5	-102.5 <sup>6</sup>	(7.9) <sup>6</sup>	112.3 <sup>3</sup>	33	1978/11/29	[15.75]	[-97.05] <sup>10</sup>	7.8 <sup>12</sup>	84.0 <sup>10</sup>
11	1911/12/16	17	-100.7 <sup>1</sup>	(7.6) <sup>2</sup>	79.5 <sup>3</sup>	34	1979/3/14	[17.46]	[-101.45] <sup>13</sup>	7.4 <sup>12</sup>	95.0 <sup>13</sup>
12	1928/3/22	15.67	-96.1 <sup>7</sup>	(7.5) <sup>6</sup>	70.9 <sup>3</sup>	35	1981/10/25	[17.75]	[-102.25] <sup>14</sup>	7.2 <sup>12</sup>	48.0 <sup>14</sup>
13	1928/6/17	15.8	-96.9 <sup>1</sup>	(7.8) <sup>6</sup>	100.1 <sup>3</sup>	36	1982/6/7-1	{16.35}	[-98.37] <sup>15</sup>	6.9 <sup>12</sup>	53.0 <sup>15</sup>
14	1928/8/4	16.1	-97.4 <sup>1</sup>	(7.4) <sup>6</sup>	63.2 <sup>3</sup>	37	1982/6/7-2	[16.4]	[-98.54] <sup>15</sup>	6.9 <sup>12</sup>	57.0 <sup>15</sup>
15	1928/10/9	16.3	-97.3 <sup>1</sup>	(7.6) <sup>6</sup>	79.5 <sup>3</sup>	38	1985/9/19	[17.79]	[-102.51] <sup>16</sup>	8.1 <sup>12</sup>	180.0 <sup>16</sup>
16	1932/6/3	[19.8]	[-105.4] <sup>8</sup>	8.0 <sup>7</sup>	222.0 <sup>8</sup>	39	1985/9/21	[17.62]	[-101.82] <sup>16</sup>	7.5 <sup>12</sup>	80.0 <sup>16</sup>
17	1932/6/18	[18.99]	[-104.6] <sup>8</sup>	7.9 <sup>7</sup>	71.0 <sup>8</sup>	40	1986/4/30	{18.42}	[-102.49] <sup>16</sup>	6.9 <sup>12</sup>	55.0 <sup>16</sup>
18	1932/6/22	18.74	-104.68 <sup>8</sup>	(6.9) <sup>8</sup>	35.5 <sup>3</sup>	41	1989/4/25	[16.58]	[-99.46] <sup>17</sup>	6.9 <sup>12</sup>	35.0 <sup>17</sup>
19	1932/7/25	18.87	-103.93 <sup>8</sup>	(6.9) <sup>8</sup>	35.5 <sup>3</sup>	42	1995/9/14	[16.48]	[-98.76] <sup>18</sup>	7.3 <sup>12</sup>	45.0 <sup>18</sup>
20	1933/5/8	17.5	-101 <sup>1</sup>	(6.9) <sup>1</sup>	35.5 <sup>3</sup>	43	1995/10/9	[19.1]	[-104.9] <sup>19</sup>	8.0 <sup>12</sup>	175.0 <sup>19</sup>
21	1934/11/30	19	-105.31 <sup>8</sup>	(7.0) <sup>8</sup>	39.9 <sup>3</sup>	44	1996/2/25	[15.78]	[-98.26] <sup>20</sup>	7.1 <sup>12</sup>	68.0 <sup>20</sup>
22	1935/6/29	18.75	-103.5 <sup>8</sup>	(6.9) <sup>8</sup>	35.5 <sup>3</sup>	45	2000/8/9	17.99	-102.66 <sup>21</sup>	(6.9) <sup>3</sup>	35.5 <sup>3</sup>
23	1937/12/23	[16.39]	[-98.61] <sup>4</sup>	7.5 <sup>7</sup>	61.2 <sup>4</sup>	46	2003/1/22	[18.7]	[-104.2] <sup>22</sup>	7.6 <sup>12</sup>	72.0 <sup>22</sup>

Notes. Numbers shown as superscripts indicate references. \*Bracketed numbers indicate the location of the center of the rupture area. ♦ M=Ms if in parenthesis, otherwise M=Mw. § L indicate the lengths of the faults along the coast (see text). References: 1) Singh et al., 1984; 2) Nishenko and Singh, 1987a; 3) L from  $\log(S)=M_s-4.1$ ; 4) Nishenko and Singh, 1987b; 5) Singh et al., 1981; 6) Anderson et al., 1989; 7) Singh and Mortera, 1991; 8) Singh et al., 1985; 9) Ortiz et al., 2000; 10) Singh et al., 1980; 11) Reyes et al., 1979; 12) Harvard CMT catalog; 13) Valdés and Novelo, 1998; 14) Havskov et al., 1983; 15) Astiz and Kanamori, 1984; 16) UNAM seismology group, 1986; 17) Zuñiga, 1993; 18) Courboux et al., 1999; 19) Pacheco et al., 1997. 20) Santoyo and Islas, unpublished report; 21) SSN catalog; 22) Singh et al., 2003.



Table 2

Results for the statistical analysis of inter-event times.

Data set	Class Int. (Years)	Test Results	$\chi^2$ 99%*	$\chi^2$ 99.9%**	Allow to reject null hypothesis.
A	5.0	73.3	36.19	43.82	yes
	10.0	38.73	21.67	27.88	yes
B	5.0	0.88	6.63	10.83	no

\* Values for the 1.0% percentage points (Abramowitz and Stegun, 1972)

\*\* Values for the 0.1% percentage points (Abramowitz and Stegun, 1972)

## FIGURE CAPTIONS.

Figure 1. Tectonic map of Mexico. Gray areas show the aftershock area of large earthquakes from 1900 to 2003. Stars represent the epicentral locations of earthquakes for which there are no aftershock areas available. Thin lines parallel to the coast show the spatial extent of the sequence 1908-1911 in Guerrero. The solid line A-B-C is the reference line for the projection of these events. TMVB shows the Trans-Mexican Volcanic Belt. OFZ: Orozco Fracture Zone; OGFZ: O'Gorman Fracture Zone; EGG: El Gordo Graben. PACIFIC, COCOS and RIV. indicate the Pacific, Cocos and Rivera oceanic plates; JA: State of Jalisco; CO: State of Colima; MI: State of Michoacan; GU: State of Guerrero; OA: State of Oaxaca.

Figure 2. Coulomb failure stress change from two possible earthquakes over their extended fault plane. The stress changes are given in bars. The aspect ratio of the fault size is  $L=2W$  for the two assumed events. For this model, we take  $dip=15^\circ$ ,  $slip=90^\circ$  and the center of the fault located at a depth of 20 km. a) The slip is assumed to have an elliptical distribution with a cosine tapering of 15% over the length and width. b) An earthquake with a moment magnitude  $M_w=7.0$ . c) An earthquake with  $M_w=8.0$ . Note that the horizontal distance between + 1 bar-contours on the extended plane is approximately twice the assumed fault length ( $L$ ).

Figure 3. Space-time plot of the Mexican subduction earthquakes with  $M_s \geq 6.9$ , taken from the catalog for the period from 1900 to 2003. The abscissa is the distance in km along the projection line A-B-C shown in Figure 1. "A" and "C" are located at the northwestern and southeastern ends of the projection line. The ordinate represents time in years beginning at 1900. Open circles indicate the epicentral location projected onto the line A-B-C at the occurrence time of earthquakes. Thick and thin horizontal lines represent the source length ( $L$ ) and the DEI of each earthquake, respectively, projected along the line A-B-C. JA, CO, MI, GU, OA same as in Figure 1.

Figure 4. Example of the method used to obtain the inter-event times, based on the spatial extent of the coseismic Coulomb failure stress. Rupture areas projected on line A-B-C of Figure 1, are shown as thick solid lines. Earthquakes, A: 27/03/1908; B: 13/10/1908; C: 31/10/1909; D: 7/6/1911; E: 16/12/1911; F: 8/5/1933; G: 15/4/1931; H: 22/2/1943; see Table 1

for details. The extent of the DEI of events A, B, C and D, are shown as thin solid lines. (a) Time intervals counted from event A. (b) Time intervals counted from event B. (c) Time intervals counted from event C. (d) Time intervals counted from event D. See text for the description of the method.

Figure 5. Histograms of inter-event times and probabilities. (a) Normalized accumulated frequency of set A (solid line) and that expected from the Poisson model (dashed line). (b) Results obtained by the method proposed in this study (set A) for a time interval of 5 years, combining bins where raw data contains less than five elements. Continuous lines here are the curves for the expected values from a Poisson model of occurrence. (c) Same as “b” for a time interval of 10 years.

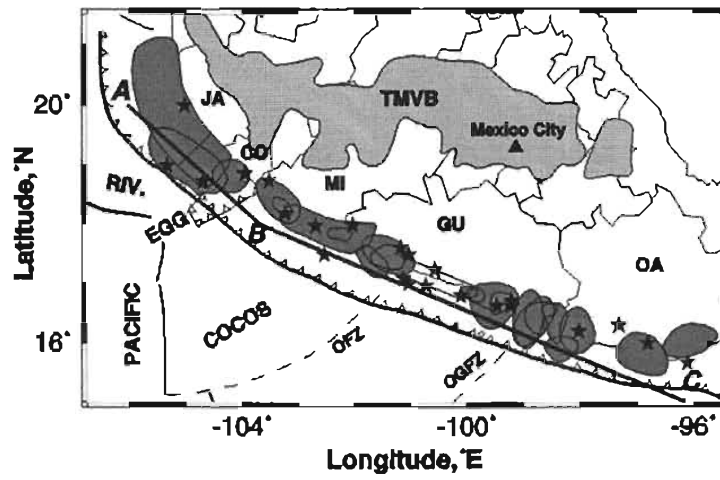


Figure 1

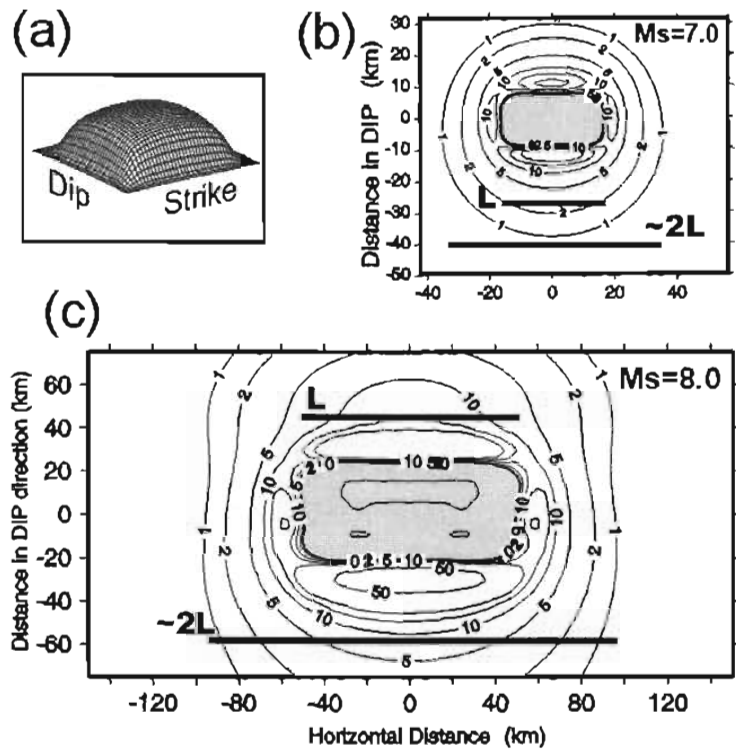


Figure 2

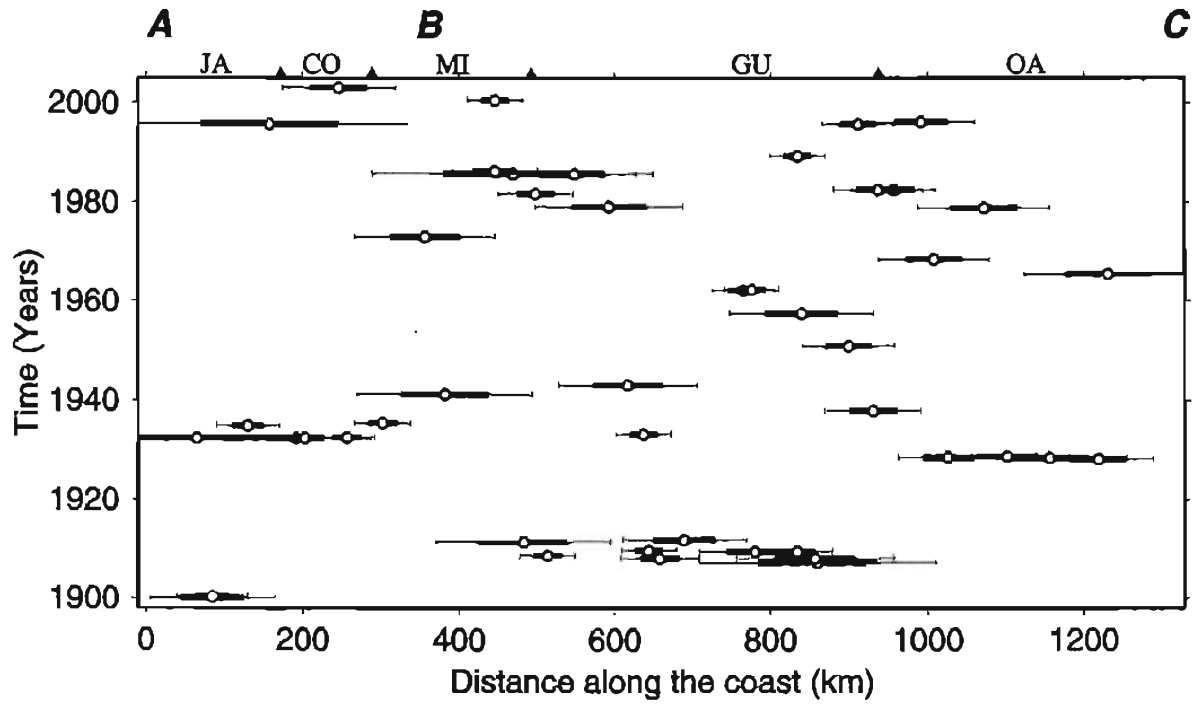


Figure 3

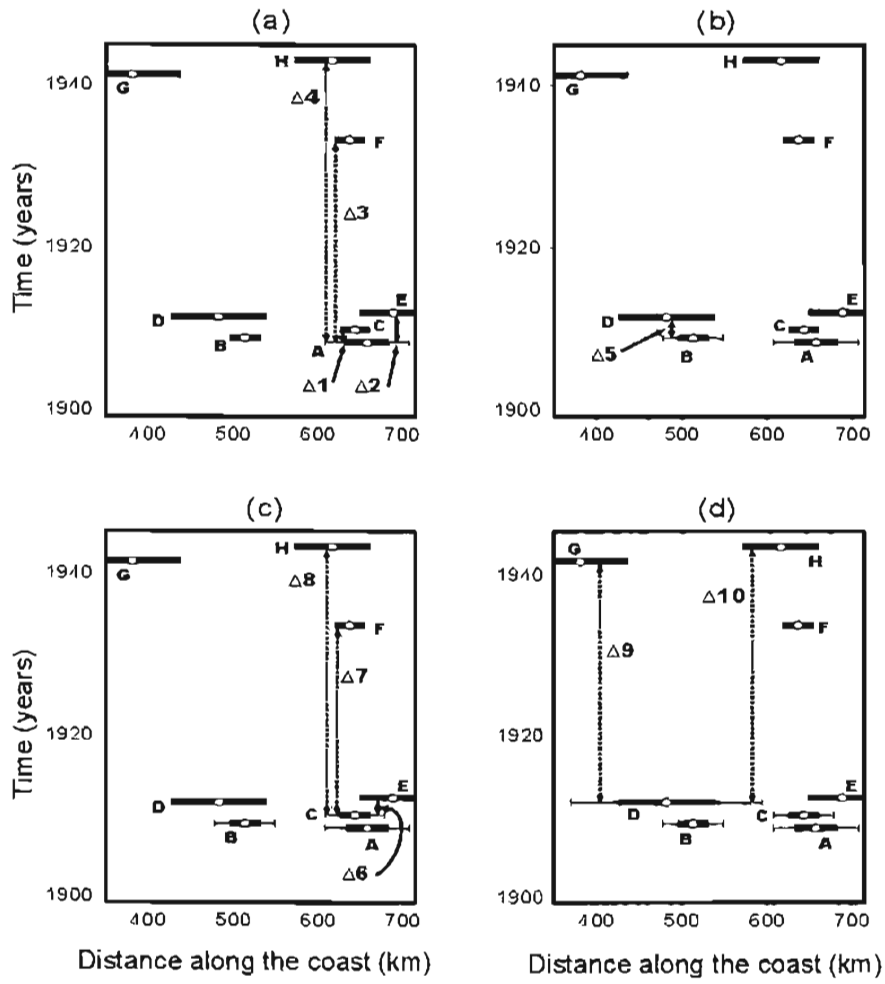


Figure 4

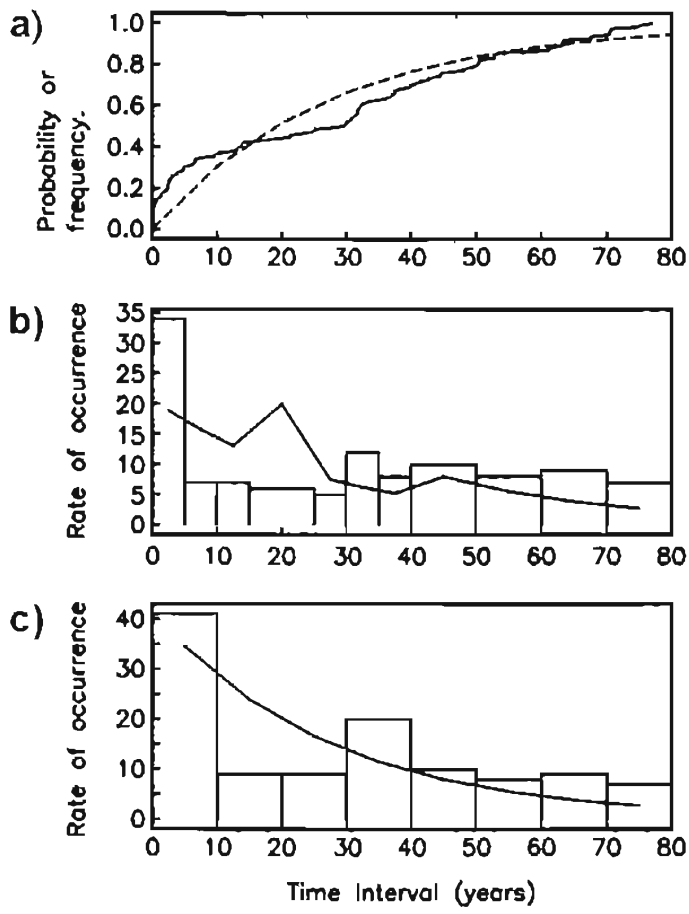


Figure 5



## Capítulo II

POSIBLE INTERACCIÓN LATERAL DE ESFUERZOS EN UNA SECUENCIA DE GRANDES SISMOS DE INTERPLACA EN LAS PLACAS SUBDUCENTES DE COCOS Y RIVERA

## Possible Lateral Stress Interactions in a Sequence of Large Interplate Thrust Earthquakes on the Subducting Cocos and Rivera Plates

*By Miguel A. Santoyo, Takeshi Mikumo, and Carlos Mendoza*

### Abstract

Large interplate earthquakes in the Mexican subduction zone sometimes cluster in space and time, and it has been suggested that this clustering could be due to stress interactions between these large events. We investigate this possibility by calculating the coseismic Coulomb failure stress change due to seven large thrust earthquakes ( $M_w > 7.3$ ) that occurred in a sequence from 1973 to 2003 on the Cocos and Rivera plates subducting beneath the North America plate. These calculations are based on the slip distribution obtained from previous kinematic waveform inversion for these earthquakes. The stress changes thus calculated are superposed in a cumulative way as a function of time and space. We also estimate the postseismic effects from viscoelastic relaxation and plate convergence on the coseismic stress change, but these effects are found to be quite small. Our results show that these earthquakes could be related to each other, and at least part of the relation may be triggering due to the coseismic stress increase from the occurrence of previous large adjacent events.

### INTRODUCTION

Seismic activity in the Pacific coast of southern Mexico is dominated by the movement of the Cocos and Rivera oceanic plates subducting beneath the continental North America plate. It has been pointed out that large interplate earthquakes in this subduction zone sometimes cluster in space and time (e.g. Singh et al., 1981; Nisbenko and Singh, 1987; Ward, 1992). A recent statistical analysis also shows that the observed space-time clustering could be due to possible stress interactions among these large events (Santoyo et al., 2005a). Numerous studies so far have shown that there is a positive correlation between the regions of coseismic stress increase inside and around the source due to a large earthquake and the increment of subsequent seismicity inside these regions (e.g. Reasenber and Simpson, 1992; King et al,

1994; Deng and Sykes, 1997; Stein et al, 1997; Harris, 1998, Stein, 1999). Some of these studies also suggested possible triggering of a large earthquake due to previous events with similar magnitudes. It has additionally been suggested that stress increases as small as 0.1 bars could influence subsequent seismicity in the surrounding region of a ruptured fault (e.g. Deng and Sykes 1997; Stein 1999). In this study, we assume an increment in the Coulomb stress of 0.25 bars to have an effective influence on subsequent events.

For the Mexican subduction zone, possible stress interactions between large interplate thrust and in-slab normal-faulting earthquakes have been discussed (Mikumo et al., 1999, 2002). Mikumo et al. (1998) also estimated coseismic stress change during several large thrust earthquakes in this zone and discussed their possible relationship, but their calculations were limited to the shear stress change inside the fault area.

In the present paper, we conduct a more comprehensive analysis using the Coulomb failure stress criterion for a sequence of large interplate thrust earthquakes ( $M_w > 7.3$ ) that occurred on the Cocos plate during 1973 to 1986 and on the Rivera plate during 1995 to 2003 to investigate if there is any stress interaction in the lateral direction between these large events. We also estimate the effects from viscoelastic relaxation process and plate convergence.

## **DATA AND METHOD**

We estimated the stress change produced by a sequence of seven large ( $M_w > 7.3$ ) thrust earthquakes on the plate interface between the subducting Cocos and Rivera plates and the North America plate. The convergence rate of the Cocos plate relative to the North America plate is about 5.2 cm/year in the northwestern section, while it is about 2.5 cm/year for the Rivera plate (DeMets and Wilson, 1997). The boundary between the two plates is uncertain, but it seems to be somewhere near the El Gordo Graben (EGG) (DeMets and Wilson, 1997). Since these two oceanic plates have different convergence rates and directions of motion, we separated our analysis in two parts: one for the five events that occurred on the Cocos plate, and another for the two events that occurred on the Rivera plate. The source parameters for these events, as well as the work we referred to for the slip distribution are shown in Table 1.

We computed the coseismic Coulomb failure stress change ( $\Delta\text{CFS}$ ) inside and in the vicinity of the fault area on the plate interface from the slip distribution for each event. The change in the Coulomb failure stress is obtained from the relation  $\Delta\text{CFS}=\Delta\tau + \mu'\Delta\sigma_n$  (e.g. Harris, 1998), where  $\Delta\tau$  is the shear stress change in the direction of the fault slip,  $\Delta\sigma_n$  is the change in the tensional stress normal to the fault plane, and  $\mu'$  is an apparent coefficient of friction  $\mu' =\mu (1-p)$ ,  $\mu$  is the static coefficient of friction and “p” is the pore pressure in the source volume.

All these stresses were calculated in a tensorial way for a 3D model using the formulations given by Okada (1985, 1992). In this calculation, we refer to the fault dimension assigned in the kinematic waveform inversion with a size of divided subfaults of 5km x 5km for all the earthquakes. In the computations, we assumed a mean shear modulus of  $\mu=3.5\times 10^{11}$  dyn/cm<sup>2</sup>, and a Poisson ratio of  $\nu=0.25$  for the region. For the apparent coefficient of friction, we used the value of  $\mu'=0.4$  adopted by Mikumo et al., (1999; 2002) for the Mexican subduction zone. In the case of the 19/09/1985 Michoacan and 9/10/1995 Colima-Jalisco events, the inversion results yielded relatively high slips near the fault edges, which generate some edge effects in the stress distribution. In order to reduce these edge effects, we applied a cosine taper function of 2% over the total fault length and width in the two spatial directions.

As the focal parameters given in Table 1 are slightly different for each earthquake, we adopted in the computation of the  $\Delta\text{CFS}$  function a general value of the strike and dip angles based on the geometry of the Benioff zone of each subducting plate. For five earthquakes on the Cocos plate we used a strike value of  $\theta=290^\circ$  and for two earthquakes on the Rivera plate a strike value of  $\theta=300^\circ$ . We assigned a dip value of  $\delta=15^\circ$  and a rake value of  $\lambda=90^\circ$  for all the earthquakes. Based on the extent of the fault areas from the kinematic model dimensions of the studied earthquakes, we take a rectangular plate interface covering an area of 475km x 240m for the Cocos plate, and for the Rivera plate we take an area of 390km x 240km. In both cases we used a mesh size of 2.0km x 2.0km for the location of the computation points.

To account for the contribution from each earthquake to the total state of stress on the plate interface, we summed up the calculated stress due to each earthquake, setting the state of stress before the first event in the sequence on each plate to be zero. The relative locations

between the events studied here were based on their epicentral locations. Finally, the state of stress over the fault interface is presented in a cumulative way as a function of time. The possible effects from postseismic stress change will be discussed in the last section.

## RESULTS

### Cocos plate

In Figure 2a we present the change of  $\Delta\text{CFS}$  over the plate interface due to the Colima earthquake of 30/01/1973 ( $M_w=7.6$ ). The epicenter of this earthquake is denoted by a yellow circle, and the epicenter of the next event in the sequence is denoted by a black star in a yellow circle. Red contours show the zones of stress increase and blue ones indicate the zones of stress drop. This event ruptured two main asperities, one on the southeastern section of the fault with a maximum stress drop of -45 bars, and another one on the northwestern section of the fault with a maximum stress drop of -37 bars. The maximum stress increase of 19 bars occurred between these two asperities about 60 km southeast of the epicenter. Here it can be observed that the epicenter of the next large earthquake (Petatlán 1979) falls approximately 130 km to the southeastern edge of the fault zone, and far outside the 0.25 bar contour due to the 1973 earthquake. This indicates that the occurrence of the 1979 event was hardly affected by the 1973 event.

The next earthquake in the sequence is the Petatlán earthquake of 14/03/1979,  $M_w=7.6$  (Figure 2b). This event had two main asperities, with a maximum stress drop of -12 bars located 30 km southeast of its epicenter. It can now be observed that the 0.25 bar-contour from this event reaches the contour of the same value due to the previous 1973 event. Here the epicenter of the third event in the sequence (Playa Azul, 1981) falls in between these two contours. This suggests possible stress interaction from the 1973 and 1979 events, and possible triggering effects on the occurrence of the 1981 earthquake.

The Playa Azul earthquake of 25/10/1981 is the third and smallest earthquake in the sequence ( $M_w=7.4$ ), but produced the highest stress drop and stress increase (Figure 2c). It had two asperities, one on the northern side of the epicenter and the other on the southern side. The maximum stress decrease of  $\Delta\text{CFS}$  occurred on the northern asperity with a value of -180 bars

and the maximum stress increase occurred on its north side, with a value of 55 bars. These high values are mostly due to large slips (~350 cm) concentrated on a relatively small area in this asperity. Because of its location between the previous two events, this earthquake has a strong positive influence on its adjacent zones, increasing the state of stress of the southeastern asperity of the 1973 earthquake as well as the northwestern side of the 1979 fault. The epicenter of the 1985 Michoacan earthquake ( $M_w=8.1$ ) is located inside the zone of increased stress due to the 1973 and 1981 events, and near the edge of the southeastern asperity of the 1973 event. The 1985 great earthquake could have been effectively affected by the 1973 and 1981 events.

The great 1985 Michoacan earthquake (19/09/1985) with a moment magnitude of  $M_w=8.1$  is the largest and most damaging earthquake in the sequence, leaving more than 20,000 deaths (García Acosta, 2001). As we mentioned above, this earthquake could have been affected by the stress increase due to the 1973 and 1981 earthquakes. This event ruptured two main asperities and one large patch, where the largest asperity occurred just to the southeast of the epicenter. This asperity produced a maximum stress drop of -120 bars, and a maximum stress increase of 23 bars. This event effectively affects the areas of stress influence from the three previous events. The combined stress changes due to these four events produced different spots of stress increase especially near the epicentral region of the 1981 Playa Azul earthquake, where the stress increase reaches a positive value of 83 bars.

The following event in the sequence on the Cocos plate is the Zihuatanejo earthquake of 21/09/1985 ( $M_w=7.6$ ). The epicenter of this event is located near a zone of stress increase but appears to be inside a zone of stress drop. However, there could be a small mislocation of the epicenter of this event, or inherent uncertainties in the slip distribution in the previous 1985 event.

A large aftershock ( $M_w=7.1$ ) to the 1985 event occurred on 30/04/1986. Its epicenter is located in the ruptured area of the 1985 event ( $18.42^\circ\text{N}$ ,  $-102.99^\circ\text{E}$ ) inside a positive 1.0 bar-contour, which also suggests a possible triggering effect on this aftershock.

## **Rivera Plate.**

This plate had generated two successive large earthquakes (3/06/1932,  $M_w=8.2$  and 18/06/1932  $M_w=7.8$ ) in the first half of the past century (Singh, et al., 1985). It seems unlikely, however, that these events more than 70 years ago provided a direct stress influence to the present seismicity (It is difficult to define an earthquake cycle in this context. I think we can leave the paragraph as it is).

The first event analyzed here is the 9/10/1995 Colima-Jalisco ( $M_w=8.0$ ) earthquake. As in the previous analysis, we set the state of stress before this event to be zero. As shown in Figure 3a, this event ruptured three main asperities; one is located on the epicentral zone and the other two on the northwest side of the epicenter, very close to the Middle America trench. The maximum stress drop of -170 bars occurred inside the largest asperity on the northwestern edge of the fault, and the second largest stress drop of -155 bars occurred on the southeastern asperity. The largest stress increase due to this earthquake is located in between the second largest and the epicentral asperities, with a maximum value of 17 bars. The next event in this sequence (Tecomán, 2003), whose epicenter is shown by a black star in a yellow circle, falls clearly inside the zone of positive stress change produced by the 1995 earthquake, in the southeastern side of its fault within a 1.0 bar contour. In this case it seems clear that the zone of stress increase due to the 1995 event provided a triggering effect on the 2003 event.

The next event in this sequence is the 22/01/2003 Tecomán ( $M_w=7.5$ ) earthquake (Figure 3b). This event ruptured two main asperities and produced a maximum stress drop of -65 bars and a maximum stress increase of about 20 bars. Here, the combined stress change due to these two events produced a relatively high stress increase zone between the two epicenters with a maximum value of 37 bars. This last event appears to have occurred in part of the Graben "El Gordo", where the occurrence of large earthquakes was unknown until this earthquake.

As can be observed in Figures 2d and 3b, the stress change due to the two events on the Rivera plate could have some effect on a possible future event on the Cocos plate; also, the stress increase due to the 1973 and 1985 events on the Cocos plate could affect the sequence of earthquakes on the Rivera plate. These observations, however, should be taken with some care

due to the uncertainties of the limits between these two oceanic plates and their related tectonic environments.

### **Postseismic stress change**

The above discussion is based entirely on the coseismic change of Coulomb failure stress. Under more realistic environments, however, there should be postseismic stress change caused by some time dependent tectonic processes. The main factors that could affect the coseismic change on the plate interface may be viscoelastic relaxation process in the lower mantle and in the asthenosphere underlying the subducting slab, and also tectonic loading of stress due to plate convergence, if postseismic slow slip did not occur on the ruptured fault. We estimate these two major effects by applying the method described by Mikumo et al. (2002) to a simplified, elliptical-shaped slip model depicted in Santoyo et al. (2005a).

To do this, we use a 3D finite-difference numerical model, which incorporates a subducting slab (with a thickness of 50 km) embedded in a horizontally-layered velocity and viscoelastic structure. The parameters assigned here are essentially the same as given in Table 1a in Mikumo et al. (2002), but we assume various Newtonian viscosities  $\eta$  and hence the corresponding Maxwellian relaxation times  $\tau$  ranging from  $\eta \sim 1 \times 10^{19}$  to  $1 \times 10^{17}$  Pa s ( $\tau \sim 10$  to 0.1 yrs) in the lower mantle and the asthenosphere. We also tested two cases with a thin dipping, low-viscosity layer either underlying or overlying the upper surface of the subducting slab. All these calculations are also tested for a half-space model of Okada (1992) incorporating the above viscoelastic structure. The time range taken here is up to 15 yrs after an earthquake, since we are interested in the time periods between 1973 and 1986 in the Cocos plate and between 1995 and 2003 in the Rivera plate subduction zones. The results show that viscoelastic stress change does not exceed  $-10\%$  in the first 5 yrs and  $-18\%$  up to the 10 yrs for a reasonable range ( $\tau > 1$  yr) of relaxation time. If the thin low-viscosity layer actually existed, the decrease could reach about  $-30\%$  and as much as  $-53\%$  during the 5 and 10 yrs, respectively. However, the viscoelastic effect reduces the absolute values of coseismic stress change, both positive and negative, and would not significantly change the overall stress patterns shown in Figures 2 and 3.



On the other hand, the tectonic loading effect on the coseismic stress change on the upper plate interface can be estimated by assigning a virtual backslip  $-vt$  on the ruptured interface, (Mikumo et al., 2002), where  $v$  is the rate of plate convergence. For the subduction zones of the Cocos and Rivera plates,  $v$  is taken as 5 cm/yr and 2 cm/yr, respectively. The calculation shows that the effect compensates the viscoelastic change by 2 % at most during the 10 yrs and hence may be omitted.

## DISCUSSION

It is to be noted that the present viscoelastic relaxation model did not yield substantial, lateral stress diffusion on the plate interface along the subduction zone. This appears consistent with a recent result from 3D finite-element viscoelastic models dealing with possible lateral propagation of a slow slip event (A. Shiraishi, personal communication, 2005). The possible existence of lateral stress diffusion has been suggested (Anderson, 1975), and actually demonstrated (e.g. Rice, 1980; Lehner et al., 1981) for plane stress deformation in an elastic lithosphere overlying a viscoelastic asthenosphere. The difference between the latter calculations and our results might come from some yet to be defined difference in the direction of applied stress with respect to the assumed fault geometry or in the depth variation of elastic and viscoelastic properties.

In the present study, it was found that the rupture starting point of a subsequent event, except possibly the 1985 Zihuatanejo event, is located in the zone of stress increase due to its previous event. There is a possibility, however, that there could be inherent small uncertainties in the relative epicentral location of two events. Another problem is some intrinsic resolution uncertainties in the slip distributions. It is to be mentioned that in the kinematic inversions, mostly limited to wave frequencies lower than 0.5 Hz, the spatial resolution of the slip may be between 5 or 6 km for rupture velocities ranging between 2.5 to 3.0 km/sec.

Although these uncertainties remain, the spatio-temporal clustering of large earthquakes in this subduction zone may be mainly accounted for by coseismic stress increase due to the preceding events that occurred in adjacent segments. In this case, the relatively short time

interval between these large events may depend on small differences between the current state of stress at a given time and the frictional strength on specific segments of the plate interface. The current stress includes the ambient tectonic stress level and its coseismic and postseismic stress changes, which are heterogeneous. On the other hand, the frictional strength could also be spatially heterogeneous, depending on the roughness of the interface, the lithospheric environment (including temperature, pore pressure, humidity, etc.), and also on other time dependent factors (e.g. Kato, 2004). This is similar to the stress corrosion mechanism often experienced in laboratory experiments (e.g. Anderson and Grew, 1977). It is probable that if any segment on the plate interface received coseismic stress increase from its adjacent segments, then they could be ruptured during a relatively short time interval. Thus, the coseismic stress change may play an important role in the triggering of large earthquakes in adjacent zones.

We have investigated the possibility of lateral stress interactions along the Mexican subduction zone, in a sequence of large interplate earthquakes ( $M_w > 7.3$ ) that occurred during 13 yrs on the Cocos plate and during 8 yrs on the Rivera plate. For this purpose, the spatial variations of the Coulomb failure stress resulting from these events have been calculated over extensive areas on the plate interfaces, based on the slip distribution obtained from previous waveform inversion for the corresponding earthquake. Possible maximum effects from viscoelastic relaxation in the lower mantle and asthenosphere have also been estimated.

It was found that the rupture starting point of a subsequent event, except possibly the case of the 1985 Zihuatanejo event, is located in the zone of stress increase due to its previous event. The effects from the viscoelastic relaxation were found to be quite small and did not yield significant lateral stress diffusion along the plate boundary. In conclusion, the spatio-temporal clustering of the large interplate earthquakes in this subduction zone may possibly be explained by lateral stress interactions due to previous earthquakes located in the adjacent segments on the plate interface.

## REFERENCES.

Anderson, D.L. (1975). Accelerated plate tectonics, *Science* **187**, 1077-1079

Anderson , O.L and P.C. Grew (1977). Stress corrosion theory of crack propagation with application to geophysics. *Rev Geophys.*, **15**, 77-105.

DeMets, C., and D. S. Wilson (1997). Relative motions of the Pacific, Rivera, North American, and Cocos plates since 0.78 Ma, *J. Geophys. Res.* **102**, 2789– 2806.

Deng J, and L.R. Sykes (1997). Evolution of the stress field in southern California and triggering of moderate-size earthquakes: A 200-year perspective, *J. Geophys. Res.* **102**, 9859-9886.

García-Acosta, V. (2001). Los sismos en la historia de México. Vol. II. *C.I.E.S.A.S.-U.N.A.M.*; Ed. Fondo de Cultura Económica.

Harris, R. (1998). Introduction to special section: stress triggers, stress shadows, and implications for seismic hazards, *J. Geophys. Res.* **103**, 24347-24358.

Kato, N. (2004). Interaction of slip on asperities: Numerical simulation of seismic cycles on a two-dimensional planar fault with nonuniform frictional property, *J. Geophys. Res.*, **109**, B12306.

King, G.C.P., R.S. Stein, and J.Lin (1994). Static stress changes and the triggering of earthquakes, *Bull. Seism. Soc. Am.* **84**, 935-953,.

Lehner, F.K., V.C. li, and J.R. Rice (1981). Stress diffusion along rupturing plate boundaries. *J. Geophys. Res.*, **86**, 6155-6169.

Mendoza (1993). Coseismic slip of two large Mexican earthquakes from teleseismic body waveforms: Implications for asperity interaction in the Michoacan plate boundary segment. *J. Geophys. Res.*, **98**, 8197-8210.

Mendoza (1995). Finite fault analysis of the 1979 March 14, Petatlan, Mexico earthquake using teleseismic P waveforms. *Geophys. J. Int.*, **121**, 675-683.

Mendoza and Hartzell (1989). Slip distribution of the 19 september 1985 Michoacan, Mexico, earthquake: Near source and teleseismic constraints. *Bull. Seism. Soc. Am.* **79**, 655-669.

Mendoza and Hartzell (1997). Fault slip distribution of the 1995 Colima-Jalisco, Mexico, earthquake. *Bull. Seism. Soc. Am.*, **89**, 1338-1344.

Mikumo, T., T. Miyatake and M.A. Santoyo (1998). Dynamic rupture of asperities and stress change during a sequence of large interplate earthquakes in the Mexican subduction zone. *Bull. Seism. Soc. Am.* **88**, 686-702.

Mikumo T., S. K. Singh and M.A. Santoyo (1999). A possible stress interaction between large thrust and normal faulting earthquakes in the mexican subduction zone, *Bull. Seism. Soc. Am.* **89**, 1418-1427.

Mikumo, T, Y. Yagi, S.K. Singh, and M.A. Santoyo (2002). Coseismic and postseismic stress changes in a subducting plate: Possible stress interactions between large interplate thrust and intraplate normal-faulting earthquakes, *J. Geophys. Res.* **107**, ESE5-1-ESE5-12.

Nishenko, S.P. and S.K. Singh (1987). Conditional probabilities for the recurrence of large and great interplate earthquakes along the Mexican subduction zone, *Bull. Seism. Soc. Am.* **77**, 2095-2114.

Okada, Y. (1985). Surface deformation due to shear and tensile faults in a half space, *Bull. Seism. Soc. Am.* **75**, 1135-1154.

Okada, Y. (1992). Internal deformation due to shear and tensile faults in a half space, *Bull. Seism. Soc. Am.* **82**, 1018-1040.

Reasenber P.A. and R.W. Simpson (1992). Response of regional seismicity to the static stress change produced by the Loma Prieta Earthquake, *Science* **255**, 1687-1690.

Rice, J.R. (1980). The mechanics of earthquake rupture, in *Physics of the earth's interior*, edited by A.M. Dziewonski and E. Boschi, pp. 555-649, Italian Physical Society/North Holland, Amsterdam.

Santoyo, M. A., S.K. Singh, T. Mikumo and M. Ordaz (2005a). Space-time clustering of large thrust earthquakes along the Mexican subduction zone: an evidence of source stress interaction. *Bull. Seism. Soc. Am.* (In press)

Santoyo M.A., T. Mikumo, and Luis Quintanar (2005b). Finite fault analysis and associated coseismic stress change of the 30 January, 1973 (Mw=7.6), Colima, Mexico earthquake, using teleseismic data. *Submitted to Geofisica Internacional.*

Shiraishi, A. (2005) personal communication,.

Singh, S.K., L. Astiz, and J. Havskov (1981). Seismic gaps and recurrence periods of large earthquake along the Mexican subduction zone: a reexamination, *Bull. Seism. Soc. Am.* **71**, 827-843.

Singh, S.K., L. Ponce and S. P. Nishenko (1985). The great Jalisco, Mexico, earthquakes of 1932: Subduction of the rivera plate, *Bull. Seism. Soc. Am.* **75**, 1301-1313.

Stein, R.S., A. Barka, and J. Dieterich (1997). Progressive failure of the north Anatolian fault since 1939 by earthquake stress triggering, *Geophys. J. Int.* **128**, 594-604.

Stein, S. (1999). The role of stress transfer in earthquake occurrence, *Nature*, 402, 605-609.

Ward S.N. (1992) An application of synthetic seismicity calculations in earthquake statistics: The middle America trench, *J.Geophys.Res.*, 97,6675-6682.

Yagi, Y., T. Mikumo, J. Pacheco and G. Reyes (2004). Source rupture process of the Tecomán, Colima, Mexico earthquake of 22 January 2003, determined by joint inversion of teleseismic body-wave and near-source data. *Bull. Seism. Soc. Am.*, 94, 1795-1807.

## **AUTHORS AFFILIATION**

Instituto de Geofísica  
Universidad Nacional Autónoma de México (UNAM)  
Circuito Insitutos s/n, Ciudad Universitaria  
Coyoacán, 04510  
México, D.F., México.  
(M.A.S., T.M.)

Centro de Geociencias, UNAM.  
Universidad Nacional Autónoma de México (UNAM)  
Campus Juriquilla 76230,  
Querétaro, México.  
(C.M.)

TABLE 1  
SOURCE PARAMETERS FOR THE EARTHQUAKES STUDIED.

No.	Earthquake	Date(D,M,Y)	Lat( $^{\circ}$ N) <sup>§</sup>	Lon( $^{\circ}$ E) <sup>§</sup>	Mw	Mech. ( $\theta$ , $\delta$ , $\lambda$ )	P.I.*	Ref <sup>†</sup>
1	Colima	30/01/1973	18.39	-103.21	7.6	305 $^{\circ}$ ,16 $^{\circ}$ ,93 $^{\circ}$	C	$\alpha$
2	Petalán	14/03/1979	17.46	-101.46	7.6	293 $^{\circ}$ ,15 $^{\circ}$ ,105 $^{\circ}$	C	$\beta$
3	Playa Azul	25/10/1981	17.75	-102.25	7.4	287 $^{\circ}$ ,20 $^{\circ}$ ,82 $^{\circ}$	C	$\gamma$
4	Michoacan	19/09/1985	18.14	-102.71	8.1	300 $^{\circ}$ ,14 $^{\circ}$ ,89 $^{\circ}$	C	$\delta$
5	Zibuatanejo	21/09/1985	17.62	-101.82	7.6	296 $^{\circ}$ ,17 $^{\circ}$ ,85 $^{\circ}$	C	$\gamma$
6	Aftershock <sup>¶</sup>	30/04//1986	18.42	-102.99	7.1	290 $^{\circ}$ ,18 $^{\circ}$ ,87 $^{\circ}$	C	—
7	Colima-Jalisco	09/10/1995	18.84	-104.58	8.0	309 $^{\circ}$ ,14 $^{\circ}$ ,92 $^{\circ}$	R	$\epsilon$
8	Tecomán	22/01/2003	18.71	-104.13	7.5	300 $^{\circ}$ ,20 $^{\circ}$ ,93 $^{\circ}$	R	$\zeta$

Notes: §Locations are taken from references shown above except for event 6 which is from Singh and Mortera, (1991); Lat=Latitude North, Lon=Longitude East. Mw=Moment magnitude. Mech=Focal mechanism ( $\theta$ =Strike,  $\delta$ =Dip,  $\lambda$ =rake) from references shown above in the last column, except event 6 from CMT Harvard. \*P.I.= Plate Interface, where C=Cocos, R=Rivera. †References for slip distributions:  $\alpha$ . Santoyo, et al., (2005b);  $\beta$ . Mendoza, (1995);  $\gamma$ . Mendoza, (1993);  $\delta$ . Mendoza and Hartzell, (1989);  $\epsilon$ . Mendoza and Hartzell, (1997);  $\zeta$ . Yagi, et al., (2004). ¶ Michoacan 19/09/1985 aftershock.

## FIGURE CAPTIONS.

Figure 1. Tectonic map of Mexico. NORTH AMERICA=North American Plate; RIVERA=Rivera Plate; PACIFIC=Pacific Plate; COCOS=Cocos Plate; TFZ=Tamayo Fracture Zone; RFZ=Rivera Fracture Zone; EPR=East Pacific Rise; EGG=El Gordo Graben; MAT= Middle American Trench; OFZ= Orozco Fracture Zone; OGFZ= O’Gorman Fracture Zone; TMVB= Trans Mexican Volcanic Belt. Numbers above arrows indicate the relative rate of convergence. The blue rectangle shows the study area for events that occurred on Cocos Plate, which are shown in Figures 2a-2e. Green rectangle shows the study area for events that occurred on Rivera Plate, which are shown in Figures 3a and 3b. The rectangle sizes and scales are both equal to allow a direct comparison between the results shown in Figures 2 and 3.

Figure 2. Coseismic Coulomb stress changes in the Cocos plate, due to the sequence of earthquakes between 1973 and 1985 studied in this work. Results are presented as a function of time. Blue zones denote stress drops and red zones denote stress increases following the color scale shown in the bottom of the figure. Yellow dots indicate the epicentral location of the earthquake shown in the figure. The time of its occurrence is shown at the upper-right side of each figure (see Table 1 for details of each earthquake). Yellow dots with a black star show the epicentral location of the next earthquake of the sequence. Tectonic features are the same as described in Figure 1. For details of the source characteristics of each earthquake, see Table 1. Stress changes in the scale are shown in bars. a) Coseismic Coulomb stress change associated with the 1973 Colima earthquake. b) Coulomb stress evolution after the occurrence of the 1979 Petatlán earthquake. c) State of the stress up to the occurrence of the 1981 Playa Azul earthquake. d) Stress changes after the great 1985 Míchoacan earthquake. e) Final state of stress in this sequence after the 1985 Zihuatanejo earthquake. Note that the epicenter of the 1986 aftershock is located in the stress increase zone due to the summed effects of the four previous events.



Figure 3. Coseismic Coulomb stress changes in the Rivera plate, due to the sequence of earthquakes between 1995 and 2003 studied in this work. Figure notes are the same as for Figure 2. a) Coseismic Coulomb stress change due to the 1995 Colima-Jalisco earthquake. b) State of stress after the occurrence of the 2003 Tecomán earthquake

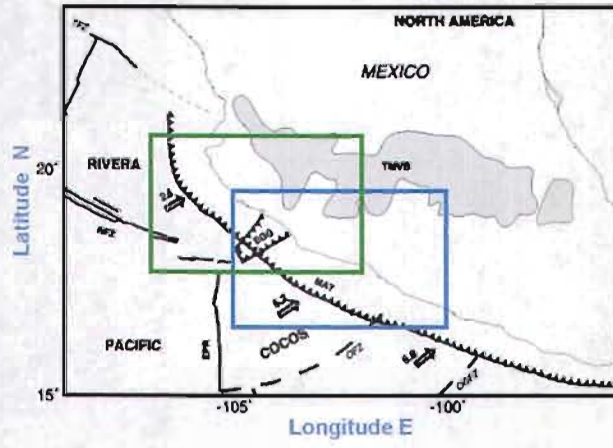


Figure 1

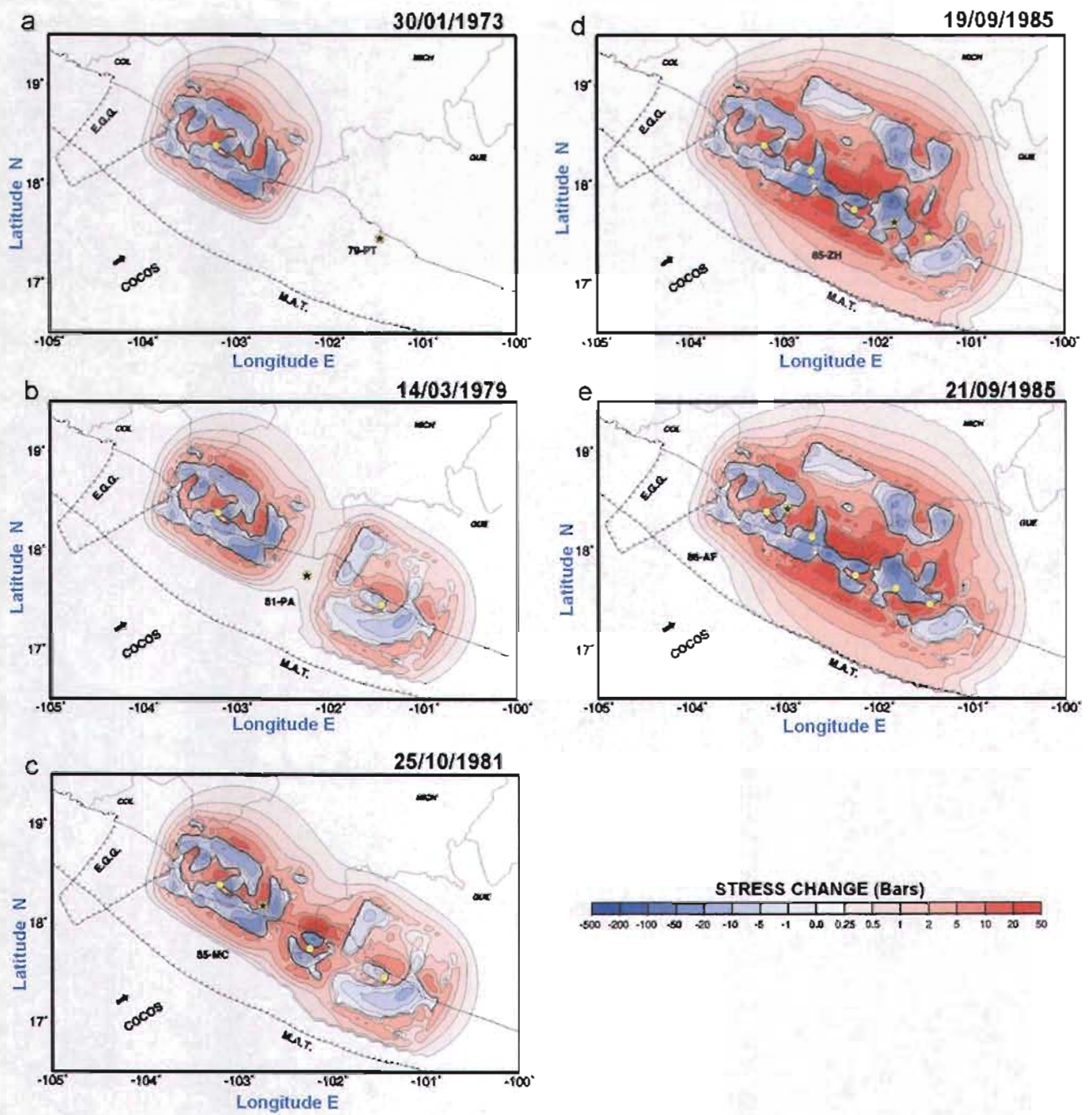


Figure 2

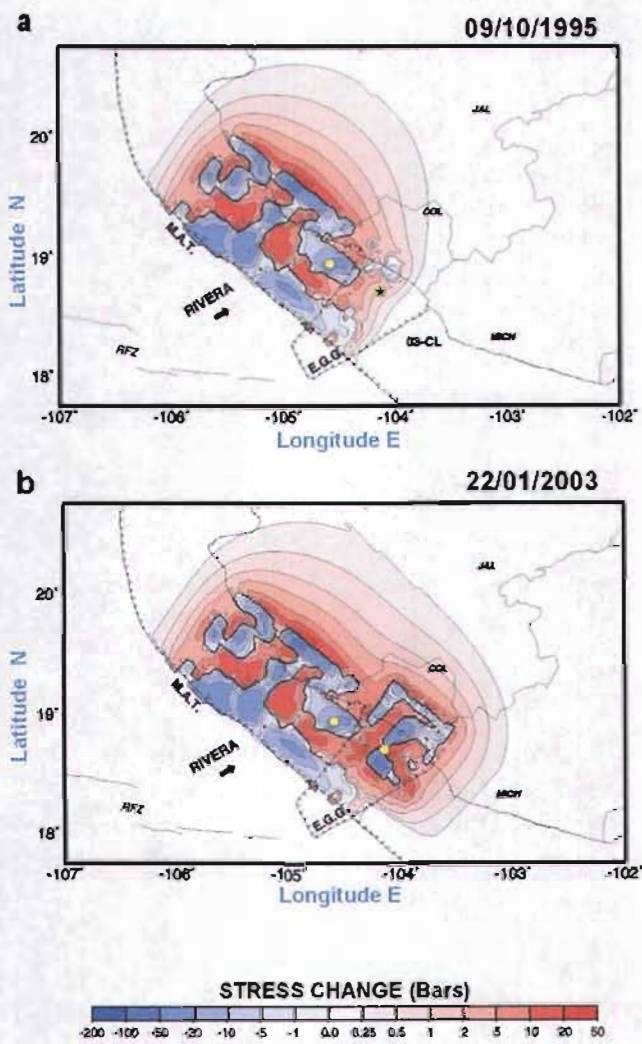


Figure 3

## Capítulo III

PROCESO DE FALLA Y SU CAMBIO DE ESFUERZOS COSÍMICOS ASOCIADO DURANTE EL SISMO INTERPLACA DEL 30 DE ENERO DE 1973, COLIMA, MÉXICO (MW=7.6).

**Faulting process and its associated coseismic stress change during the 30 January, 1973, Colima, Mexico interplate earthquake (Mw=7.6).**

*By Miguel A. Santoyo, Takeshi Mikumo and Luis Quintanar*

**ABSTRACT.**

A large thrust subduction earthquake (Mw=7.6) occurred on January 30, 1973, on the plate interface between the subducting oceanic Cocos plate and the continental North America plate. This event appears to have occurred close to a tectonic triple junction between the North America, Cocos and Rivera Plates, and might be related to two sequences of subsequent large earthquakes that occurred around this region. Although several authors have analyzed the focal mechanism and depth of this earthquake, we analyzed its point source characteristics and performed a linear kinematic waveform inversion for the slip distribution over the fault plane. Our results show a shallow thrust mechanism (St=285°, Dip=16°, Ra=85°), consistent with the tectonic environment in the region, with a hypocenter depth of 16 km and a total moment release of  $2.98 \times 10^{27}$  dyn-cm. The results also show a slip distribution with two main patches, with a maximum dislocation of 199cm and 173cm respectively. Based on these results, we calculated the associated coseismic stress change, and estimated the spatial extent of the possible lateral stress influence on the subsequent seismicity. The coseismic stress change shows that this earthquake ruptured two main asperities one downdip and southwest and the other updip and northwest of the hypocenter with a stress change of -31 and -40 bars. The extent of the surrounding zone of stress increase could have influence on the subsequent seismicity up to 120 km from the hypocenter.

**INTRODUCTION**

The northwestern portion of the Mexican subduction zone constitutes a rather complicated tectonic region, which is characterized by high seismic activity directly related with the subduction of the Rivera and Cocos oceanic plates under the North America plate (Figure 1). The Rivera plate is a relatively small plate with a convergence rate of 2.5 cm/year relative to North America (DeMets, et al., 1994), which had produced some of the greatest earthquakes in the last century, i.e. the 3/06/1932, Ms=8.2 and 18/06/1932, Ms=7.6, Jalisco earthquakes

(Singh et al., 1985) and the 9/10/1995, Mw=8.0, Colima-Jalisco earthquake (e.g. Pacheco et al, 1997). Although the southeastern edge of this plate is uncertain, this may be limited by a triple junction near El Gordo Graben (EGG), which could also limit the Cocos plate (Figure 1) (Kostoglodov and Bandy, 1995). The Cocos plate, on the other hand, has larger convergence rates with respect to North America than the Rivera plate, which ranges between 5.2 cm/year near its northwest edge (Figure 1), to 8.2 cm/year near the Tehuantepec ridge at the southeastern portion of the Mexican subduction zone (DeMets, et al., 1997). The subduction of the Cocos plate is also responsible for large and great thrust earthquakes (e.g. the 29/11/1978, Mw=7.8, Oaxaca earthquake and the 19/09/1985, Mw=8.1, Michoacan earthquake) (e.g. Singh and Mortera, 1991), and also for large normal-faulting events (e.g. the 11/1/1997, Mw=7.1, Arteaga earthquake and the 30/09/1999, Mw=7.5, Oaxaca event) (e.g. Santoyo et al, 2005a, Singh et al , 2000).

Recent studies have revealed the possibility of stress interaction between large-thrust and inslab normal-faulting earthquakes (e.g. Mikumo *et al.*, 1999; Mikumo *et al.*, 2002), and also among large-thrust interplate events in this subduction zone (e.g. Mikumo *et al.*, 1998; Santoyo *et al.*, 2005b). In order to discuss a seismic recurrence cycle and the associated seismic hazard in Mexico, a detailed study of large earthquakes and their postseismic activity has become indispensable.

The 30 January 1973 (Mw=7.6) earthquake is a low-angle thrust event that ruptured the interface between the North-America plate and the northwestern edge of Cocos plate. Its epicenter (-103.21°E, 18.39°N; Lomnitz, 1977) located inland is close to the EGG and the diffuse triple junction near the Rivera plate (Figure 1). Six subsequent major seismic events, two of them located northwest (the 9/10/1995 Colima-Jalisco and 22/01/2003 Tecomán earthquakes; Santoyo et al, 2005b), and another four located southeast (the 25/10/1981 Playa Azul, 19/09/1985 Michoacan, 21/09/1985 Zihuatanejo and 14/03/1979 Petatlán earthquakes; Santoyo et al., 2005b), have been studied by different authors from a finite fault point of view (Figure 2). A detailed study of the source and its associated coseismic stress change of the 1973 event, becomes essential to look for a possible spatial and temporal relation between

these two large seismic sequences and to improve our knowledge of the seismicity and the state of stress in the region.

Several authors have studied different point source characteristics of this earthquake. Lomnitz (1977) located the mainshock epicenter with the aid of a distance residual algorithm, using the P arrival times recorded at 254 local and teleseismic stations. His results show a location error of less than 5 km for the epicenter ( $-103.21^{\circ}\text{E}$ ,  $18.39^{\circ}\text{N}$ ) with a source depth of 32 km. Reyes *et al.* (1979) obtained a focal mechanism solution (strike= $330^{\circ}$ , dip= $30^{\circ}$ , rake= $65^{\circ}$ ) for a source depth of 35 km, based on the P wave polarities in regional and teleseismic recordings. They also studied the epicentral distribution of 2 weeks aftershock activity, and concluded that the earthquake most probably occurred on the interface between the Cocos and North America plates. Chael and Stewart (1982) also studied the source properties and obtained a different solution (strike= $266^{\circ}$ , dip= $17^{\circ}$ , rake= $55^{\circ}$ ) with a source depth of 20 km. They suggest a complex source process because of the complexity of the teleseismic time histories. Singh and Mortera (1991), using the seismograms from station DBN (DeBilt, Holland), obtained a rather complex source time function composed of several subevents, all located at a shallow depth of 8 km. They mention, however, that this result appears somehow strange in contrast to neighboring events, especially the 15/04/41 earthquake where the source time function is much simpler than for the 1973 event. Pardo and Suarez (1993) described the geometry of the Benioff zone in the region, finding that the angle of plate subduction changes from  $8^{\circ}$  near the trench to about  $30^{\circ}$ , 300 km away from the trench. Their finding suggests that the dip of the interface at the location of the 1973 event is of about  $17^{\circ}$  at a depth of 21 km. Finally, based on the mechanism obtained by Chael and Stewart, Quintanar (1991) obtained a spatial distribution of the seismic moment release using an iterative inversion method proposed by Kikuchi and Kanamori (1982) and later extended by Kikuchi and Fukao (1985). From this distribution, he found a main patch downdip from the epicenter and two other patches southeast and northwest of the nucleation point.

The objective of this work is to obtain more reliable focal information, to perform a detailed finite fault inversion for the spatial distribution of slip, and to compute the associated



coseismic stress change over the plate interface. To do this, we based our analysis on teleseismic P waveform seismograms, recorded at 8 WWSSN stations.

## DATA

We examined the LPZ P waveform arrivals recorded on 8 WWSSN digitized analog seismograms, with a sampling interval of 0.5 sec. Only teleseismic stations located between 30° and 90° were considered, in order to avoid the distorted P waves that propagate inside the earth's upper mantle and through the earth's outer core respectively. These stations are listed in Table 1, and as it can be seen here, they have a good azimuthal coverage.

TABLE 1  
Data for stations used in this study

St. <sup>*</sup>	Az. <sup>#</sup>	Dist. <sup>&amp;</sup>	B.Az. <sup>%</sup>
AFI	249.50	74.80	66.36
AKU	25.80	71.42	273.38
ARE	136.03	46.61	316.59
ESK	34.79	80.64	288.58
KIP	283.07	51.41	83.17
LPB	132.99	48.96	313.59
SOM	159.59	76.72	326.96
STU	37.68	90.32	298.65

Notes: \* St.=Station name; # Az.=Azimuth from epicenter; & Dist.= Distance from epicenter; B.Az.= Back azimuth from station to epicenter.

The recordings were corrected for the instrumental response, filtered with a three-pole low-pass butterworth filter ( $f_c=0.3\text{Hz}$ ) and integrated into the displacement time histories.

## POINT SOURCE CHARACTERISTICS

As described before, different focal mechanisms and depths have been obtained from previous studies for this earthquake. As a first step, we performed a point source inversion for the main focal properties and depth. To do this, we inverted the teleseismic displacement waveforms, using the Nábêlek's (1984) maximum-likelihood inversion technique. The crustal velocity model used for the source region is that adopted by Santoyo et al (2005a) for the Michoacan region (Table 2). A global crustal velocity model shown in Table 3 was used for the teleseismic receivers. Here we also included the attenuation parameter  $T^*$  of 1.0 second for P waves (Futterman, 1962).

TABLE 2.

Crustal velocity model for the source region			
$h^{\dagger}$ (km)	$\alpha^*$ (km/sec)	$\beta^{**}$ (km/sec)	$\rho^{\#}$ (gr/cm <sup>3</sup> )
0.0	5.3	3.35	2.50
4.0	6.0	3.45	2.76
15.0	6.5	3.80	2.84
35.0	7.4	4.27	2.90

Notes: †h= Depth of the upper interface; \*  $\alpha$ = P wave Velocity;  
 \*\*  $\beta$ = S wave velocity; #  $\rho$ = Density of the medium

TABLE 3.

Crustal velocity model for teleseismic receivers			
$h^{\dagger}$ (km)	$\alpha^*$ (km/sec)	$\beta^{**}$ (km/sec)	$\rho^{\#}$ (gr/cm <sup>3</sup> )
0.0	6.10	3.52	2.70
60.0	7.80	4.45	3.40

Notes: †h= Depth of the upper interface; \*  $\alpha$ = P wave Velocity;  
 \*\*  $\beta$ = S wave velocity; #  $\rho$ = Density of the medium.

To obtain the main focal characteristics, we first fixed the source depth at 20 km, and performed a linear inversion for the focal mechanism, source time function and total moment release. After the inversion, the focal mechanism solution obtained was found to be; strike=285°, dip=16° and rake=85°, a total moment release of  $2.98 \times 10^{27}$  dyn-cm, and a total duration of 26 sec for the source time function. In Figure 3 we show the solution, together with a comparison between the observed records (solid lines) and the synthetic seismograms (dashed lines). The focal mechanism and the relative location of the teleseismic stations are shown on the lower focal hemisphere. For the estimation of the best source depth we performed an RMS error analysis fixing the above parameters, computing the synthetic seismograms for different source depths, and comparing them with the observations. Figure 4 shows the results from this analysis where we obtained a minimum RMS error at a depth of 16.5 km.

## FAULTING PROCESS

Once the main point source characteristics were estimated, we performed a finite fault inversion for the slip distribution over the fault plane. The method of waveform inversion used in this study was originally developed by Hartzell and Heaton (1983) and has been applied successfully to several Mexican earthquakes (e.g. Mendoza and Hartzell, 1989; Mendoza, 1993, 1995; Courboux et al., 1997; Santoyo, et al., 2005a). For the inversion, we assumed that the fault plane is the interplate interface with a strike of 285° and a dip of 16° to the

northeast. Here, we assumed a fault area of 140 km by 80 km in the strike and dip directions respectively based on the aftershock distribution (Figure 2), and discretized it into 493 square subfaults of equal size (5km x 5km), which are embedded in the horizontally layered structure of Table 2. The hypocenter was located at the center of the fault plane (-103.21°E, 18.39°N) at a depth of 16 km. The fault dimension thus assumed covers the depths between 5 and 27 km.

Synthetic seismograms are then calculated for each pair of subfaults and teleseismic stations, applying the generalized ray theory proposed by Helmberger (1974) and Langston and Helmberger (1975) for teleseismic distances. The point source responses (Green's functions) are shifted by the time delay corresponding to the rupture propagation from the hypocenter. We assumed here a constant rupture velocity that implies circular rupture fronts centered at the nucleation point or the hypocenter. The responses of each subfault are calculated for a triangular source time function of a given duration (STFD), which was assumed the same for all the subfaults on the fault plane.

Based on this assumption, the observed data together with the synthetic seismograms form an over-determined linear system of the type  $\mathbf{AX} \approx \mathbf{B}$ . Here, the matrix  $\mathbf{A}$  contains the synthetic seismograms with its respective time shifting due to the rupture delay,  $\mathbf{B}$  is a vector with the observed records arranged in the same order as in the synthetics in matrix  $\mathbf{A}$ , and  $\mathbf{X}$  is the solution vector containing the dislocation weighting values which represent the amount of slip that must be applied to each subfault in order to fit the observations.

The matrix equation shown here can be solved by a simple least-squares technique; however, the solution could become unstable if matrix  $\mathbf{A}$  is ill-conditioned (Hartzell and Heaton, 1983). To solve this problem, the inversion was stabilized by a Householder decomposition of the matrix equations (Lawson and Hanson, 1974; Menke 1984), imposing a positivity constraint to the solution. To further stabilize the inversion, we appended, to the linear system, additional smoothing and moment-minimization constraints of the form  $\lambda \mathbf{FX} = \lambda \mathbf{D}$ , where  $\lambda$  is a scalar weighting factor. Smoothing is imposed by constructing  $\mathbf{F}$  and  $\mathbf{D}$  such that the difference between adjacent dislocations be zero. Moment minimization is obtained by letting  $\mathbf{F}$  be the

identity matrix and  $\mathbf{D}$  the zero vector, effectively reducing the length of  $\mathbf{X}$ . To identify the proper weighting factor  $\lambda$ , several inversion runs are conducted until the largest value of  $\lambda$  is reached that still allows the observed records to be fitted by the synthetic waveforms. In this case, spatial smoothness constraints are imposed to reduce some noise effects included in the solution, which could come from some unconsidered path effects or simplification of the velocity model.

For this inversion we used the velocity recordings instead of the displacement data at the 8 mentioned stations, mainly because these waveforms supply more information in high frequencies than the displacement seismograms, which allow us to obtain a better spatial resolution on the slip distribution.

To estimate the values of the STFD and rupture velocity that best fit the observations, we performed several inversion runs, varying the STFD between 2.0 sec and 3.0 sec and the rupture velocity between 2.5 km/sec and 3.5 km/sec. Due to the inherent trade-off between these two unknowns, the value for the STFD was obtained as a function of the rupture velocity to have a smooth rupture along the fault. After this analysis, we observed that a rupture velocity of 2.7 km/sec and a source time function duration of 2.5 sec for each subfault, produced a more coherent solution and better fit between the observed and synthetic seismograms.

In order to assure the reliability of the source depth already estimated, we also performed an additional RMS analysis for the source depth, based on the finite source inversion. In this case we computed the synthetic seismograms and performed several inversion runs for different depths of the fault plane. We show in Figure 5 the results from this analysis, having a minimum RMS error for a source depth of 17 km. From these results, we conclude that a source depth between 16 and 17 km is a reliable value.

The inversion results using the above parameters show the best agreement between the synthetic and observed velocity seismograms (Figure 6). The dislocation pattern is shown in Figure 7. Slips are shown in cm and the black star shows the hypocenter location on the fault

plane. The “x” axis represents the length in the horizontal (strike) direction and the “y” axis represents the width in the dip direction. From the slip distribution obtained, it can be observed that the rupture produced two main patches: One of them 20 km downdip from the hypocenter with a maximum slip of 199 cm, and the other one updip and southeast of the hypocenter, with a maximum slip of 173 cm. The total moment release obtained from this inversion is  $2.78 \times 10^{27}$  dyn-cm, with an overall source time function duration of 26 sec, and a roughly triangular shape with some high frequency small variations on the seismic moment release (Figure 8).

### **COULOMB FAILURE STRESS CHANGE**

The 30/01/1973 earthquake occurred under a relatively complex tectonic environment, where the subducting Cocos and Rivera plates subduct beneath the continental North America plate. This event may have some spatial relations to the two earthquake sequences that occurred a few tens of years later, one on the Rivera plate interface and the other one on the Cocos plate interface (Figures 1 and 2). To investigate this possible relation, we estimate the coseismic stress change inside the fault area of this earthquake, and also the spatial extent of the stress influence of this earthquake over the two plate interfaces.

Taking into account the final slip distribution, we calculated the coseismic change of the Coulomb failure stress function ( $\Delta CFS$ ) due to this earthquake. To do this, we computed the Coulomb failure stress from the relation  $\Delta CFS = \Delta\tau + \mu' \Delta\sigma_n$  (e.g. Harris, 1998), where  $\Delta\tau$  is the shear stress change in the direction of the fault slip,  $\Delta\sigma_n$  is the change in the tensional stress normal to the fault plane, and  $\mu'$  is an apparent coefficient of friction  $\mu' = \mu (1-p)$ , where  $\mu$  is the static coefficient of friction and  $p$  is the pore pressure in the source volume.

All these stresses were calculated in a tensorial way for a 3D model using the formulations given by Okada (1985, 1992). In the computations, we used the mean shear modulus for the site,  $\mu = 3.5 \times 10^{11}$  dyn/cm<sup>2</sup>, with a Poisson ratio of  $\nu = 0.25$ . For the tectonic apparent coefficient of friction, we used the value of  $\mu' = 0.4$  adopted by Mikumo et al. (2002) for the Mexican subduction zone. Based on the extent of the fault area of this earthquake we take, for the computation of the stress, a rectangular plate interface covering an area of 300 km by 275 km

on the strike and dip directions respectively. Here, we used a mesh size of 2.0km x 2.0km for the location of the computation points.

Figure 9 show the Coulomb failure stress change for this earthquake over the extended fault plane, resolved in the same plane and in the slip direction. Here, the “x” axis (abscissa) represents the distance along the strike direction, which is approximately parallel to the coast, and the “y” axis (ordinate) represents the distance in the dip direction also indicating the depth. Contours are given in bars. Black star shows the hypocenter on the fault plane. It can be observed in this figure that the earthquake ruptured two main asperities: One downdip and northwest of the hypocenter with a maximum stress drop of -31 bars and a total length of about 100 km in the horizontal direction, and the other updip and southwest of the hypocenter with a maximum stress drop of -40 bars and a similar size of the first one. There are also two zones of stress increase with a maximum vaue of 25 bars inside the fault area, and also stress increase zones extending to the surrounding the fault area.

## DISCUSSION AND CONCLUSIONS

Previous studies by different authors about the source characteristics of this earthquake highly differ in the fault geometry, focal depth and source time function duration, etc. In this work, we believe that our results show much more tectonically consistent focal mechanism and the source depth. The focal mechanism obtained here agrees well with the tectonic setting and the geometry of the Benioff zone described by Pardo and Suarez (1993) for the region. Our estimate of the source depth by means of two different RMS error analysis is based on a point source and finite fault inversions. In both cases, the minimum RMS error occurs at 16-17 km depth. This analysis shows that previous estimations of the source depth of this event were both underestimated (Singh and Mortera, 1991) and overestimated (e.g Reyes et al, 1979). Also the source time functions obtained by previous authors show different durations and complexities. Quintanar (1991) obtained a simple triangular source time function with a 27 sec duration, and Singh and Mortera (1991) obtained a rather complex source time function. Our results mainly show a simple function with some high frequencies and a duration of 26 sec.

It is to be mentioned that the difference between our source time function and the one obtained by Singh and Mortera (1991) could be explained by different assumptions in the computation of synthetics and for the number of the waveforms analyzed. They used a simple homogeneous half-space earth model over the source region, while we used a multi-layered model appropriate to the region. In this case, the complexities in the wave train usually produced by a layered earth and recorded on the seismogram at the DBN station, which is the only one station they used, could have been attributed to the source.

Numerous studies so far have shown that there is a positive correlation between the zones of coseismic stress increase inside and around the source region due to a large earthquake and the increment of subsequent seismicity in these regions (e.g. Reasenberg and Simpson, 1992; King et al, 1994; Deng and Sykes, 1997; Stein et al, 1997; Harris, 1998, Stein, 1999). Some of these studies also suggested possible triggering of a large earthquake due to previous events with similar magnitudes. In addition, it has been suggested that stress increases as small as 0.1 bars could influence subsequent seismicity in the surrounding region of a ruptured fault (e.g. Deng and Sykes 1997; Stein 1999).

If we assume an increment in the Coulomb stress of 0.5 bars to have an effective influence on subsequent events, the stress increase zone surrounding the fault area reaches about 1.5 times the length and two times the width of the fault area. This result shows that this event could have effective influence on subsequent events as far as 120 km apart from its hypocenter.

## **ACKNOWLEDGMENTS**

Carlos Mendoza kindly provided some codes for the inversion procedures. Synthetics for teleseismic distances were computed based on the program TELEDB by Charles A. Langston. The Coulomb failure stress computations were performed using the code DIS3D by Laurie Erickson. We thank Jaime Yamamoto for his suggestions on the WWSSN stations. This work was partially supported by the CONACYT project No. 41209-F.

## **AUTHORS AFFILIATION**

Instituto de Geofísica, UNAM. Ciudad Universitaria, 04510, México D.F., México.

## REFERENCES

- Chael, E.P. and G.S. Stewart (1982). Recent large earthquakes along the Middle American trench and their implications for the subduction process, *J. Geophys. Res.* 87, 329-338.
- Courboux, F., M.A. Santoyo, J. Pacheco and S.K. Singh (1997). The 14 September 1995 (M=7.3) Copala, México earthquake : A Source study using teleseismic, regional, and local data, *Bull. Seism. Soc. Am.* 87, pp. 999-1011.
- DeMets, C., R. Gordon, D. Argus and S. Stein (1994). Effect of recent revisions to the geomagnetic reversal time scale on estimates of current plate motions. *Geophysical Research Letters* 21 (20), 2191– 2194.
- DeMets, C., and D. S. Wilson (1997) Relative motions of the Pacific, Rivera, North American, and Cocos plates since 0.78 Ma, *J. Geophys. Res.*, 102, 2789-2806.
- Deng J, and L.R. Sykes (1997). Evolution of the stress field in southern California and triggering of moderate-size earthquakes: A 200-year perspective, *J. Geophys. Res.*, 102, 9859-9886.
- Futterman, W.I. (1962). Dispersive body waves. *J. Geophys. Res.* 67, 5279-5291.
- Harris, R. (1998). Introduction to special section: stress triggers, stress shadows, and implications for seismic hazards, *J. Geophys. Res.*, 103, 24347-24358.
- Hartzell S. H. and T.H. Heaton (1983). Inversion of strong ground motion and teleseismic waveform data, for the fault rupture history of the 1979 Imperial Valley, California, earthquake. *Bull. Seism. Soc. Am.*, 76, 1553-1583.
- Helmberger, D. (1974). Generalized ray theory for shear dislocations. *Bull. Seism. Soc. Am.*, 64, 45-64.



King, G.C.P., R.S. Stein, and J.Lin (1994). Static stress changes and the triggering of earthquakes, *Bull. Seism. Soc. Am.* 84, 935-953,.

Kikuchi, M. and Y. Fukao (1985). Iterative deconvolution of complex body waves from great earthquakes: The Tokachi-Oki earthquake of 1968. *Phys. Earth Planet. Interiors*, 37, 235-248.

Kikuchi, M. and H. Kanamori (1982). Inversion of complex body waves. *Bull. Seism. Soc. Am.*, 72, 491-506.

Kostoglodov V. and W. Bandy (1995). Seismotectonic constraints on the convergence rate between the Rivera and North American plates, *J. Geophys. Res.*, 100, 17,977-17,989,.

Langston, C. and D. Helmberger (1975). A procedure for modelling shallow dislocation sources. *Geophys. Journ. Roy. Astr. Soc.*, V. 42, 117-130.

Lawson C.L. and R.J. Hanson (1974). Solving least squares problems. *Ed. Prentice Hall Inc., Englewood Cliffs, New Jersey, 340p.*

Lomnitz, C. (1977). A procedure for eliminating the indeterminacy in focal depth determination. *Bull. Seism. Soc. Am.*, 67, 533-535.

Menke, W. (1989). Geophysical data analysis: Discrete inverse theory. *Ed. Academic Press Inc., San Diego, CA., USA, 289p.*

Mendoza and Hartzell (1989). Slip distribution of the 19 september 1985 Michoacan, Mexico, earthquake: Near source and teleseismic constraints. *Bull. Seism. Soc. Am.* 79, 655-669.

Mendoza (1993). Coseismic slip of two large Mexican earthquakes from teleseismic body waveforms: Implications for asperity interaction in the Michoacan plate boundary segment. *J. Geophys. Res.*, 98, 8197-8210.

Mendoza (1995). Finite fault analysis of the 1979 March 14, Petatlan, Mexico earthquake using teleseismic P waveforms. *Geophys. J. Int.*, 121, 675-683.

Mendoza and Hartzell (1997). Fault slip distribution of the 1995 Colima-Jalisco, Mexico, earthquake. *Bull. Seism. Soc. Am.*, 89, 1338-1344.

Mikumo, T., T. Miyatake and M.A. Santoyo (1998). Dynamic rupture of asperities and stress change during a sequence of large interplate earthquakes in the Mexican subduction zone. *Bull. Seism. Soc. Am.* 88, 686-702.

Mikumo T., S. K. Singh, and M.A. Santoyo (1999). A possible stress interaction between large thrust and normal faulting earthquakes in the mexican subduction zone, *Bull. Seism. Soc. Am.* 89, 1418-1427.

Mikumo, T., M.A. Santoyo and S.K. Singh (2000). Dynamic rupture and stress change in normal faulting earthquakes in the subducting Cocos plate. *Geophys. J. Int.*, 140, 611-620.

Mikumo, T., Y. Yagi, S.K. Singh, and M.A. Santoyo (2002). Coseismic and postseismic stress changes in a subducting plate: Possible stress interactions between large interplate thrust and intraplate normal faulting earthquakes, *J. Geophys. Res.*, 107, B1, ESE5-1-ESE5-12.

Nabelek, J.L. (1984). Determination of earthquake source parameters from inversion of body waves. *PhD. dissertation, Massachusetts Institute of Technology, Cambridge, Mass.*

Okada, Y. (1985). Surface deformation due to shear and tensile faults in a half space, *Bull. Seism. Soc. Am.* 75, 1135-1154.

Okada, Y. (1992). Internal deformation due to shear and tensile faults in a half space, *Bull. Seism. Soc. Am.* 82, 1018-1040.

Pardo, M. and G. Suarez (1993). Shape of the subducted Rivera and Cocos plates in southern Mexico: Seismic and tectonic implications. *J. Geophys. Res.*, 100, 12357-12373.

Quintanar L. (1991). Tomographie de la source sismique par inversion des ondes P télésismiques. *PhD. dissertation, Université Paris 7, Paris, France.*

Reasenber, P.A. and R.W. Simpson (1992). Response of regional seismicity to the static stress change produced by the Loma Prieta Earthquake, *Science* 255, 1687-1690.

Reyes, A., J.N. Brune, and C. Lomnitz (1979). Source mechanism and aftershock study of the Colima, Mexico earthquake of January 10, 1973, *Bull. Seism. Soc. Am.*, 69, 1819-1840.

Santoyo, M. A., S. K. Singh and T. Mikumo (2005a). Source process and stress change associated with the 11 January, 1997 (Mw=7.1) Michoacan, Mexico, Inslab Earthquake. *Geofisica internacional*. In press.

Santoyo, M. A., T. Mikumo, and C. Mendoza (2005b). Possible Lateral Stress Interactions in a Sequence of Large InterplateThrust Earthquakes on the Subducting Cocos and Rivera Plates. *Submitted to Bull. Seism. Soc. Am.*

Singh, S. K. and F. Mortera (1991), Source-time functions of large Mexican subduction earthquakes, morphology of the Benioff zone, and the extent of the Guerrero gap, *J. Geophys. Res.* 96, 21487-21502.

Singh, S.K., M. Ordaz, L. Alcantara, N. Shapiro, V. Kostoglodov, J. Pacheco, S. Alcocer, C. Gutierrez, R. Quaas, T. Mikumo, and E. Ovando (2000). The Oaxaca earthquake of September 30, 1999 (Mw=7.5): A normal faulting event in the subducted Cocos plate. *Seism. Res. Lett.*, 71, 67-78

Stein, R.S., A. Barka, and J. Dieterich (1997). Progressive failure of the north Anatolian fault since 1939 by earthquake stress triggering, *Geophys. J. Int.* 128, 594-604.

Stein, S. (1999). The role of stress transfer in earthquake occurrence, *Nature*, 402, 605-609.

## Figure Captions

Figure 1. Tectonic map of Mexico. NORTH AMERICA=North American Plate; RIVERA=Rivera Plate; PACIFIC=Pacific Plate; COCOS=Cocos Plate; TFZ=Tamayo Fracture Zone; RFZ=Rivera Fracture Zone; EPR=East Pacific Rise; EGG=El Gordo Graben; MAT= Middle American Trench; OFZ= Orozco Fracture Zone; OGFZ= O'Gorman Fracture Zone; TMVB= Trans Mexican Volcanic Belt. Numbers above arrows indicate the relative rate of convergence. The black star shows the epicentral location of the 30/01/1973 Colima Earthquake.

Figure 2. Epicentral map of the 30/01/1973 earthquake. NORTH AMERICA=North American Plate; COCOS=Cocos Plate; EGG=El Gordo Graben; MAT= Middle American Trench. Black star indicates the epicentral location of the 30/01/1973 Earthquake. Solid thin lines show the rupture areas of the 25/10/1981 Playa Azul, 19/09/1985 Michoacan, 21/09/1985 Zihuatanejo, 09/10/1995 Colima-Jalisco and 22/01/2003 Tecomán earthquakes (from Santoyo et al, 2005b). The focal mechanism of the 30/01/1973 earthquake obtained in this study, is plotted on the lower hemisphere of the stereographic projection. The rectangle centered on the epicenter show the fault plane assumed here for the finite fault analysis, which is projected on a horizontal surface. The grid inside the rectangle indicates the subdivision of the fault plane in the 493 (5km x 5km) subfaults, used in the inversion for the kinematic slip distribution.

Figure 3. Focal mechanism and P waveforms fit for the 30/01/1973 earthquake, obtained from the point source teleseismic inversion. Recorded waveforms are shown by solid lines, and the corresponding synthetic seismograms are shown by dashed lines. Stations are shown in the lower focal hemisphere with open circles. Amplitudes in scale are in  $\mu$  (microns).

Figure 4. RMS errors (in  $\mu$ , microns) in for the point source inversion vs focal depth. The lowest RMS error occurs for depths between 15 km and 17.5 km.

Figure 5. RMS errors (in  $\mu$ /sec) for the finite fault inversion vs focal depth. Here the lowest RMS error occurs for a depth of 16 km.

Figure 6. 2-D kinematic inversion results. Comparison between the recorded (solid lines), and synthetic velocity seismograms (dashed lines) at the eight teleseismic stations used in this study.

Figure 7. Dislocation pattern obtained from the 2-D kinematic inversion. Slips are shown in cm. The two main rupture asperities are located downdip and updip-southeast of the hypocenter. Fault plane is viewed from the northeast. Distances are given in km. The upper edge of the fault plane is located at a depth of 4 km.

Figure 8. Source time function obtained in this study for the 30/01/1973 event. Amplitudes are shown in dyn-cm/sec.

Figure 9. Coulomb failure stress associated with the slip distribution of the 30/01/1973 over the fault plane. Contours are shown in bars. Two main asperities can be observed, one downdip-northwest and another updip-southeast of the hypocenter. Note that the stress increase area outside the fault area extends up to 150 km from the epicenter on each side of the rupture.

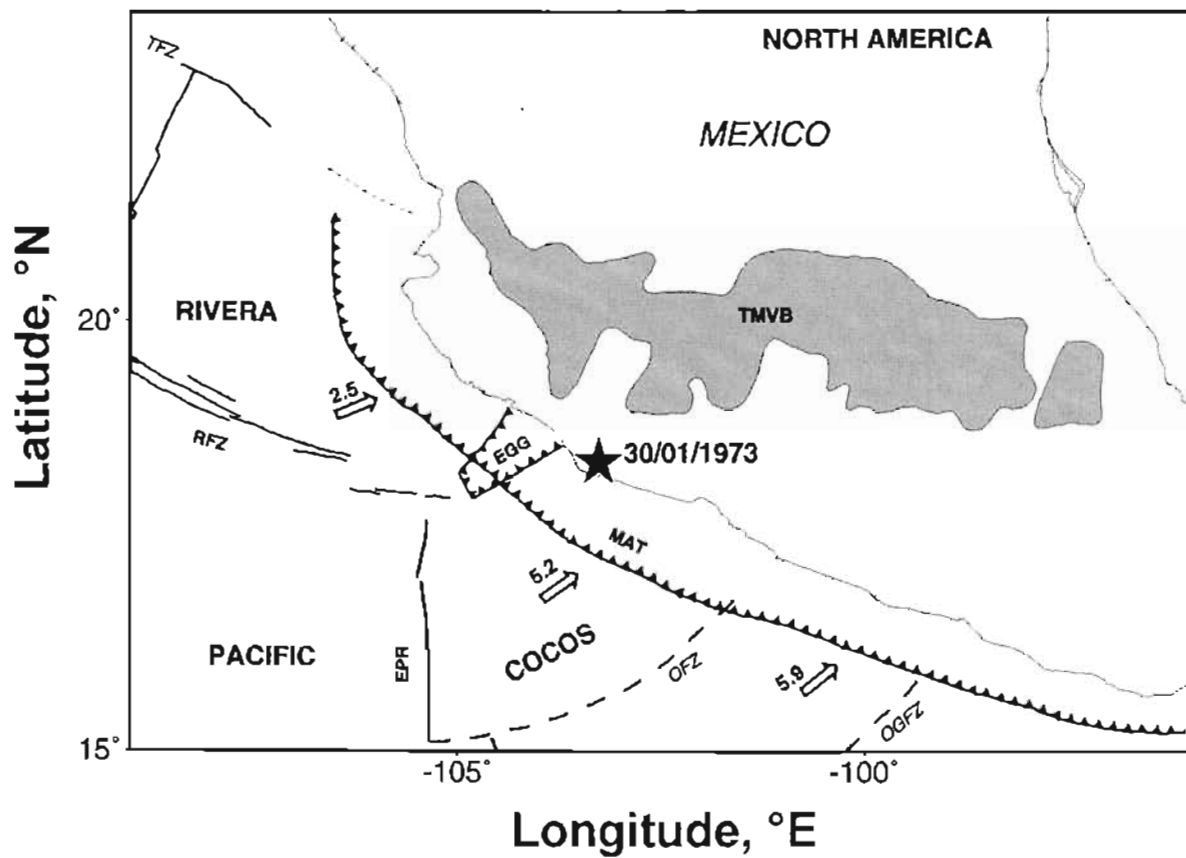


Figure 1

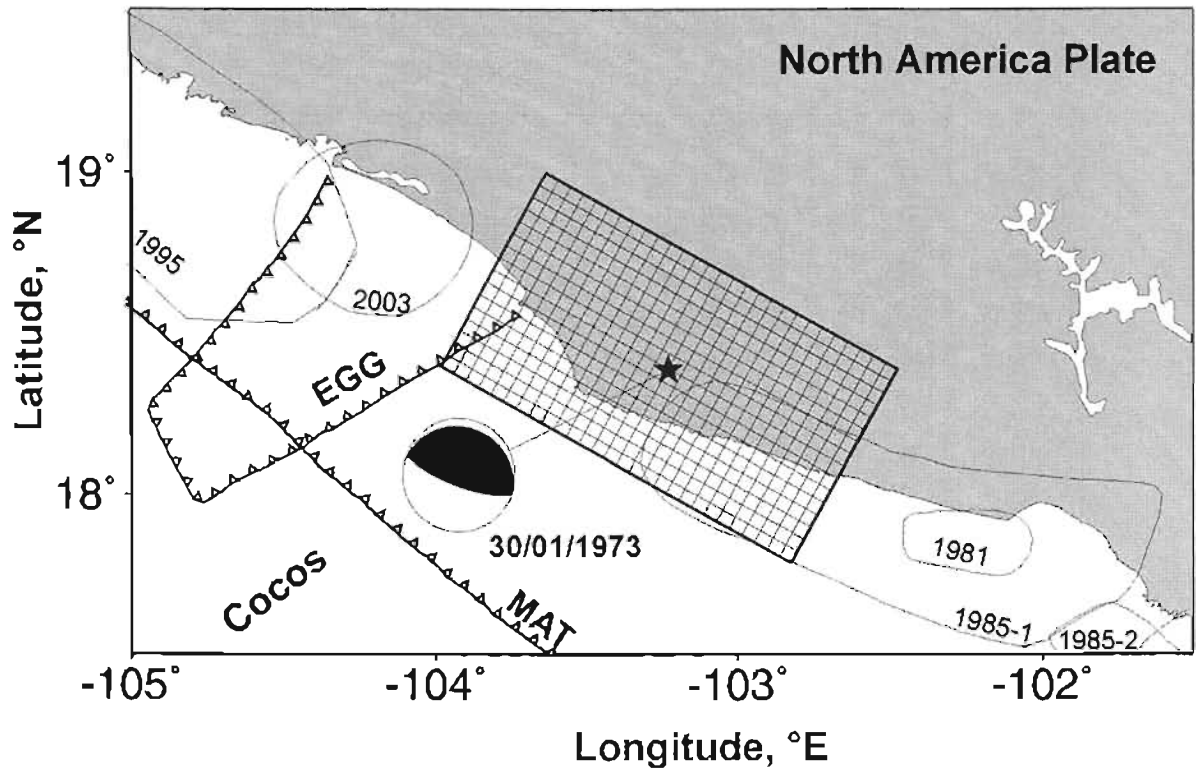


Figure 2



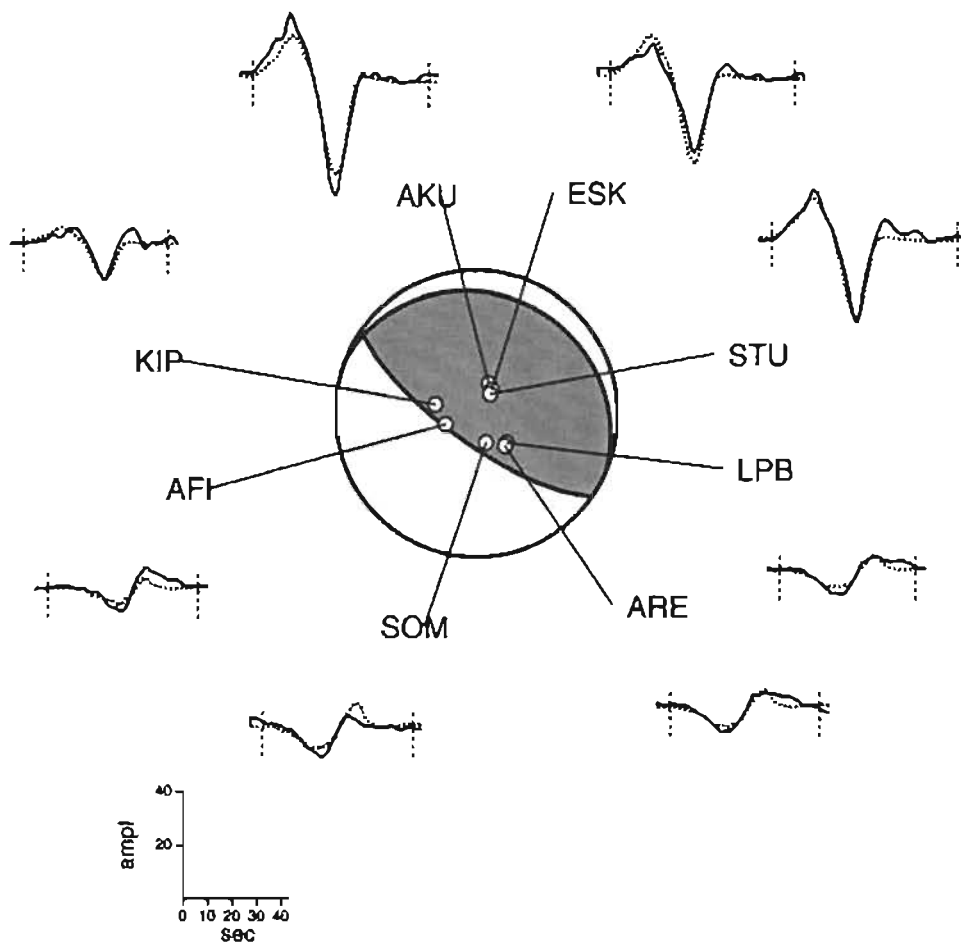


Figure 3

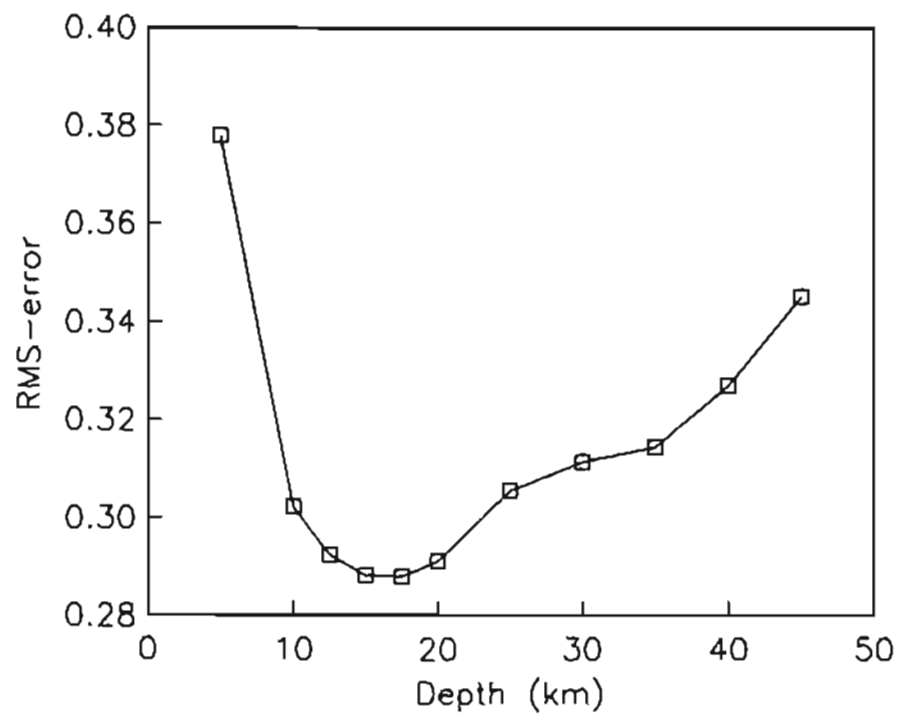


Figure 4

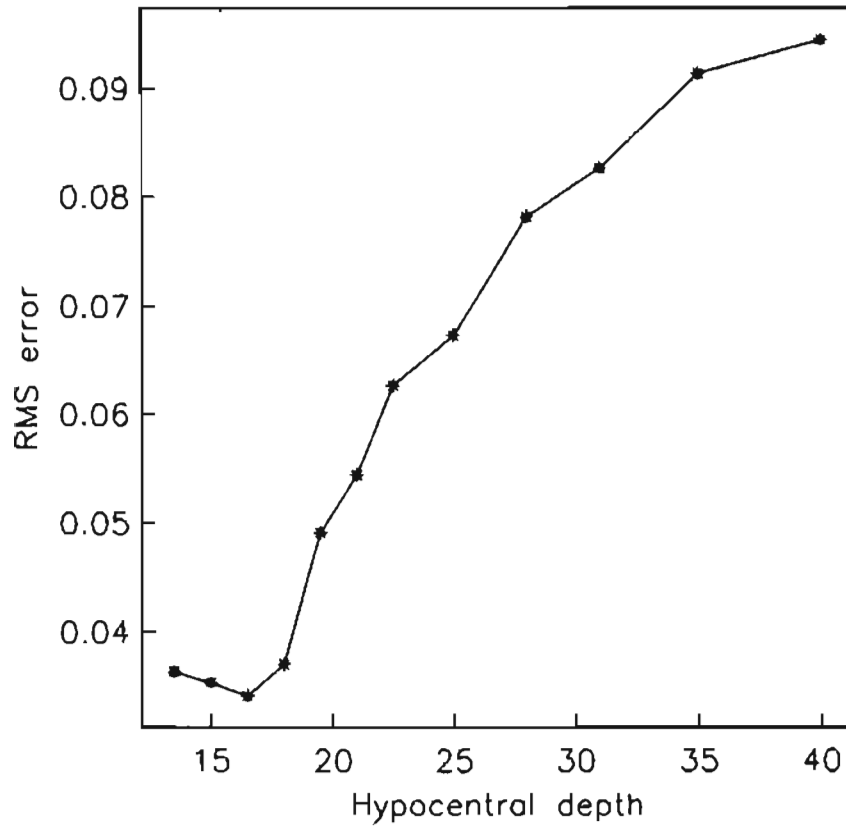


Figure 5

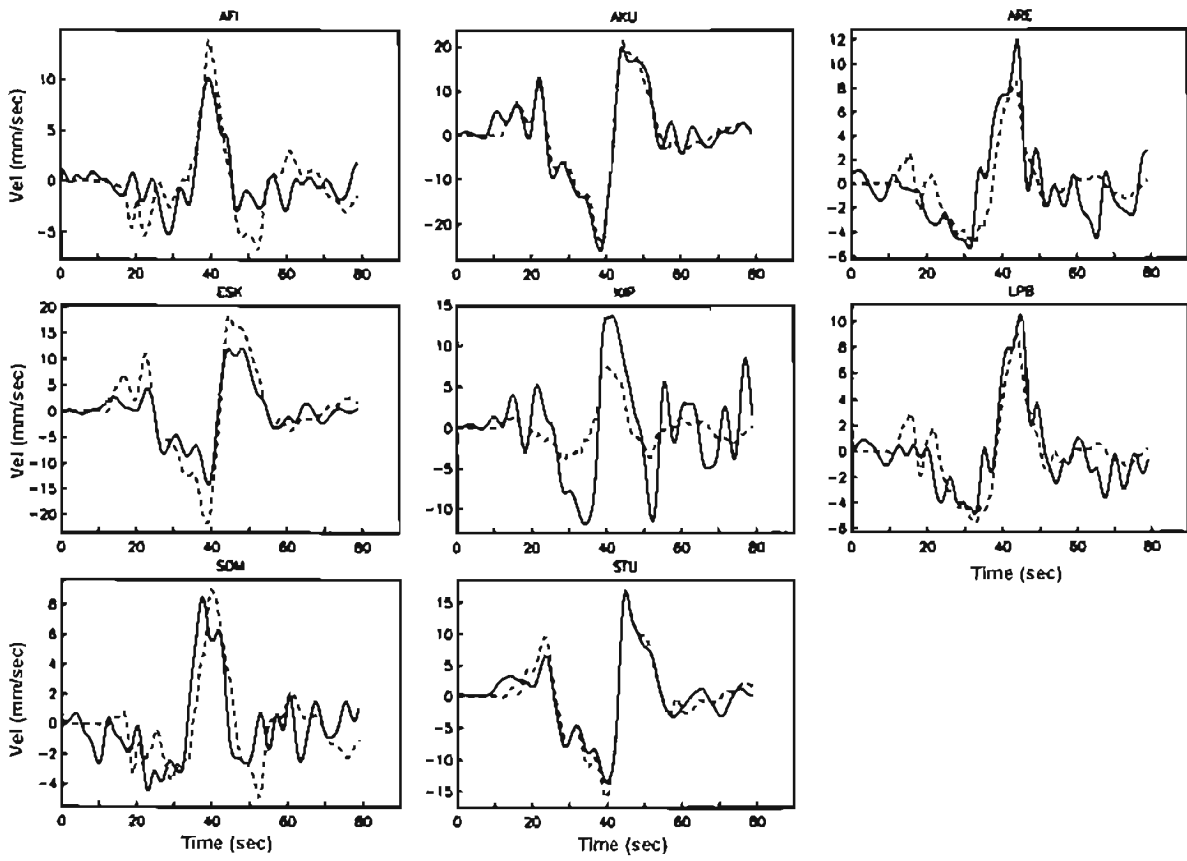


Figure 6

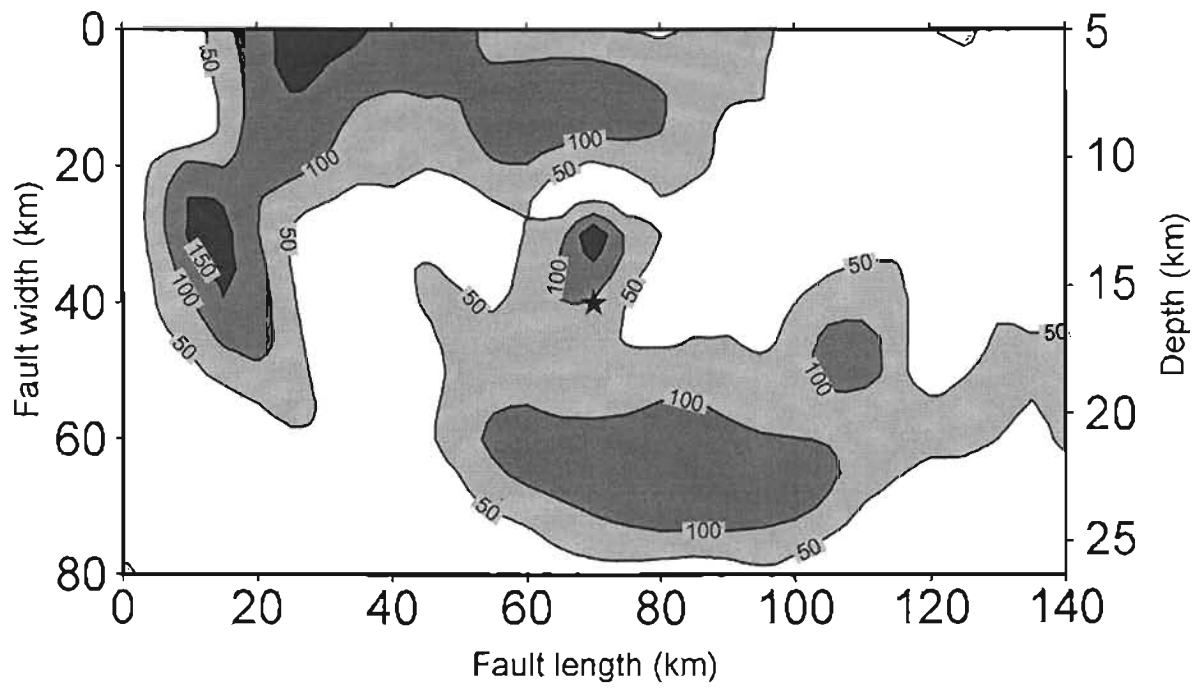


Figure 7

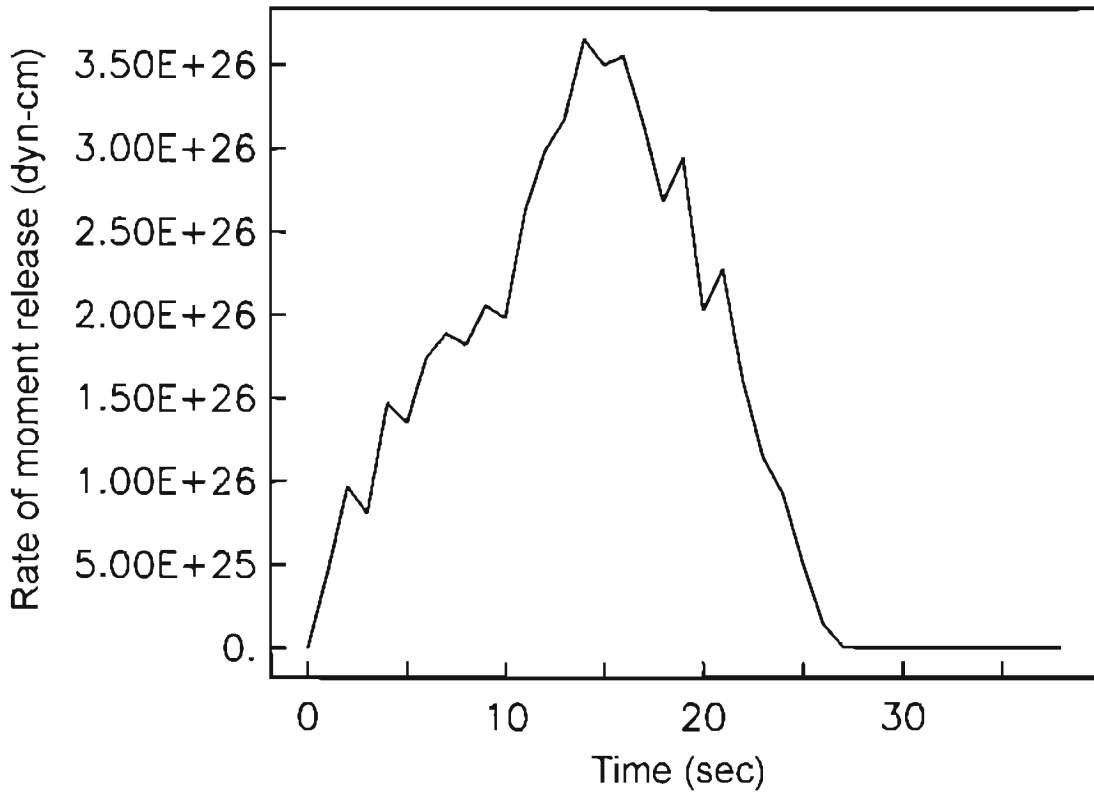


Figure 8

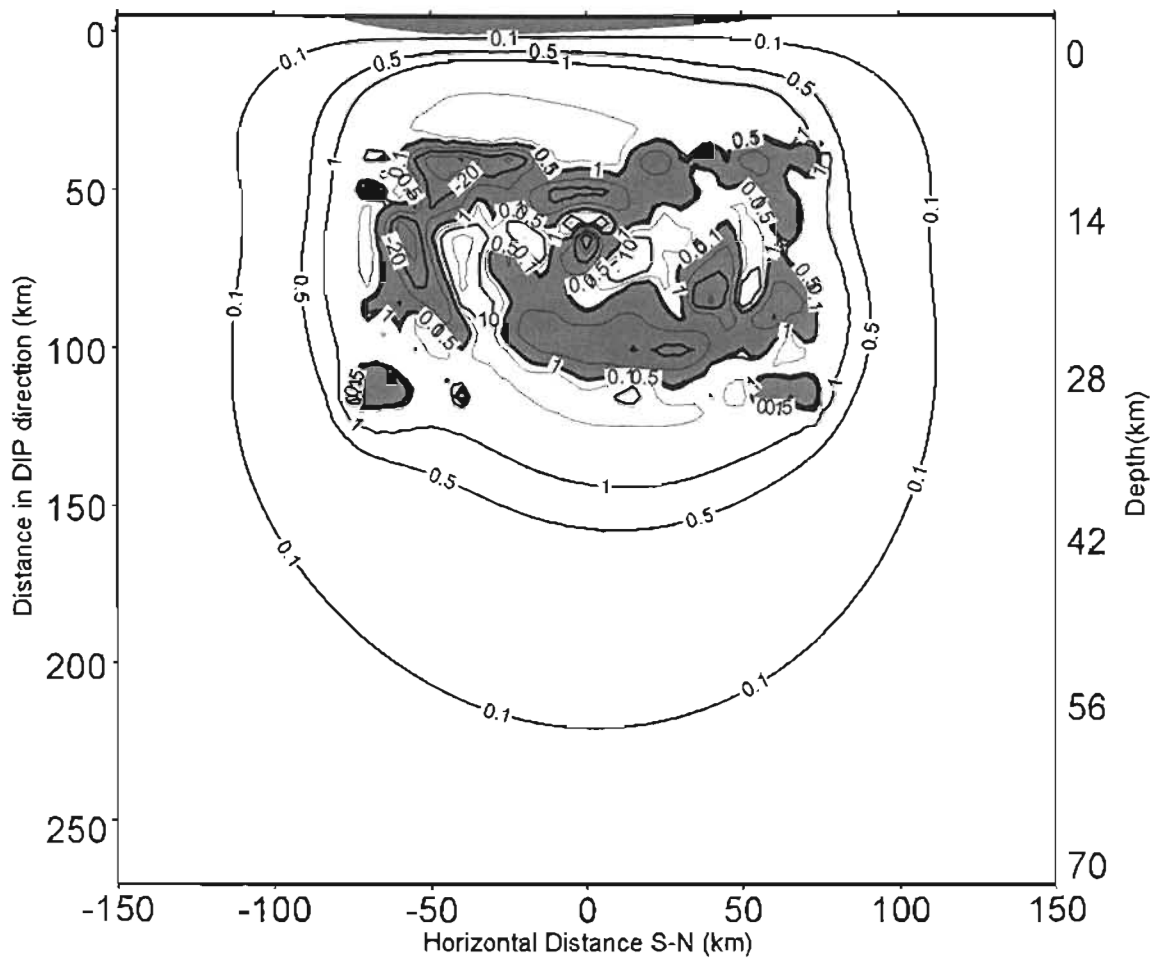


Figure 9

## Capítulo IV

PROCESO DE RUPTURA Y CAMBIO DE ESFUERZOS ASOCIADO CON EL SISMO INTRAPLACA DEL 11 DE ENERO DE 1997 (MW=7.1), EN MICHOACÁN, MÉXICO



**Source process and stress change associated with the 11 January, 1997  
(Mw=7.1) Michoacan, Mexico, Inslab Earthquake**

*By Miguel A. Santoyo, Shri K. Singh and Takeshi Mikumo*

**RESUMEN**

Con base en registros sísmicos obtenidos a distancias locales, regionales y telesísmicas, estudiamos las características de la fuente y el cambio de esfuerzos asociado del sismo de Michoacán del 11 de enero de 1997. Este evento fué localizado justo bajo la zona de ruptura del gran sismo de subducción de Michoacán de 1985. De la inversión de datos telesísmicos, obtenemos una falla cercana a la vertical a 35 km de profundidad, con una duración total de la fuente de 15 segundos, una magnitud de momento sísmico  $M_w=7.1$  y una velocidad de ruptura promedio de 2.8 km/seg. El análisis de registros locales y telesísmicos muestra que la ruptura presentó una fuerte directividad al sureste, con una función de tiempo de la fuente compleja, dos subeventos principales y una duración de 13 segundos. La distribución de dislocaciones sobre el plano de falla, obtenida a partir de inversión lineal cinemática 2-D y con datos locales y telesísmicos de banda ancha, muestra un patrón de ruptura complejo donde la mayor parte de la liberación de momento sísmico ocurre en la porción sureste de la falla. La comparación entre los cambios de esfuerzos de Coulomb cosísmicos debido al evento principal, y la localización y el mecanismo focal de sus réplicas, sugiere que la sismicidad post-sísmica pudo haber sido disparada por los cambios de esfuerzos debidos al sismo principal.

**PALABRAS CLAVE:** Inversión cinemática de la fuente, esfuerzos de Coulomb, interacción de sismos.

## ABSTRACT

We study the source characteristics and the associated coseismic stress change of the January 11, 1997 Michoacan earthquake, based on teleseismic, regional and near-source recordings. This event was located just beneath the ruptured zone of the 1985 Michoacan thrust event. From the inversion of teleseismic recordings, we obtain a nearly-vertical faulting at 35 km-depth, a total source duration of 15 sec, a moment magnitude of  $M_w=7.1$ , and a mean rupture velocity of 2.8 km/sec. An analysis of teleseismic and local seismograms shows that the rupture had a strong directivity to the southeast, with a rather complex source-time function with two main subevents and a total duration of 13 sec. The dislocation distribution obtained from 2D kinematic linear inversion, using both local strong motion and broad-band teleseismic data, shows a complex rupture pattern with the main seismic moment release occurring in the southwest portion of the fault. A comparison between the coseismic Coulomb failure stress change during the main shock, and the location and mechanism of the aftershocks, suggests that post-event seismicity may have been triggered by the stress changes due to the main event.

**KEY WORDS:** Kinematic source inversion, Coulomb failure stress, earthquake interaction.

## INTRODUCTION

The 11 January, 1997 earthquake ( $M_w=7.1$ ) took place just beneath the area of the main ruptured zone of the great 1985 Michoacan earthquake ( $M_w=8.1$ ), within the subducted slab, after a relatively short period of 12 years (Figure 1). The focal mechanism and other source parameters preliminarily reported by different institutions and authors (see Table 1) showed an intermediate-depth, nearly-vertical faulting event. From teleseismic waveform inversion, M. Kikuchi (personal communication, 1997) obtained a general dislocation pattern with two main asperities to the southeast side of the rupture area, under the assumption that the vertical nodal plane was the fault plane. Mikumo et al. (2000) calculated the dynamic stress change inside the fault area of this earthquake, based on the slip distribution obtained only from the local

seismograms. They found that high stress drop zones are confined to the deeper part of the fault, surrounded by zones with low stress drop.

In this study, by the aid of teleseismic, regional and local recordings, we investigate in detail the main source characteristics (location, depth, focal mechanism, fault-plane orientation, directivity and complexity of the rupture), the distribution of dislocations, and the associated stress change in a 3D space and its relation with the aftershock seismicity.

### **FOCAL CHARACTERISTICS USING TELESEISMIC DATA.**

In order to retrieve a more reliable focal solution than those obtained by automated procedures, we inverted the teleseismic body-wave recordings for point- and line-sources, using the Nábělek's (1984) maximum-likelihood inversion technique. For this purpose, we low-pass filtered the available long period P and SH velocity waveform data using a Butterworth filter ( $F_c=0.5$  Hz), selecting waveforms with a good signal to noise ratio

The selection process yielded recordings from 23 teleseismic stations located at distances between  $30^\circ$ - $92^\circ$ , with a good azimuthal coverage (see Figure 2). The recordings were also corrected for the instrumental response, rotated, and integrated once in order to obtain the transverse and radial displacement time histories.

The crustal velocity model in the source region is based on the one obtained by Fuentes (1997), and adjusted by a grid search analysis of the P and S wave arrival times from the 16/1/97 aftershock local recordings. The 16/1/97 aftershock was considered as an empirical Green function of the mainshock event, due to its magnitude ( $M_w=5.5$ ) and its hypocentral location, which occurred close enough to the mainshock hypocenter to consider that the body waves from the two events sample the same structure in the source region. In Table 2 we show the crustal model that provides a best fit to the arrival times to the local stations that recorded this aftershock. For the teleseismic receivers, we used the global crustal velocity model shown in Table 3. Here we also included the attenuation parameter  $T^*$  (Futterman, 1962) of 1.0 second for P waves and 4.0 seconds for S waves. The epicenter location used here ( $18.06^\circ$ N,  $102.79^\circ$ W) was relocated using local and regional seismograms.

Comparing the SH waveforms among some stations located in opposite directions from the epicenter (e.g. NNA and FFC; see Figure 3), we found a significant difference in their duration, which indicates a strong directivity effect. As this effect was also observed at many other teleseismic and local stations, we performed a teleseismic directivity analysis. Here, we initially modeled the event as a propagating horizontal line source with velocity  $V_r$ , measuring the rms-errors with respect to the azimuth and the rupture velocity. In Figure 4a, we find that the minimum RMS for the directivity falls around the value of  $Az=105^\circ$ , and the rupture velocity between  $V_r=2.6$  km/sec and  $V_r=2.8$  km/sec (Figure 4b). After these analyses, we performed the waveform inversion for the focal mechanism, depth and source time function. Results show an almost vertical dip-slip faulting mechanism, strike= $105^\circ$ , dip= $89^\circ$ , rake= $110^\circ$ , with a source time function duration of 15 sec and a centroid depth of 34 km. The RMS error in this case is  $E_{rms}=4.94 \times 10^{-2} \mu$ . Figures 5a and 5b show the resulting focal mechanism and the observed and synthetic seismograms of P and SH waves. Comparing this error with that obtained from the inversion using a single point source ( $E_{rms}=6.01 \times 10^{-1} \mu$ ), we found a better agreement for the horizontally propagating source. This line source waveform inversion yielded an average seismic moment release of  $M_0=4.9 \times 10^{26}$  dyn-cm ( $M_w=7.1$ ).

## **KINEMATIC ANALYSIS OF THE SOURCE**

To investigate the slip distribution and the rupture history at the source, we performed a kinematic inversion using first only local strong-motion recordings, and second both local-strong motion and broadband teleseismic data. Synthetic seismograms for local and regional distances were computed using the discrete wave-number method described by Bouchon and Aki (1977) and Bouchon (1979). For teleseismic distances the synthetics were computed using the generalized ray theory procedure proposed by Helmberger (1974), and Langston and Helmberger (1975). The crustal velocity structure around the source region used in both methods was the same as shown in Table 2.

### *Kinematic analysis using strong-motion seismic recordings.*

For this purpose, we selected the recordings from four closest, three-component accelerograph stations: CALE, VILD, INPT and UNIO (Figure 1). This choice is based on the fact that near-

source records are less contaminated by path propagation effects. In Figure 1 we also show the epicentral locations of the mainshock and its aftershocks (Table 4). The acceleration records were integrated once following the procedure proposed by Iwan et al. (1985) to obtain the ground velocities, and then low-pass filtered ( $F_c=1.0$  Hz) using a three-pole Butterworth filter. Recordings from stations CALE (EW), UNIO (NS and EW) and VILD (EW) are contaminated by some undesirable glitches, so we un-glitched the seismograms by averaging the adjacent acceleration values before the processing of the data.

We performed a 2D finite source inversion of the slips over the source plane, using only local and regional data. In order to discriminate the actual fault plane from the two nodal planes, we observed that the nearly-vertical plane meets important constraints: First, the vertical plane becomes nearly parallel to the coast and to the trench, which is not the case for the auxiliary plane. Second, as we will see later, kinematic inversion over the vertical fault plane gives a better fit between the synthetic and observed seismograms than for the auxiliary plane.

To obtain the slip distribution over the nearly-vertical fault plane, we discretized it into 416 square subfaults of equal size (2km x 2km), embedded in a horizontally layered structure. Based on this assumption, the observed data together with the synthetic seismograms computed using the techniques already mentioned, form an over-determined linear system of the type  $\mathbf{AX} \approx \mathbf{B}$ . Here, the matrix  $\mathbf{A}$  contains the synthetic seismograms with its respective time shifting due to the rupture,  $\mathbf{B}$  is a vector with the observed records arranged in the same order as in the synthetics in matrix  $\mathbf{A}$ , and  $\mathbf{X}$  is the solution vector containing the dislocation weighting values which represent the amount of slip that must be applied to each subfault in order to fit the observations.

The matrix equation shown here can be solved by a simple least-squares technique; however, the solution becomes unstable because matrix  $\mathbf{A}$  could be ill-conditioned (Hartzell and Heaton, 1983). To solve this problem, the inversion was stabilized by a Householder decomposition of the matrix equations (Lawson and Hanson, 1974; Menke 1984), and imposing a positivity constraint to the solution. To further stabilize the inversion, we appended to the linear system, additional smoothing and moment-minimization constraints of the form  $\lambda \mathbf{FX} = \lambda \mathbf{D}$ , where  $\lambda$  is a

scalar weighting factor. Smoothing is imposed by constructing  $\mathbf{F}$  and  $\mathbf{D}$  such that the difference between adjacent dislocations is zero. Moment minimization is obtained by letting  $\mathbf{F}$  be the identity matrix and  $\mathbf{D}$  the zero vector, effectively reducing the length of  $\mathbf{X}$ . To identify the proper weighting factor  $\lambda$ , several inversion runs are conducted until the largest value of  $\lambda$  is reached that still allows the observed records to be fitted by the synthetic waveforms. In this case, spatial smoothness constraints are imposed to reduce some noise effects included in the solution, which could come from some unconsidered path effects or the simplification of the velocity model.

For the kinematic inversion, we again assumed a constant rupture velocity of 2.8 km/sec (same as that estimated from the teleseismic analysis), as this produced a more coherent solution and better fit between the observed and synthetic seismograms. Due to this constant rupture velocity, the rupture initiates at the hypocenter and propagates with circular rupture fronts. We assumed also that the value of the rise time was the same for all the subfaults. Following this assumption, the rise time value was varied in different inversion runs, between 0.5 and 2.0 seconds to obtain a value that best fit the observations. In this case, we obtained a mean source duration of 1.2 seconds. As mentioned earlier, the fault plane was discretized into a uniform mesh of 2.0 x 2.0 km, obtaining a total of 416 subfaults, using the focal mechanism obtained from the teleseismic inversion (strike=105°, dip=89°). The rupture initiation point was located at 10 km from the northwestern edge, and 14 km from the upper edge of the fault.

The inversion results show a good agreement between the synthetic and observed velocity seismograms with an RMS error of  $1.53 \times 10^{-2}$  cm/sec (Figure 7.a). It can be observed that the rupture propagates almost horizontally from the hypocenter to the southeast direction. The dislocation pattern obtained (Figure 7.b) is mainly confined to depths between 25 km and 50 km with a horizontal length of approximately 35 km. It can also be observed that the main asperity with the largest moment release is located at the southeastern side of the fault plane close to the end of the rupture, 20 to 30 km southeast of the hypocenter. The maximum slip here obtained from this inversion is 450 cm and the total seismic moment release is  $M_0 = 4.6 \times 10^{26}$  dyn-cm respectively. The total overall time duration obtained for the source time function (curve A, Figure 6) is about 13 seconds with two main subevents: the first one 4

seconds after the initiation of the rupture, and the second and largest one, approximately 11 seconds after the initiation time, during the last phase of the rupture. The dimension of the main ruptured asperity (second subevent) is about 15x20 km., as shown in the dislocation pattern in Figure 7b.

As a further check on the vertical plane as the real fault plane, we performed tests following a procedure by Delouis and Legrand (1999). Here, we inverted the waveforms at the same stations, but taking the auxiliary plane as the fault plane. In this case we used the same parameters as for the nearly-vertical plane. The RMS errors of the misfit between the observed and synthetic seismograms for the two planes are significantly different:  $2.37 \times 10^{-2}$  cm/sec for the auxiliary plane and  $1.53 \times 10^{-2}$  cm/sec for the vertical plane. On the other hand, the slip distribution obtained over the auxiliary plane was very dispersed, contrary to the pattern observed for the vertical plane. These results clearly show that the horizontal plane could hardly represent the real fault plane.

*Joint inversion for slips over the fault plane using local and teleseismic data.*

A large number of broadband teleseismic stations between 30° and 95° recorded the mainshock event with a good azimuthal coverage. We selected 12 best-distributed stations in azimuth with respect to the epicenter (ADK, COR, CPUP, DBIC, ESK, FFC, HRV, KONO, LPAZ, RAR, SJG, SNZO) for the analysis. For the joint inversion we incorporated the 12 broadband teleseismic displacements of the P wave arrival on the vertical component, which were band-pass filtered from 0.01 to 2 Hz, and corrected for the instrumental response before the inversion. Beside the mentioned stations, some other stations in the southern hemisphere also recorded this event; however, since the signal-to-noise ratio for these stations was very poor, we excluded them from the analysis.

For the joint inversion, we used a rupture velocity of 2.8 km/s, and the same fault plane discretization as in the previous case. We computed the synthetic seismograms using the same crustal model shown in Table 2 for the source region, and a general model in Table 3 for the receiver sites. In order to obtain the best agreement between the observed and synthetic time histories, we searched for the optimum weight to assign to each type of data in the inversion;

that is, one value for the local and regional data, and another value for teleseismic data. We tested the inversion results for three weighting schemes: 1:2, 1:4, 1:8 (teleseismic : local data) with a normalized error in the misfit between the observed and synthetic seismograms. From this test, we found that the best case was 1:4, with a normalized error of  $8.99 \times 10^{-2}$ . The observed and synthetic seismograms from this final inversion are compared in Figure 8, and the dislocation pattern obtained is shown in Figure 9.

The seismic moment release obtained first by local inversion ( $M_0 = 4.6 \times 10^{26}$  dyn-cm) and second by the joint inversion ( $M_0 = 4.9 \times 10^{26}$  dyn-cm) is very close to those reported by other authors. These values give a mean moment magnitude of  $M_w = 7.1$ .

### **COULOMB FAILURE STRESS CHANGE**

Mikumo et al. (2000) calculated the dynamic stress change inside the fault area of this earthquake, based on the slip distribution obtained from the local seismograms. They found that high stress drop zones are confined to the deeper part of the fault, surrounded by zones with low stress drop. Mikumo et al. (1999) also found that the 1997 earthquake took place in the zone of maximum coseismic stress increase due to the 1985 event, and that the 1997 normal faulting earthquake occurred under possible stress transfer from the 1985 earthquake to the interior of the subducting Cocos plate.

In this section, we investigate the possible influence of the 11/01/97 mainshock event on its aftershock seismicity. Taking into account our final distribution of slips, we calculated the coseismic change of the Coulomb failure stress function ( $\Delta CFS$ ) due to this earthquake, not only over the fault plane but also over a vertical cross section perpendicular to the strike direction. To do this, we computed the Coulomb failure stress by the use of the relation  $\Delta CFS = \Delta \tau + \mu' \Delta \sigma_n$  (e.g. Harris, 1998), where  $\Delta \tau$  is the shear stress change in the direction of the fault slip,  $\Delta \sigma_n$  is the change in the tensional stress normal to the fault plane, and  $\mu'$  is an apparent coefficient of friction  $\mu' = \mu (1-p)$ , where  $\mu$  is the static coefficient of friction and  $p$  is the pore pressure in the source volume. Here, we used the formulation given by Okada (1985, 1992) to compute the coseismic  $\Delta CFS$ . In the computations, we used the mean shear modulus for the site,  $\mu = 3.5 \times 10^{11}$  dyn/cm<sup>2</sup>, with a Poisson ratio of  $\nu = 0.25$ . For the tectonic apparent



coefficient of friction, we used the value of  $\mu'=0.4$  adopted by Mikumo et al. (2000) for the Mexican subduction zone.

Figures 10 and 11 shows the  $\Delta$ CFS plots for this earthquake. In Figure 10, we show the Coulomb failure stress over the fault plane. Here, the “x” axis (abscissa) represents the distance along the strike direction, which is approximately parallel to the coast, and the “y” axis (ordinate) represents the distance in the dip direction also indicating the depth. Contours are given in bars. Black dots show the aftershock hypocenters projected over the fault plane. It can be observed in this figure that most of the aftershocks are distributed over the main asperity inside the zone of stress drop caused by normal faulting. The stress drop zone can be expected to, in turn, become a zone of stress increase for subsequent inverse faulting. Actually, almost all of these aftershocks indicate inverse faulting mechanism (Table 4). The  $\Delta$ CFS due to the mainshock slips was resolved onto the plane strike= $290^\circ$ , dip= $70^\circ$ , over the cross section A-A' in Figure 11, perpendicular to the main fault plane (see Figure 1). In this figure, we show the plot of  $\Delta$ CFS contours and the aftershock hypocenters projected over this section. Here we see that almost all of these aftershocks fall inside the contours of stress increase for inverse faulting due to the mainshock, as expected. It is important to note that in this case aftershocks are occurring outside of the fault plane on the downdip side of the slab, which suggests that they are not defining the fault plane.

## CONCLUSIONS

The focal mechanism of this event shows a very steep, dip slip normal faulting in the oceanic subducting slab. Although high-angle, in-slab normal faulting events are common in the Mexican subduction zone (e.g. Singh et al., 1981, 2000), this is the first reported event of a great magnitude with a nearly-vertical mechanism. The falling block in the focal mechanism suggests that the driving mechanism of this event could be related with the gravitational pull of the subducting slab.

On the other hand, the dislocation pattern obtained from the 2D kinematic inversion shows a complex slip distribution, with the main seismic moment release occurring at the southeast of the hypocenter, and breaking a main asperity with an area of approximately 20x30 km (Figure

9). Comparing the slip distribution with the location of its aftershocks, we observe that these aftershocks occurred mainly in the zones of high slip - stress drop on the fault. It is to be noted from the location of their hypocenters that, all the aftershock seismicity seems to have occurred also within the subducted slab. The Coulomb failure stress resolved in the direction of the focal mechanism of the aftershocks (steep-angle, reverse faulting) shows that almost all the aftershock also occurred in the zone of stress increase due to the mainshock, outside of the fault plane, which means that they are not defining the fault plane itself. Several authors have reported a positive correlation between the coseismic stress changes on the neighborhood of the source region, and the increase of seismicity in the stress increase areas (e.g. King *et al.*, 1994; Stein *et al.*, 1994; Toda *et al.*, 1998; Deng and Sykes, 1997; Harris, 1998; Freed and Lin, 1998; Stein 1999). The results of this study suggest that this aftershock seismicity observed after the occurrence of the 11/01/97 event may have been triggered by the main event.

#### **ACKNOWLEDGMENTS**

We wish to thank Javier Pacheco for his constructive discussions and remarks. We thank also Roberto Quaas from CENAPRED, Citlalli Pérez from I.I. UNAM, and Clara Javier from CFE, for providing the strong motion recordings. Carlos Mendoza kindly provided some codes for the inversion procedures. Synthetics for local distances were computed using the program AXITRA by Olivier Coutant. Synthetics for teleseismic distances were computed based on the program TELEDDB by Charles A. Langston.

#### **AUTHORS AFFILIATION**

Instituto de Geofísica, UNAM. Ciudad Universitaria, 04510, México D.F., México.

## REFERENCES

- Bouchon M. (1979). Discrete wave number representation of elastic wave field in three space dimensions, *J. Geophys. Res.*, 84, 3609-3614.
- Bouchon M. and K. Aki (1977). Discrete wave number representation of seismic source wave fields, *Bull. Seism. Soc. Amer.* 67, 259-277.
- Delouis, B. and D. Legrand (1999). Focal mechanism determination and identification of the fault plane of earthquakes using only one or two near source seismic recordings. *Bull. Seism. Soc. Amer.*, 89, 1558-1574
- Deng J, and L.R. Sykes (1997). Evolution of the stress field in southern California and triggering of moderate-size earthquakes: A 200-year perspective, *J. Geophys. Res.* 102, 9859-9886.
- Freed, A. M. and J. Lin (1998). Time- dependent changes in failure stress following thrust earthquakes. *J. Geophys. Res.*, 24300-24300xx
- Fuentes, C. (1997). Determinación de la estructura cortical para el sur de México utilizando dispersión de ondas superficiales. *MS dissertation, UNAM, México.*
- Futterman, W.I. (1962). Dispersive body waves. *J. Geophys. Res.* 67, 5279-5291.
- Hartzell S. H. and T.H. Heaton (1983). Inversion of strong ground motion and teleseismic waveform data, for the fault rupture history of the 1979 Imperial Valley, California, earthquake. *Bull. Seism. Soc. Am.*, 76, 1553-1583.
- Harris, R. (1998). Introduction to special section: stress triggers, stress shadows, and implications for seismic hazards, *J. Geophys. Res.* 103, 24347-24358.

Helmberger, D. (1974). Generalized ray theory for shear dislocations. *Bull. Seism. Soc. Am.*, 64, 45-64.

Iwan, W.D., M.A. Moser and C. Peng (1985). Some observations of strong-motion earthquake measurement using a digital accelerograph, *Bull. Seism. Soc. Amer.*, 75, 1225-1246.

King, G.C.P., R.S. Stein, and J.Lin (1994). Static stress changes and the triggering of earthquakes, *Bull. Seism. Soc. Am.* 84, 935-953,.

Langston, C. and D. Helmberger (1975). A procedure for modelling shallow dislocation sources. *Geophys. Journ. Roy. Astr. Soc.*, V. 42, 117-130.

Lawson C.L. and R.J. Hanson (1974). Solving least squares problems. *Ed. Prentice Hall Inc.*, Englewood Cliffs, New Jersey, 340p.

Menke, W. (1989). Geophysical data analysis: Discrete inverse theory. *Ed. Academic Press Inc.*, San Diego, CA., USA, 289p.

Mikumo, T. S.K. Singh and M.A.Santoyo (1999) A possible stress interaction between large thrust and normal faulting earthquakes in the mexican subduction zone. *Bull. Seism. Soc. Am.*, 89, 6, 1418-1427.

Mikumo, T., M.A. Santoyo and S.K. Singh (2000). Dynamic rupture and stress change in normal faulting earthquakes in subducting Cocos plate. *Geophys. J. Int.*, 140, 611-620.

Nabelek, J.L. (1984). Determination of earthquake source parameters from inversion of body waves. *PhD. dissertation*, Massachusetts Institute of Technology, Cambridge, Mass.

Okada, Y. (1985). Surface deformation due to shear and tensile faults in a half space, *Bull. Seism. Soc. Am.* 75, 1135-1154.

Okada, Y. (1992). Internal deformation due to shear and tensile faults in a half space, *Bull. Seism. Soc. Am.* **82**, 1018-1040.

Singh, S.K., J. Havskov and L. Astiz (1981). Seismic gaps and recurrence periods of large earthquakes along the Mexican subduction zone. *Bull. Seim. Soc. Am.*, **71**, 827-843.

Singh, S.K., M. Ordaz, L. Alcantara, N. Shapiro, V. Kostoglodov, J. Pacheco, S. Alcocer, C. Gutierrez, R. Quaas, T. Mikumo, and E. Ovando (2000). The Oaxaca earthquake of September 30, 1999 (Mw=7.5): A normal faulting event in the subducted Cocos plate. *Seism. Res. Lett.*, **71**, 67-78.

Stein, S. (1999). The role of stress transfer in earthquake occurrence, *Nature*, **402**, 605-609.

Stein, R.S., G.C.P. King, and J. Lin (1994). Stress triggering of the 1994 M=6.7 Northridge, California earthquake by its predecessors, *Science*, **265**, 1432-1435.

Toda S., R. S. Stein, P. A. Reasenberg, J. H. Dieterich, and A. Yoshida (1998). Stress transferred by the 1995 Mw=6.9 Kobe, Japan, shock: Effect on aftershocks and future earthquake probabilities, *J. Geophys. Res.* **103**, 24543-24565.

UNAM Seismology Group (1986). The september 1985 Michoacan earthquakes: Aftershock distribution and history of rupture, *Geophys. Res. Lett.* **13**, 573-576.

## FIGURE CAPTIONS

Figure 1. Map of the epicentral region of the 11/01/1997 earthquake. Local strong motion stations are indicated by solid triangles. CALE= Caleta de Campos; VILD= La Villita; INPT= Infiernillo; UNIO= La Unión. The mainshock epicenter is shown by a solid star. Aftershocks are shown by solid dots. The projection of the fault plane on the surface is shown as a solid line almost parallel to the coast. Aftershocks area of the 1985 Michoacan earthquake is shown with a closed dotted line (UNAM Seismology Group, 1986). Line A-A' indicate the location of the cross section plane for stress computations (see text). *Inset*: Tectonic setting for the south Pacific coast of Mexico. PA= Pacific plate; CO= Cocos plate; RV=Rivera plate; continental Mexico belongs to the North America plate. The location of the epicentral region is indicated by a rectangle.

Figure 2. World map showing, the teleseismic stations used in this study.

Figure 3. S waveform displacements in the transverse component, obtained at NNA and FFC stations from the 11/01/97 mainshock. Note a shortened S wave pulse at station NNA (solid line) located southeast of the epicenter, and the broadened pulse at station FFC (dashed line) located northwest of the epicenter.

Figure 4a. RMS errors for the teleseismic inversion vs directivity azimuth of a line source with horizontal rupture propagation. The lowest RMS corresponds to an azimuth of  $105^\circ$ .

Figure 4b. RMS errors for the teleseismic inversion vs rupture velocity for a line source with horizontal rupture propagation, with an azimuth of  $105^\circ$ . The lowest RMS errors occur for values of  $R_v$  between 2.7 and 2.9 km/sec.

Figure 5a. Focal mechanism and P waveforms fit for the 11/01/97 mainshock, obtained from the teleseismic inversion. Recorded waveforms are shown by solid lines, and synthetic seismograms are shown by dashed lines. Stations are shown located in the lower focal hemisphere with open circles.

Figure 5b. SH wave inversion results from the teleseismic inversion. Recorded waveforms are in solid lines, and synthetic seismograms are shown by dashed lines.

Figure 6. Source time functions for the 11/01/97 mainshock, obtained in this study from three different inversions. Curves A, B, and C indicate source time functions obtained from an idealized line source, 2-D dislocation linear inversion, and joint inversion of local and teleseismic seismograms, respectively. The amplitudes are in dyn-cm/sec.

Figure 7a. Comparison between the recorded (solid lines), and synthetic velocity seismograms (dashed lines) for the four local stations used in this study, for the 2-D kinematic inversion.

Figure 7b. Dislocation pattern obtained from the 2-D kinematic inversion. Slips are shown in cm. The main rupture asperity is located at the S-E portion of the fault plane. Fault plane is viewed from southwest. Depths are given in km. The upper edge of the fault plane is located at a depth of 20 km.

Figure 8. Comparison between the recorded seismograms (solid lines) and the synthetic seismograms (dashed lines), obtained from the joint linear inversion using displacement teleseismic and velocity local data.

Figure 9. Dislocation pattern for the 11/01/97 mainshock obtained from the joint linear inversion using both teleseismic and local data. Slips are shown in cm. The thin line outside the gray contours represents a 50 cm curve.

Figure 10. Coulomb failure stress over the fault plane. Contours are in bars. Black dots indicate the projected aftershock locations over the fault plane.

Figure 11. Cross-section A-A' of Figure 1. Coulomb failure stress is resolved in the direction of the aftershocks focal mechanism. Contours are in bars. Black dots represent the location of the aftershocks projected on plane of the cross-section.

TABLE 1  
Source parameters of the mainshock of 11 January 1997.

Time (H: M: S)	Latitude (°N)	Longitude (°W)	Depth (km)	Mo. (Dyn-cm)	Focal Mech. (Str, Dip, Rake)	Duration (Sec)	Source
20:28:39.6	18.34	102.58	40	$6.06 \times 10^{26}$	292, 82, -106	18.8	1
20:28:25.7	18.25	102.81	13	$5.5 \times 10^{26}$	115, 90, 93	—	2
20:28:25.0	18.72	102.57	31	$4.82 \times 10^{26}$	289, 81, -96	—	3
—	18.25	102.81	40-50	$5.2 \times 10^{26}$	119, 90, 97	17.0	4
20:28:25.7	18.25	102.80	13	$1.12 \times 10^{27}$	278, 10, 73	30.0	5
20:28:29.0	18.06	102.79	35	$4.51 \times 10^{26}$	105, 87, -110	14.0	6

Sources: 1-Harvard University CMT catalog. 2.- NEIC, United States Geological Survey. 3.- Earthquake Research Institute, Tokyo University. 4.- M. Kikuchi, personal communication. 5.- Source time function catalog, University of Michigan. 6.- This work.



TABLE 2.  
Crustal velocity model for the source region

$h^{\dagger}$ (km)	$\alpha^*$ (km/sec)	$\beta^{**}$ (km/sec)	$\rho^{\#}$ (gr/cm <sup>3</sup> )
0.0	5.3	3.35	2.50
4.0	6.0	3.45	2.76
15.0	6.5	3.80	2.84
35.0	7.4	4.27	2.90

Notes: †h= Depth of the upper interface; \*  $\alpha$ = P wave Velocity;  
\*\*  $\beta$ = S wave velocity; #  $\rho$ = Density of the medium

TABLE 3.  
Crustal velocity model for teleseismic receivers

$h^{\dagger}$ (km)	$\alpha^*$ (km/sec)	$\beta^{**}$ (km/sec)	$\rho^{\#}$ (gr/cm <sup>3</sup> )
0.0	6.10	3.52	2.70
60.0	7.80	4.45	3.40

Notes: †h= Depth of the upper interface; \*  $\alpha$ = P wave Velocity;  
 \*\*  $\beta$ = S wave velocity; #  $\rho$ = Density of the medium.

TABLE 4  
Source parameters of the 11/01/97 aftershocks.

Date (Y,M,D)	Lat (°N)	Lon (°W)	Depth (km)	M (Mw)	Focal Mech. (St; Dp; Rk)		
97-01-16	18.095	102.669	33	5.5	310	60	90
97-10-25	18.181	102.659	34	3.9	315	60	80
97-11-20	18.11	102.81	28	4.1	280	40	70
98-01-15	18.105	102.705	30	3.5	280	45	90
00-04-11	18.094	102.663	34	5.3	290	60	95
00-08-09-1	18.073	102.564	32	6.5	294	48	93
00-08-09-2	18.033	102.574	34	5.2	315	85	120
00-08-09-3	18.082	102.673	29	4	289	70	130
00-08-09-4	18.045	102.646	31	4.7	280	70	110
00-08-09-5	18.063	102.638	31	4.5	270	55	95
00-08-09-6	18.072	102.628	37	3.9			
00-08-10	18.073	102.562	39	4.5	280	65	120
00-08-12	18.066	102.668	32	3.5			
00-08-13-1	18.073	102.609	34	4.6	300	65	130
00-08-13-2	18.073	102.658	36	4.1	305	70	90
00-08-14	18.085	102.615	37	4.4	270	65	125
00-11-27	18.055	102.636	32				
00-08-18	18.119	102.652	31	3.6	310	70	80
00-12-01	18.058	102.628	31	5.5	285	70	120

Notes: All focal parameters were calculated from local strong motion data. Lat=Latitude; Lon=longitude; M= Magnitude; St= strike angle; Dp= Dip angle; Rk= Rake angle.

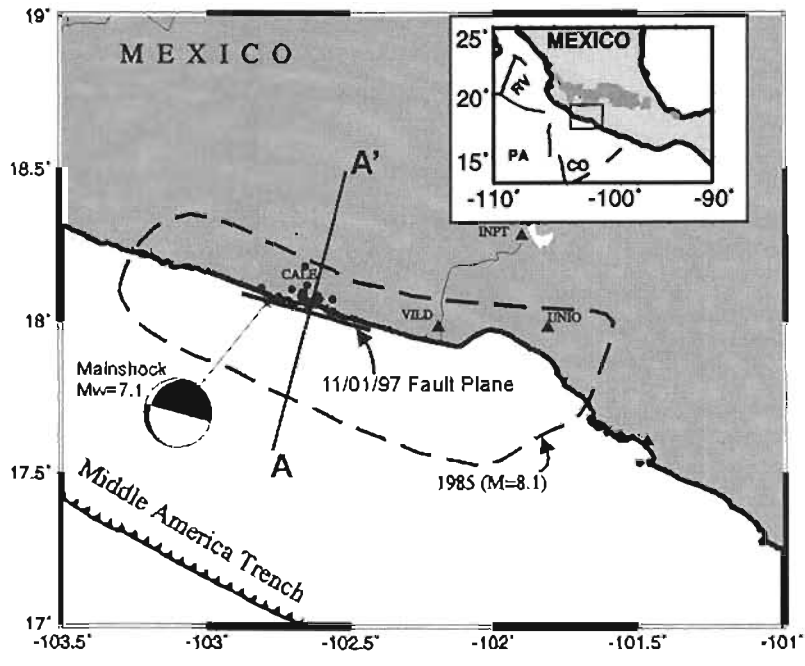


Figure 1



Figure 2

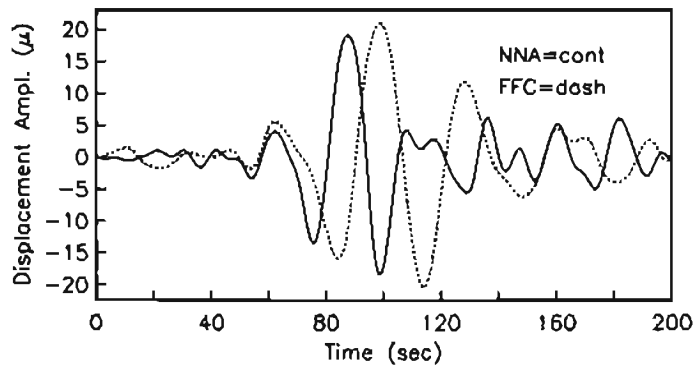


Figure 3

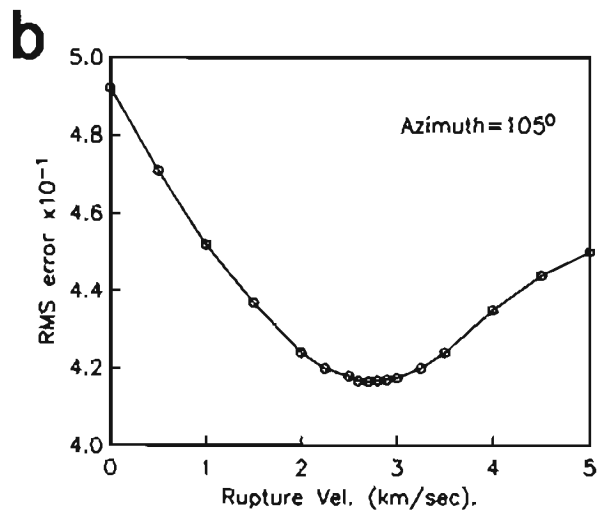
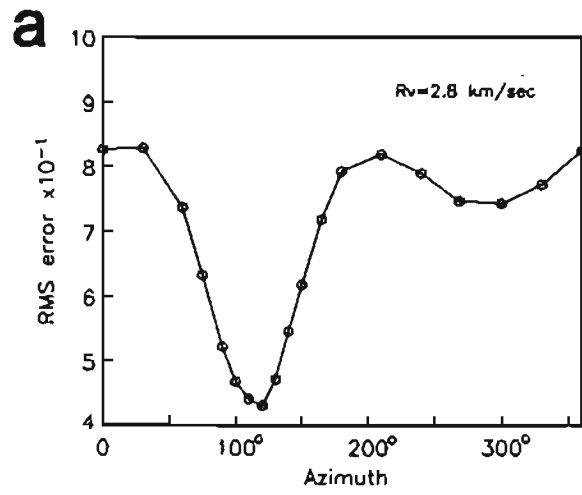


Figure 4

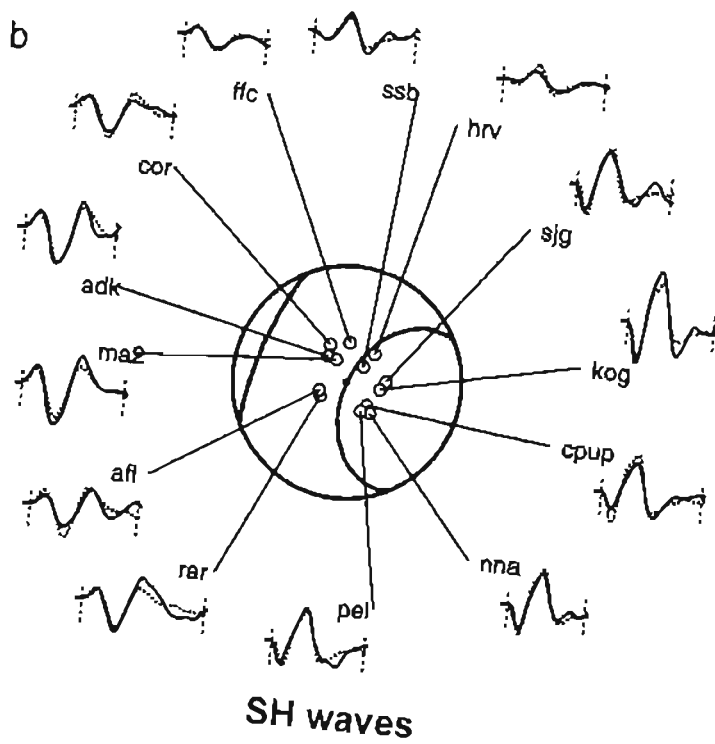
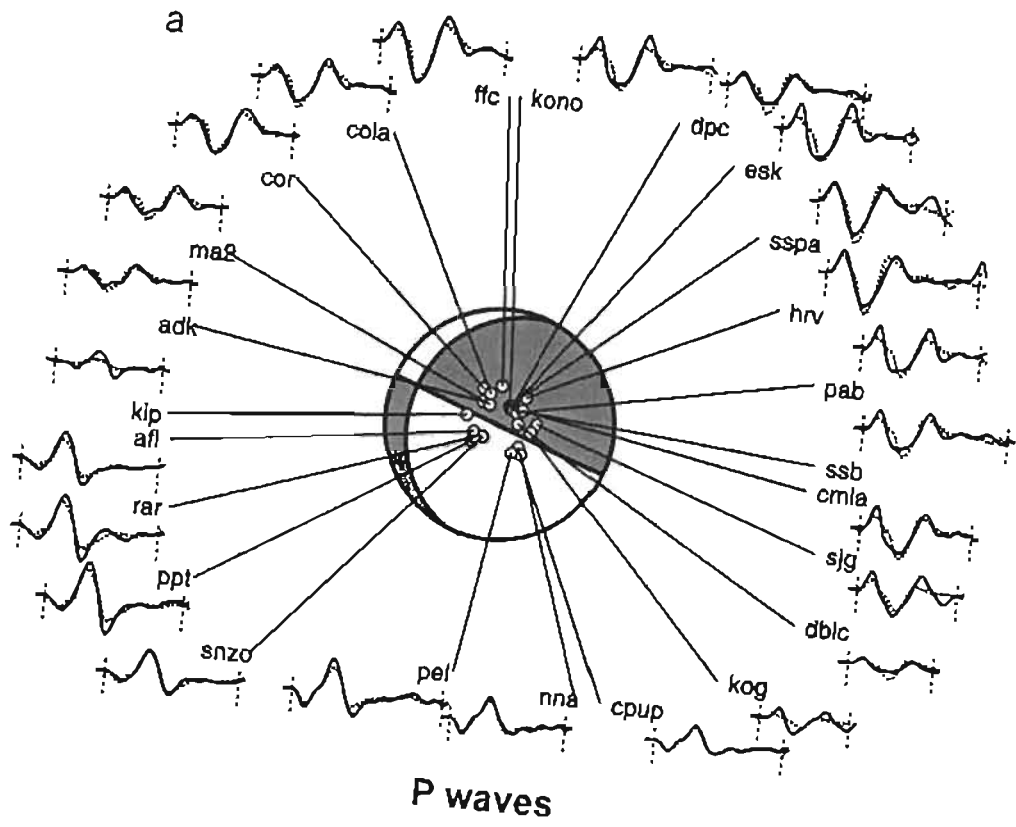


Figure 5



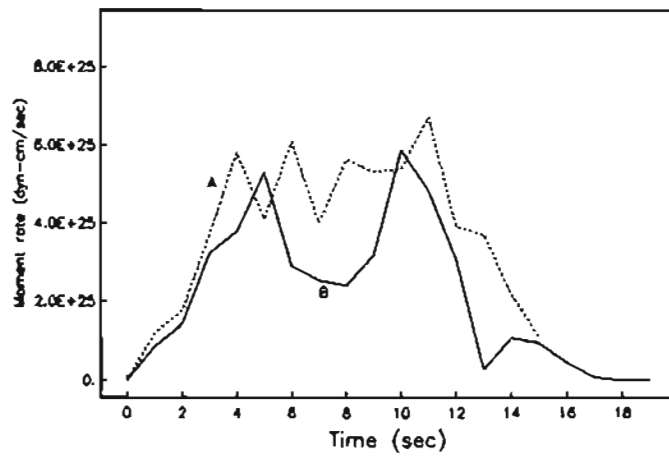


Figure 6

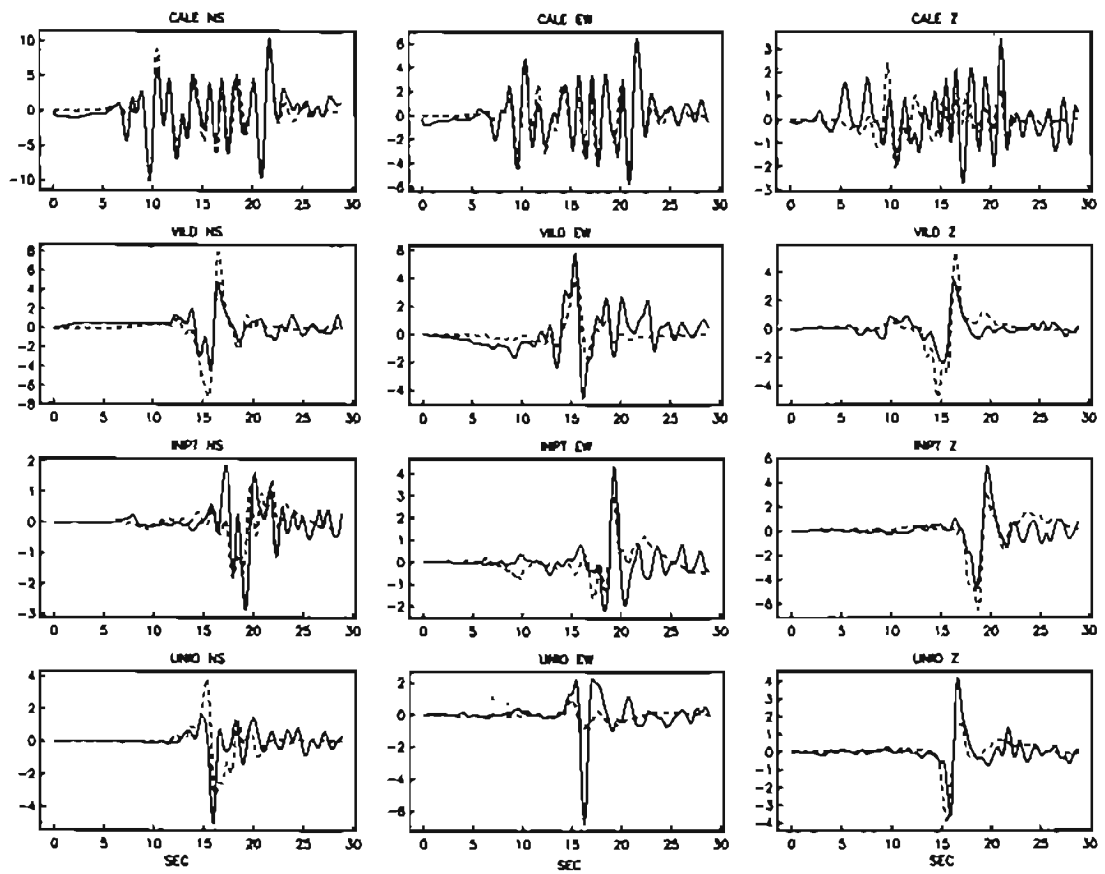


Figure 7a

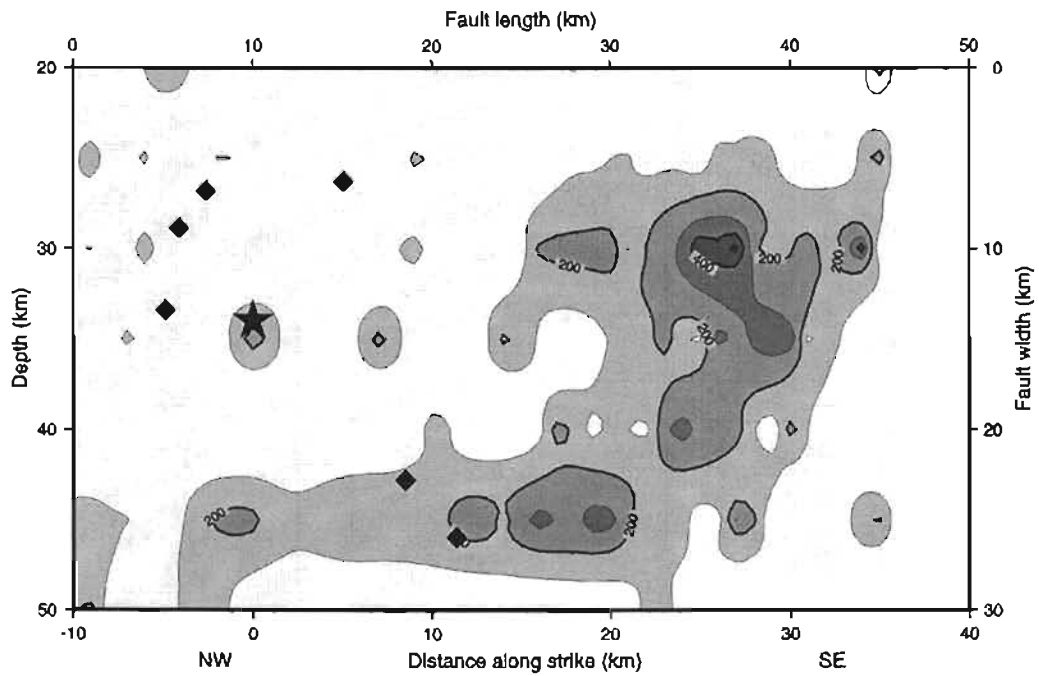


Figure 7b

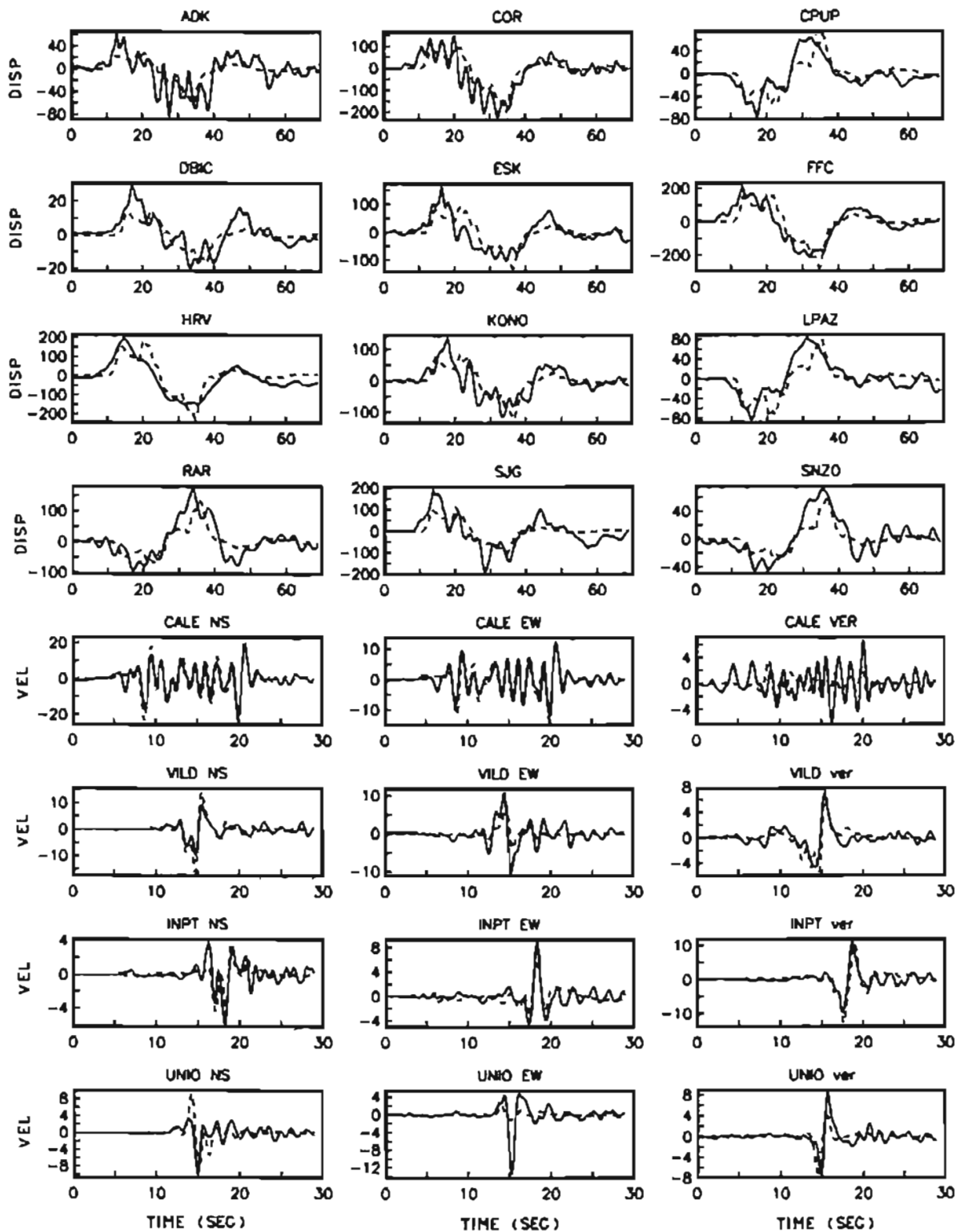


Figure8

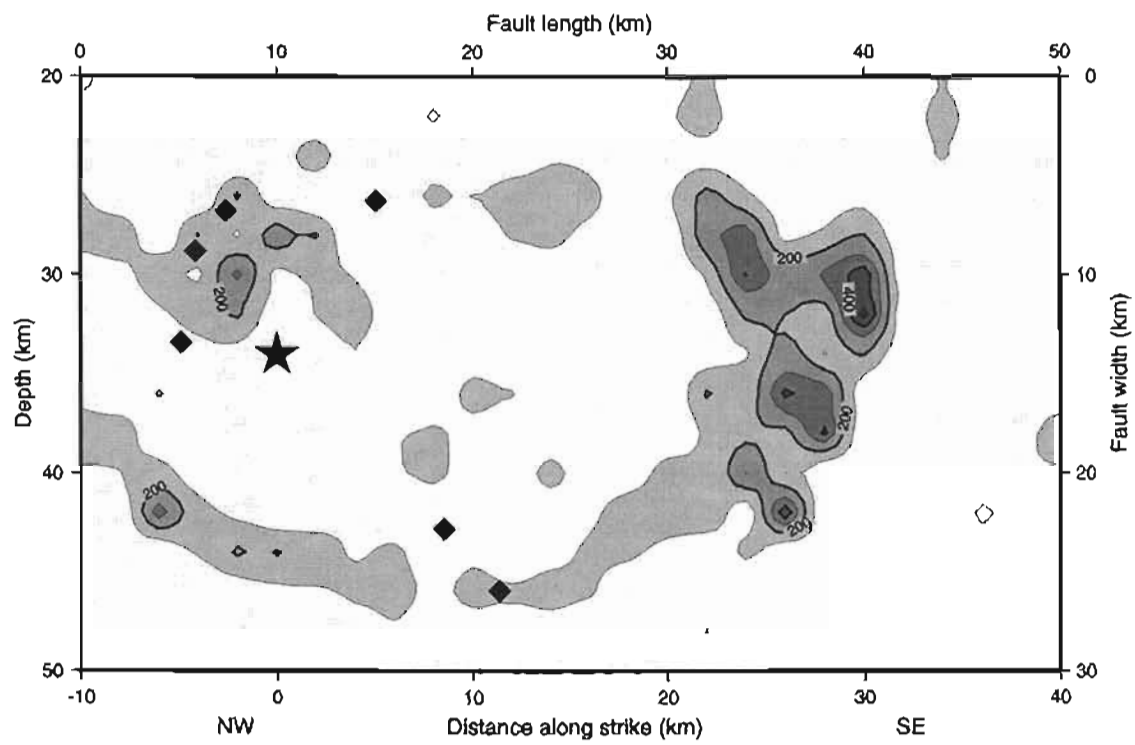


Figure 9

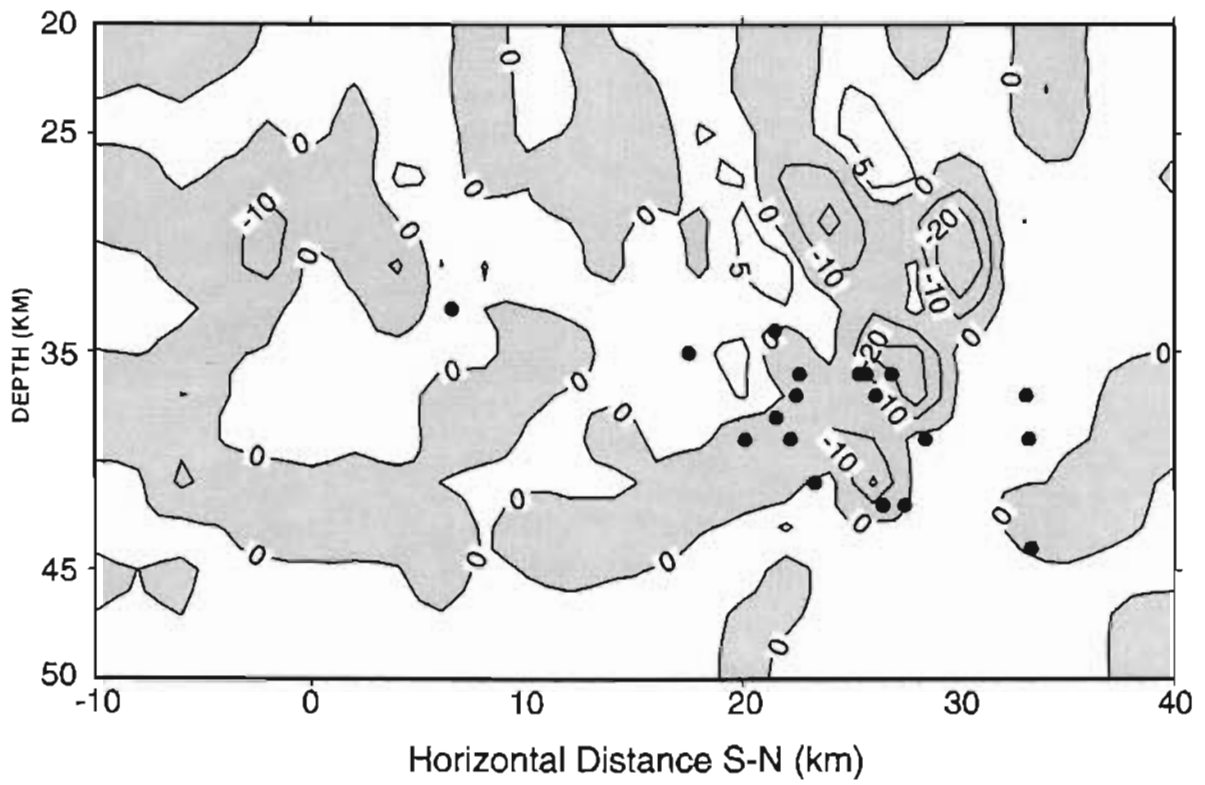


Figure 10

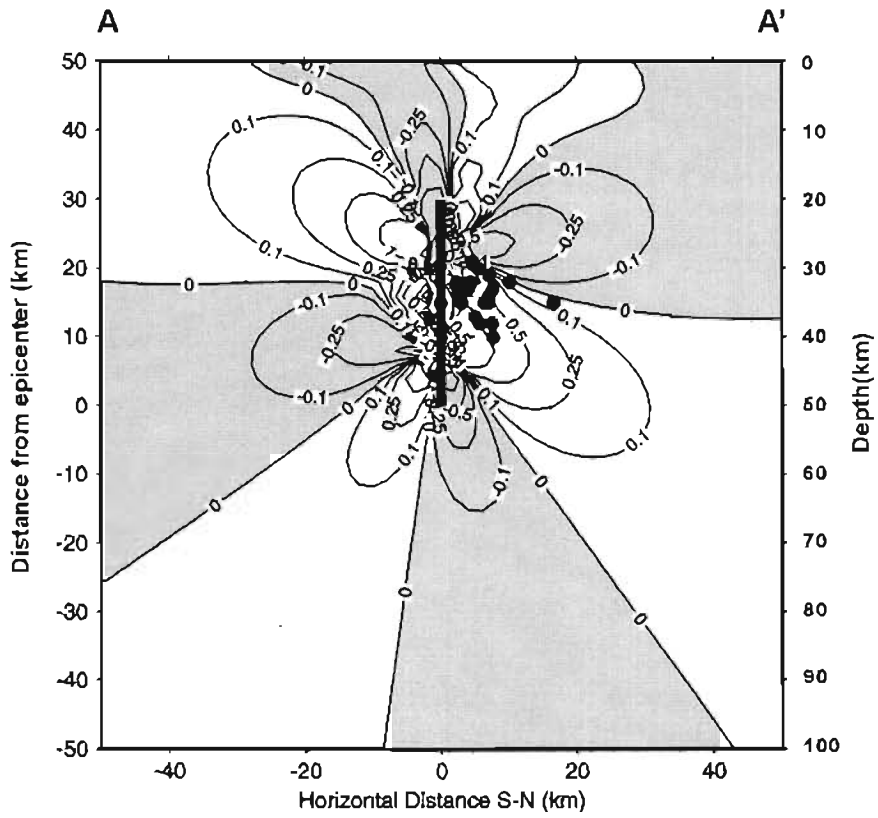


Figure 11

## Capítulo V

POSIBLE INTERACCIÓN DE ESFUERZOS ENTRE UN GRAN SISMO DE SUBDUCCIÓN Y UN SISMO DE FALLAMIENTO NORMAL EN LA ZONA DE SUBDUCCIÓN MEXICANA

# A Possible Stress Interaction between Large Thrust and Normal Faulting Earthquakes in the Mexican Subduction Zone

by Takeshi Mikumo, Shri Krishna Singh, and Miguel A. Santoyo

**Abstract** A large, nearly vertical, normal-faulting earthquake ( $M_w = 7.1$ ) took place in 1997 in the subducting Cocos plate just beneath the ruptured fault zone of the 1985 Michoacan, Mexico, earthquake ( $M_w = 8.1$ ). We investigate the possibility of stress interaction between the two large events through a 3D analysis of coseismic-stress change that was due to the first event, taking into consideration the postseismic change and the dynamic rupture process of the second event. In the middle portion of the subducting plate at depths below 30 km, the calculated coseismic increase in the vertical-shear stress and in the Coulomb-failure stress beneath the high stress-drop zones of the 1985 earthquake is in the order of 0.4 to 0.8 MPa. It was also found that the 1997 earthquake took place in the zone of maximum coseismic-stress increase. Possible postseismic-stress changes due to the subduction process or to the loading of the overriding continental lithosphere and from aseismic slip would enhance the coseismic-stress change and hence the possibility of occurrence of a normal-faulting earthquake in the subducting plate. The dynamic rupture pattern of the 1997 event seems to be consistent with the inferred stress interactions.

## Introduction

A large, nearly vertical, normal-faulting earthquake ( $M_w = 7.1$ ) occurred on 11 January 1997 beneath the Michoacan segment of the Mexican subduction zone (Santoyo *et al.*, 1999). Although intermediate-depth, normal-faulting events occur relatively frequently in the Cocos plate, which subducts beneath the Mexican continent (e.g. Singh *et al.*, 1985; Pardo and Suarez, 1995; Cocco *et al.*, 1997), the location of the present earthquake is quite unusual because it took place just beneath the extensively ruptured fault zone of the great 1985 Michoacan, Mexico earthquake ( $M_w = 8.1$ ) on 19 September 1985.

Large lithospheric normal-faulting earthquakes also occur in several other subduction zones: Sanriku (Kanamori, 1971) and Shioya-oki (Abe, 1977), northeastern Japan, west Shikoku (Shiono and Mikumo, 1975), Mariana (Yoshida *et al.*, 1992), Rat Islands, Aleutian (Abe, 1972a), northern Peru (Abe, 1972b), northern Chile (Kausel and Campos, 1992); Sumba (Spence, 1986; Lynnes and Lay, 1988), and Tonga (Eissler and Kanamori, 1982; Spence, 1986; Christensen and Lay, 1988; Lundgren and Okal, 1988). Most of the aforementioned earthquakes that occurred in a partially decoupled plate were interpreted to be caused by tensile stress due to the gravitational pull of the denser subducting slab, rupturing nearly the entire plate thickness. Some of these reported events took place in the updip portion of the slab a few days to several years after a large thrust earthquake, which seems to have ruptured the coupled interface. In the Mexican sub-

duction zone, on the other hand, some normal-faulting earthquakes took place in the downdip portion up to ten years following the occurrence of large shallow-thrust events (Singh *et al.*, 1985; Cocco *et al.*, 1997). However, the causal relationship between the two types of earthquakes, if any, is not well understood (Singh *et al.*, 1985).

The 1997 earthquake with a nearly vertical fault plane (Santoyo *et al.*, 1999) was located right below the ruptured zone of the 1985 large-thrust event (Fig. 1a, b), while other normal-faulting earthquakes took place near the trench or the outer rise farther updip of the thrust plane, or some far downdip. The goal of the present study is to find if there is any possible stress interaction between the two recent earthquakes in the Mexican subduction zone. We apply a 3D stress analysis and make some qualitative considerations on possible postseismic stress changes. We will show that the stress transfer from the 1985 earthquake down to the subducting plate could be one of possible sources that enhance the possibility of occurrence of the 1997 earthquake.

## Model and Method of Calculations

One useful method to investigate a possible stress interaction between any two events is to estimate the coseismic stress change caused by the first event near the fault zone of the second event and its postseismic change up to the time of the latter event.



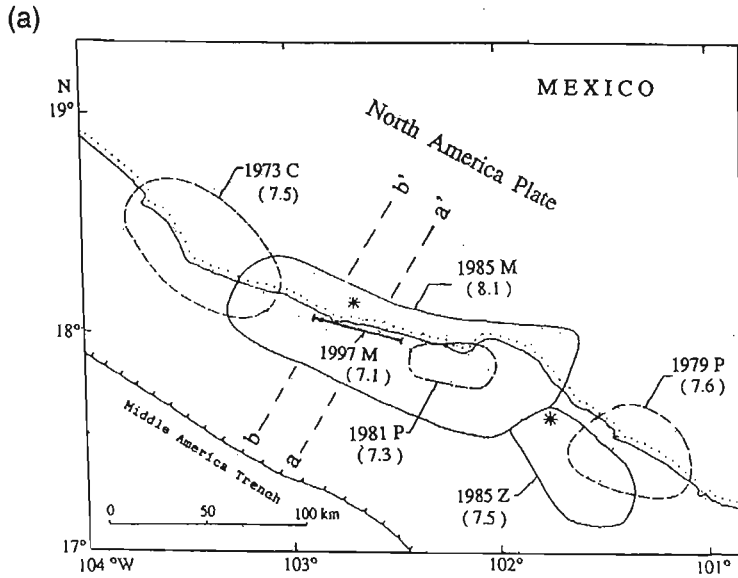
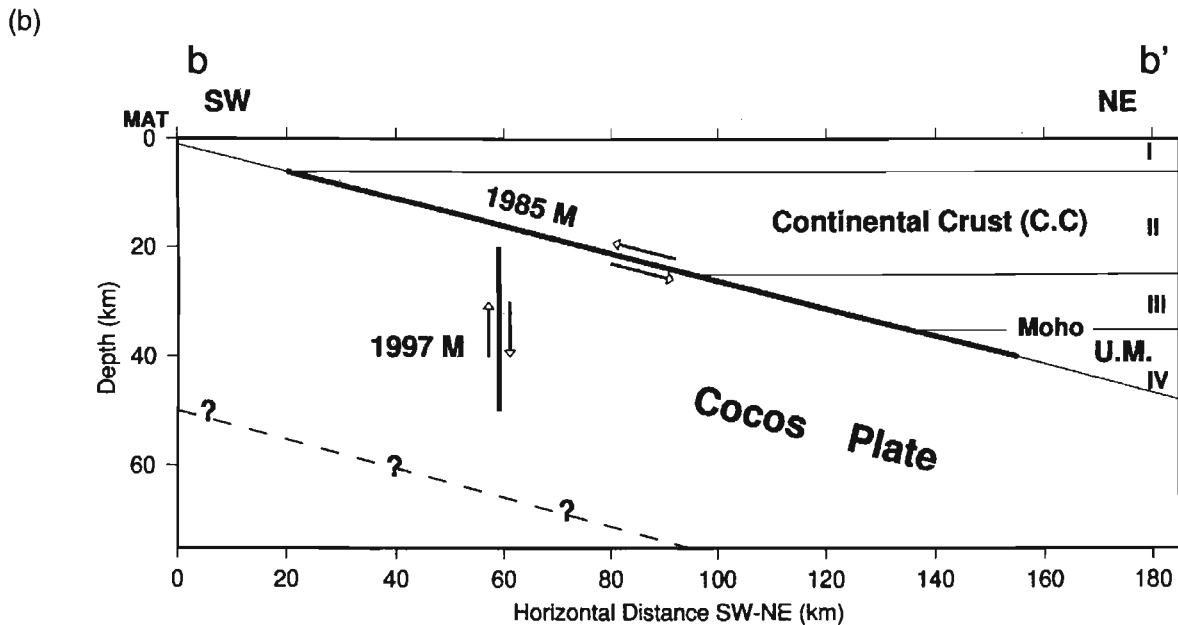


Figure 1. (a) Location of the 1997 earthquake (Santoyo *et al.*, 1999) and the aftershock areas of recent large earthquakes in the Michoacan-Guerrero regions of Mexico (modified from UNAM Seismology Group, 1986). Their magnitudes in parentheses are given in *Ms*. (b) Schematic side view of the 1985 thrust event and the 1997 normal fault, which are indicated by bold lines, with respect to the subducting Cocos plate and the overlying continental crust (C.C.) and uppermost mantle (U.M.). The velocity and density structures with layer indices are given in Table 1.



We calculate here the coseismic change of all stress components due to the 1985 thrust earthquake, not only on the fault but in the subducting plate and the overlying continental crust and uppermost mantle. The model used here is an extension of a 3D dynamic-rupture model (Mikumo *et al.*, 1998) and incorporates a shallow-dipping fault located above the subducting plate, which is embedded in a horizontally layered half-space (Fig. 2a, b). The method of calculation essentially follows the previous approach (Mikumo and Miyatake, 1993; Mikumo *et al.*, 1998). In this method, all displacement and stress components in the 3D model space and dynamic-rupture propagation on the fault are calculated by solving elastodynamic equations under appropriate boundary conditions, with a second-order finite-differ-

ence scheme. We assume that the initial shear stress is applied parallel to the dipping fault (see Figure 2b) and that it gradually increases due to the approach of the rupture front and drops immediately to the level of dynamic friction at the time of rupture arrival, when it exceeds the prescribed peak stress level. The difference between the initial and final stresses is taken as static-stress drop. The boundary conditions to be satisfied are (1) the continuity of the normal stress and displacement components across the fault, (2) the traction-free ground surface, (3) the continuity of all stress and displacements components at each of the layer interfaces, and (4) absorbing boundary conditions (Clayton and Engquist, 1977) at the side and the bottom boundaries of the model space.

(a)

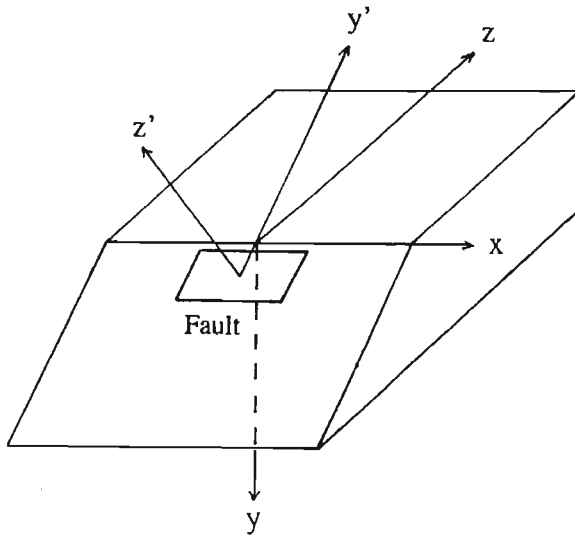
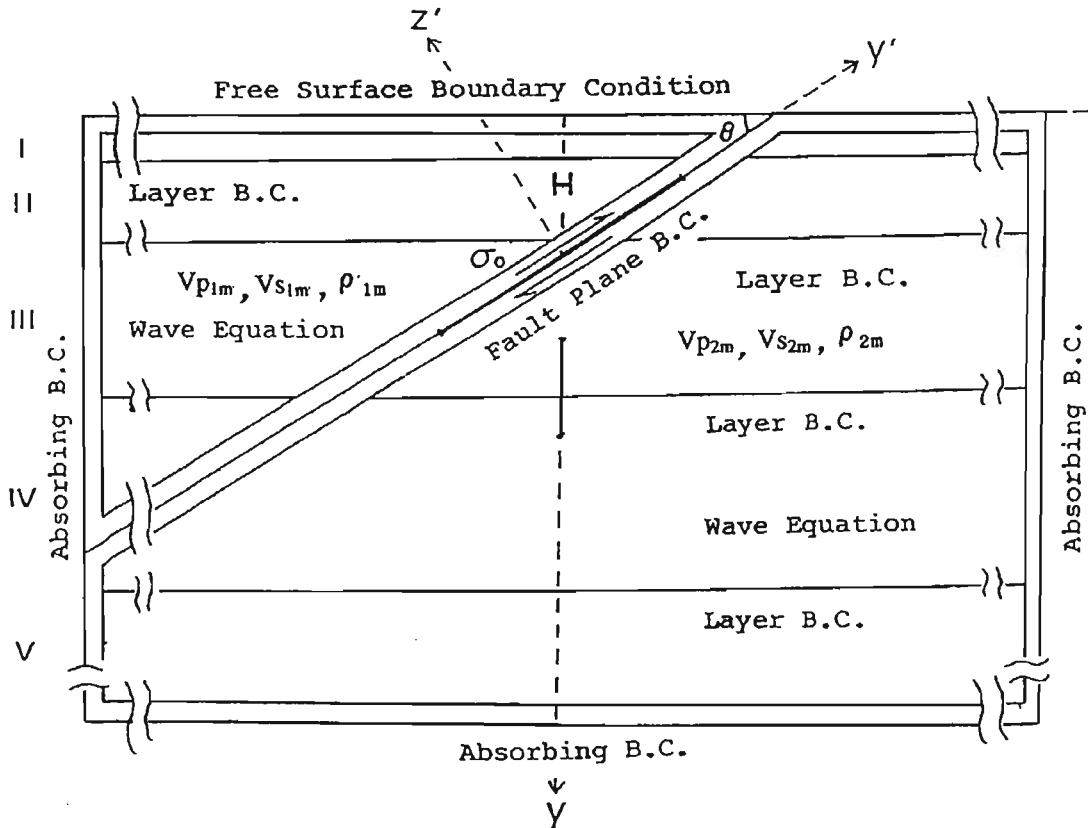


Figure 2. (a) Location of a dipping fault and the 3D model used here with the coordinate axes illustrated. (b) Side view of the 3D model space incorporating a horizontally layered-velocity structure (modified from Mikumo and Miyatake, 1993).

(b)



To evaluate the spatial distribution of dynamic- and static-stress changes, we use a nonlinear, iterative least-squares technique by incorporating some of the kinematic fault parameters as observational constraints. Given approximate estimates of static-stress drop on the fault plane as starting values, we calculate the distribution of fault slips

from the above dynamic model and compare them with the previously obtained kinematic slips. The ratio between the kinematic and dynamic slips at each point on the fault is then multiplied to the previously estimated stress drop in the next iteration. This procedure is repeated until the rms difference between the kinematic and dynamic slips over the

fault can be minimized within a reasonably small value, which gives a best-fitting model. The distribution of dynamic- and static-stress changes on the fault as well as in the model space are obtained from the final model. (For more details, see Mikumo and Miyatake, 1993; Mikumo *et al.*, 1998).

The spatial distribution of dynamic- and static-stress drops over the fault plane of the 1985 Michoacan thrust earthquake has been evaluated (Mikumo *et al.*, 1998) in this way from the distribution of kinematic fault slip (Mendoza and Hartzell, 1989) based on waveform inversion of strong-motion records. The present calculation, incorporating the same observations, uses a finer grid spacing (5.0 km on the fault, 1.25 km in the vertical direction, and 4.85 km in the horizontal direction for a fault dip of 14°). The extent of the 3D model space is taken as 350 km × 105 km × 240 km in the x, y, and z directions, respectively (Fig. 2).

The crust and uppermost mantle structure assumed here is taken from a 3-layer velocity model (Mendoza and Hartzell, 1989) which is given in Table 1. Since this model has been used by Mendoza and Hartzell to derive the distribution of kinematic slips on the 1985 earthquake fault, we also use it in calculating the corresponding stress change. However, a more refined structure in the Michoacan region (Valdes and Meyer, 1996) shows slightly higher velocities (5–10%) in the subducting Cocos plate overridden by oceanic crusts with slightly lower velocities. For this reason, we performed the present calculations by assuming elastic wave velocities and densities which are 0, 5, and 10% higher in the subducting slab than in the overlying crust and uppermost mantle at the same layer (Table 1, Figs 1b and 2b). The effects of this velocity contrast on our results are described in the next section. The results shown in the figures that follow correspond to the first case.

## Results

Although the calculation provides dynamic changes of all stress components during the rupture process of the 1985 event, here we are looking only at the final values (i.e., static-stress changes) of four stress components (see Figure 2 for the coordinate system);  $\Delta\sigma_{y'z'}$  (shear stress along the dipping fault),  $\Delta\sigma_{y'y'}$  (compressional stress along the direction parallel to the fault),  $\Delta\sigma_{yz}$  (shear stress in the vertical direction), and  $\Delta\sigma_{zz}$  (horizontal tensional stress). The value  $\Delta\sigma_{yz}$  corresponds to the change in shear stress due to the 1985 event, resolved into the vertical-fault direction of the 1997 event, and  $\Delta\sigma_{zz}$  corresponds to the change in normal stress due to the 1985 event in the direction perpendicular to the 1997 fault. These two components constitute the well-known Coulomb stress  $\Delta\sigma_{cfs} = \Delta\sigma_{yz} + \mu' \Delta\sigma_{zz}$ , where  $\mu'$  is the apparent coefficient of friction for the effective confining pressure, that is, the difference between the normal stress and the fluid-pore pressure (King *et al.*, 1994). Since the most appropriate value of  $\mu'$  is still not well known, we take three different values of  $\mu' = 0.0, 0.4, \text{ and } 0.6$ . In the case

Table 1  
Crust and Uppermost Mantle Velocity Model used in This Study  
(after Mendoza and Hartzell, 1989)

Layer (m)	H(km)	$V_p$ (km/sec)	$V_s$ (km/sec)	$\rho$ (g/cm <sup>3</sup> )	$c_m$
I	0	5.80	3.35	2.68	1.00, 1.05, 1.10
II	6	6.40	3.69	2.78	1.00, 1.05, 1.10
III	25	7.00	4.04	2.85	1.00, 1.05, 1.10
IV	35	8.00	4.62	3.00	1.00, 1.05, 1.10

m, layer index number; H, top depth of the m-th layer;  $V_p$ , P-wave velocity;  $V_s$ , S-wave velocity;  $\rho$ , density;  $c_m = V_{p2m}/V_{p1m} = V_{s2m}/V_{s1m} = \rho_{2m}/\rho_{1m}$  (1 and 2 correspond to the portions of the overlying crust and uppermost mantle and the subducting slab, respectively).

of  $\mu' = 0$ ,  $\Delta\sigma_{cfs} = \Delta\sigma_{yz}$ . The Coulomb failure stress criterion has been widely used to predict possible regions of subsequent failure and aftershock locations of crustal earthquakes, as recently summarized by Harris (1998).

Figure 3 shows the distribution of stress change  $\Delta\sigma_{y'z'}$  over the fault plane (180 km × 140 km, dipping at 14° toward north-northeast) of the 1985 earthquake. Four high stress-drop (stress decrease) zones corresponding to the rupture of existing asperities can be identified; two of them are located in the relatively shallow fault section, and the other two are in the deeper part. The maximum stress drop exceeds 130 bars. The negative stress drop (coseismic stress increase) zone spreads around and in between the high stress-drop zones. The coseismic stress change  $\Delta\sigma_{y'z'}$  on two vertical profiles, a-a' and b-b' in Figures 1a and 3 is shown in Figure 4. The profiles a-a' and b-b' go across the portion of the maximum stress drop on the 1985 fault and the hypocenter of the 1997 earthquake, respectively. Note that this shear stress component decreases below and above the upper half of the dipping fault both in the subducting slab and in the overlying crust, while it increases below some depth in the middle portion of the slab and also near the updip and downdip portions of the plate interface. These patterns are similar for the two profiles. Figure 5 gives coseismic change  $\Delta\sigma_{y'y'}$  along the two profiles, which clearly shows, as expected, the zones of compressional stress increase updip above the thrust plane and in the middle and downdip below the plane, while the zone of stress decrease can be recognized updip below the thrust plane and downdip above the plane.

The coseismic changes in shear stress  $\Delta\sigma_{yz}$  and in the Coulomb failure stress  $\Delta\sigma_{cfs}$  ( $\mu' = 0.4$ ) along the two profiles are shown in Figure 6a and b. The patterns of their distribution are quite similar to those in Figure 4 and are mainly characterized by three zones of stress increase and stress decrease, which appear to be separated by several lobes. Small bumps seen in zero contours may be due to less accuracy of the second-order finite-difference calculations near the contours.

The most remarkable feature is that the shear stress and the Coulomb stress increase in the subducting slab below a depth of about 30 km just beneath the high stress-drop zone of the 1985 thrust event (indicated hereafter by P-zone),

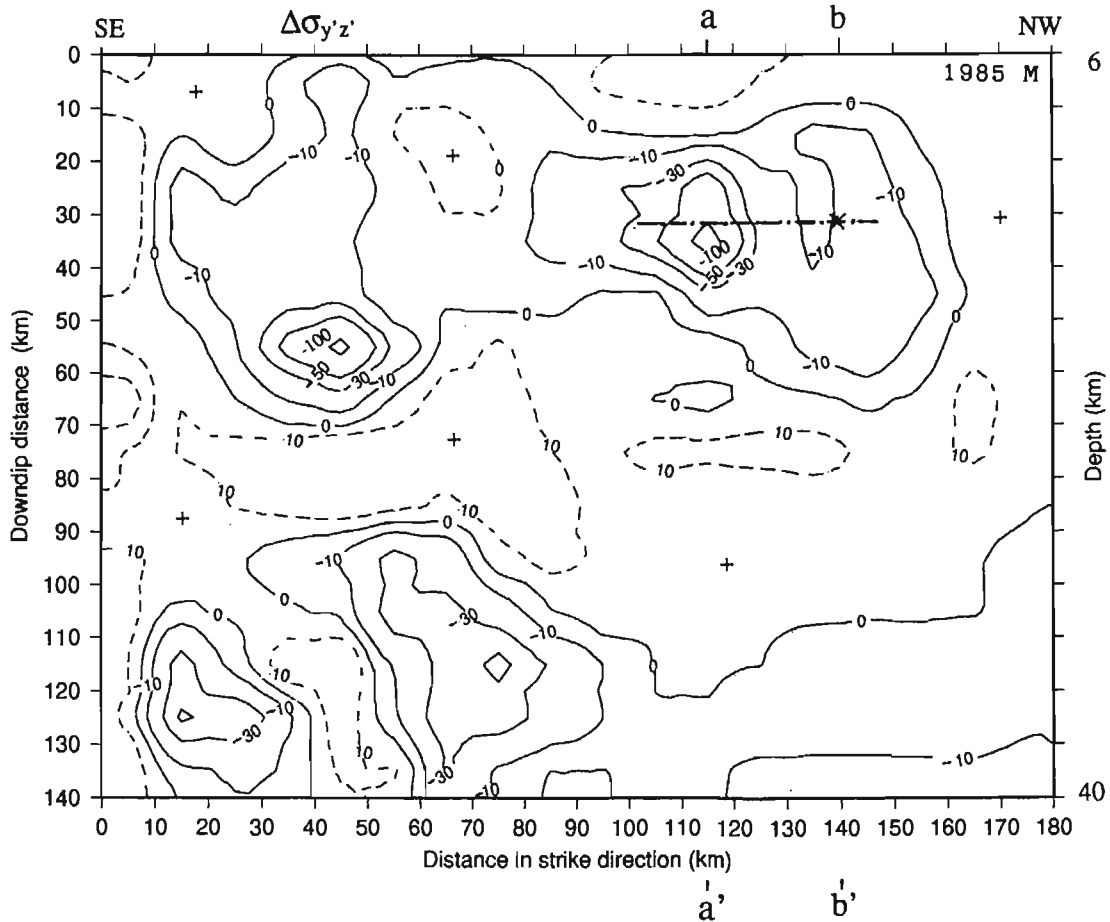


Figure 3. Distribution of the calculated shear stress drop  $\Delta\sigma_{y'z'}$  (in bars) on the fault plane of the 1985 thrust earthquake. Full and broken contours indicate stress decrease and increase, and plus sign denotes the zone of stress increase, respectively. A chain line at a downdip depth of about 30 km shows the location of the 1997 vertical fault projected onto the 1985 thrust fault plane. An asterisk indicates the hypocentral location of the 1997 event. Two profiles a-a' and b-b' are taken to pass through the region of the maximum stress drop and and the hypocenter of the 1997 earthquake.

while the zone of stress decrease obliquely extends down below its updip and downdip portions of the slab. Zones of stress increase also exist near the updip and downdip portions. Incidentally, these patterns are quite similar to those for the failure stress calculated for shallow dipping thrust earthquakes in the upper crust (Freed and Lin, 1998). The maximum magnitude of coseismic stress increase in the P-zone in the middle portion of the subducting slab reaches 8 bars for the profile a-a' (Fig. 6a) and about 4 bars in the b-b' profile (Fig. 6b). The magnitudes do not change significantly for the two cases of  $\Delta\sigma_{yz}$  ( $\Delta\sigma_{cfs}$  for  $\mu' = 0$ ) and  $\Delta\sigma_{cfs}$  for  $\mu' = 0.4$ . For the case of  $\mu' = 0.6$  (not shown here), the P-zone of stress increase spreads more towards the downdip portion of the slab, and its maximum increase exceeds 9 bars. The location of the 1997 vertical fault, which is shown in Figure 1b and indicated by an arrow in Figure 6a and b, has some uncertainty in the horizontal direction,

and the depth of the fault ranges between 20 and 50 km. The starting point of rupture at about 35 km and the major part of the fault are surely located within the P-zone of stress increase. Accordingly, it appears that the 1997 earthquake took place within the contour of the maximum stress increase in the P-zone.

It was found that higher velocities and densities of 10% in the subducting plate enhance the stress changes on the fault (Fig. 3) up to a maximum of about 15% and also enhance the maximum magnitude of stress increase in the P-zone up to about 10 bars and 5 bars (for  $\mu' = 0.4$ ) along the a-a' and b-b' profiles, respectively. However, the actual velocity contrast between the oceanic crust overriding the subducting slab and the overlying crust and uppermost mantle does not reach 10% but seems to be less than 7% at the depth range of the 1985 thrust fault (Valdes and Meyer, 1996). Thus, the magnitude of the stress changes in and

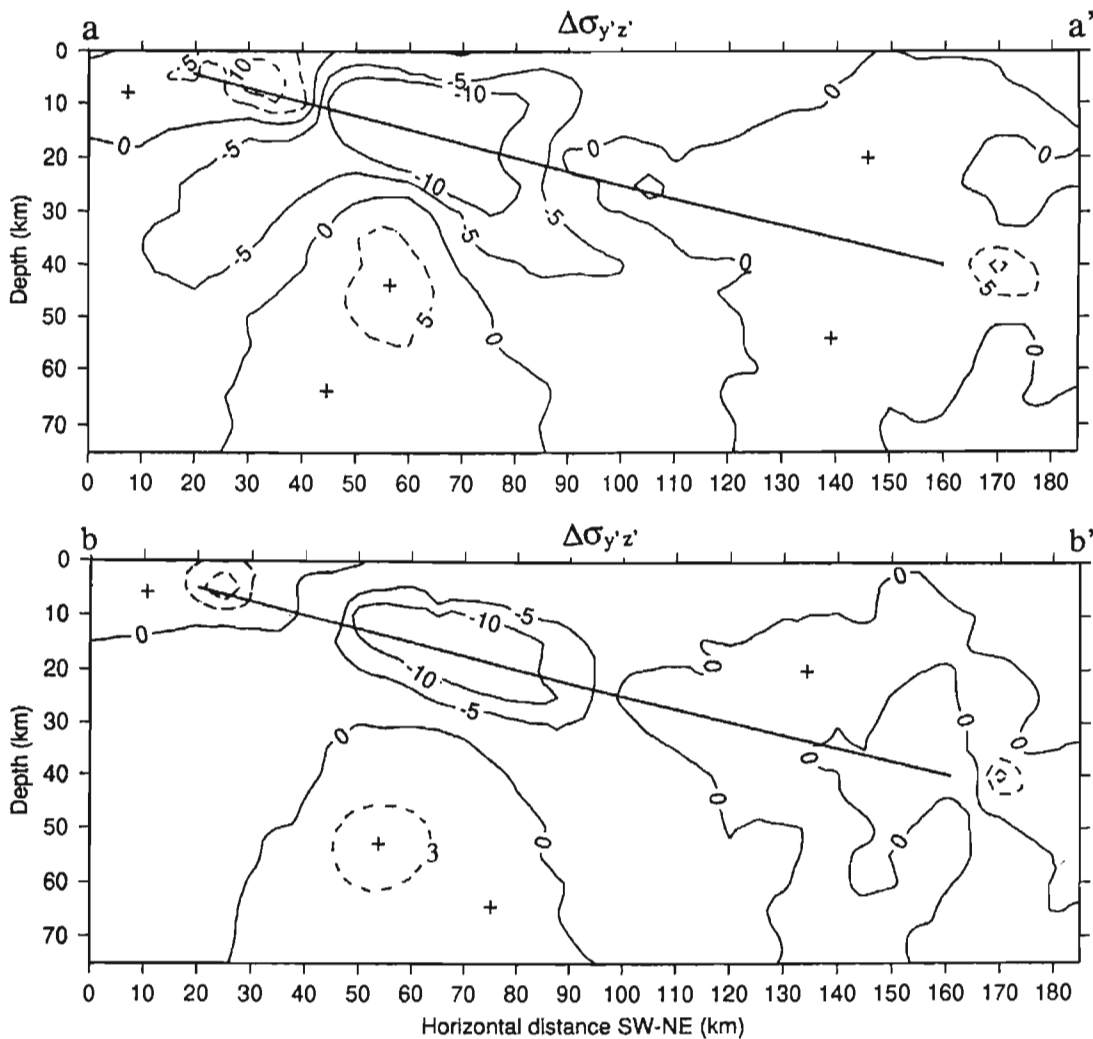


Figure 4. Coseismic changes of shear stress  $\Delta\sigma_{y'z'}$  (in bars) working parallel to the 1985 thrust fault plane, along the two profiles a-a' and b-b' shown in Figures 1a and 3. The bold oblique line indicates the 1985 dipping fault. Full and broken contours indicate stress decrease and increase, and plus and minus signs denote the zones of stress increase and decrease, respectively. The same explanations apply to Figures 5-7.

around the P-zone is not very sensitive to the velocity structure assumed here and does not significantly affect our estimates. Although it is uncertain whether this order of stress increase is large enough to actually trigger the 1997 normal-faulting event 12 years after the 1985 large thrust earthquake, the magnitude is significantly larger than those so far reported (e.g., Harris, 1998). This may be due to the proximity of the two events, the high stress drop in specific-fault zones, and to the much larger fault extent of the 1985 Michoacan earthquake.

Figure 7 shows the calculated coseismic-stress change  $\Delta\sigma_{yz}$  due to the 1985 earthquake over the vertical plane including the 1997 fault (fault length, 50 km; fault width, 30 km at depths between 20 and 50 km). Shear stress in the

upper-fault section dropped to a considerable extent due to the 1985 event, and it increased up to 4 to 5 bars in the lower half of the fault. The zones of stress increase and decrease appear to be separated by an oblique lobe traversing nearly the middepth of the fault. It is interesting to note that high-stress drop and major slip occurred in the lower-fault section during the 1997 earthquake, which suffered a stress increase from the 1985 earthquake; only minor slip and smaller stress drop were observed in the upper-fault zone of the 1997 event, where shear stress has dropped after the 1985 event (Santoyo *et al.*, 1999; Mikumo *et al.*, 1999). This evidence also suggests that the 1997 nearly vertical, normal-faulting earthquake took place under stress transfer from the 1985 thrust earthquake to the subducting plate.

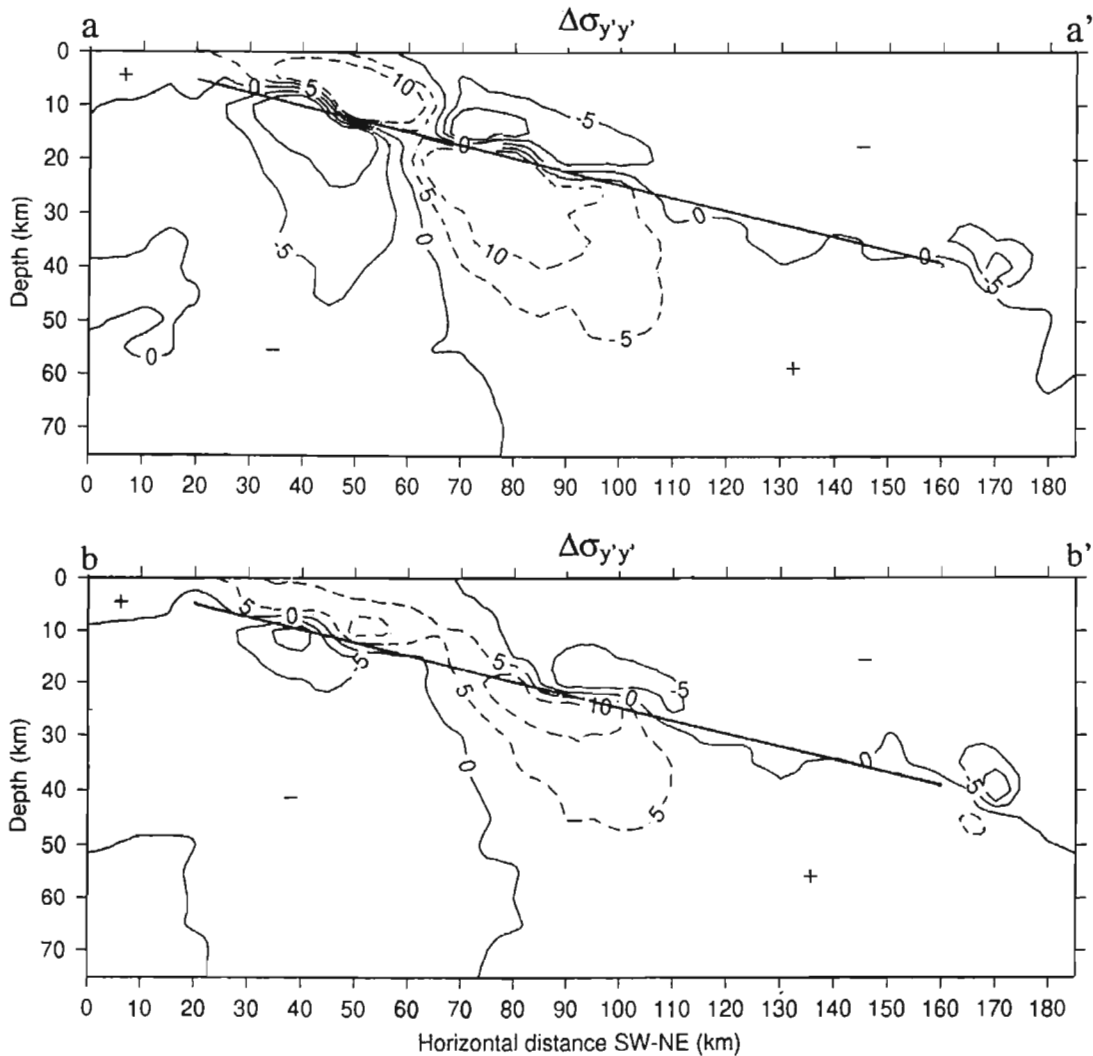


Figure 5. Coseismic changes of compressional stress  $\Delta\sigma_{y'y'}$  (in bars) working parallel to the 1985 thrust fault along the two profiles a-a' and b-b'.

### Discussion

Postseismic stress changes that can affect the pattern of coseismic changes and hence the occurrence of the subsequent earthquake may come from possible aseismic slip on the 1985 fault zone and on the updip or the downdip extension of the fault, viscoelastic relaxation of the overlying mantle and the asthenosphere, and loading of extensional stress due to the subduction process. In this article, we do not calculate these changes but qualitatively discuss their possible effects.

Evidence of further aseismic slip on the 1985 fault has not been detected due to the lack of geodetic observations in the area, although it seems likely to have occurred. If it actually occurred on the same fault with a few tens of percent of the coseismic slip, the postseismic increase in the shear stress in the subducting slab would also be of about this order

of magnitude. This change would add to the estimated coseismic-stress change, and hence enhance the possibility of occurrence of the 1997 event in this zone. If it occurred on some portion of the updip or downdip segment, a small oblique zone of stress decrease similar to that in Figure 6 would extend into the peripheral zone of coseismic stress increase. This would slightly erode its increase or would almost not affect it.

The viscoelastic stress-relaxation process within a subducted slab during thrust earthquake cycles in coupled subduction zones has been discussed on the basis of simple 1D calculations (Dmowska *et al.*, 1988) and 2D finite-element models (Taylor *et al.*, 1996; Gardi *et al.*, 1999) incorporating Maxwellian viscoelasticity. Their results (e.g. Taylor *et al.*, 1996) indicate that the coseismic changes in the uniaxial stress component ( $\Delta\sigma_{y'y'}$  in Figure 5) in the subducting slab just below the thrust zone slowly recovers with time (i.e.,

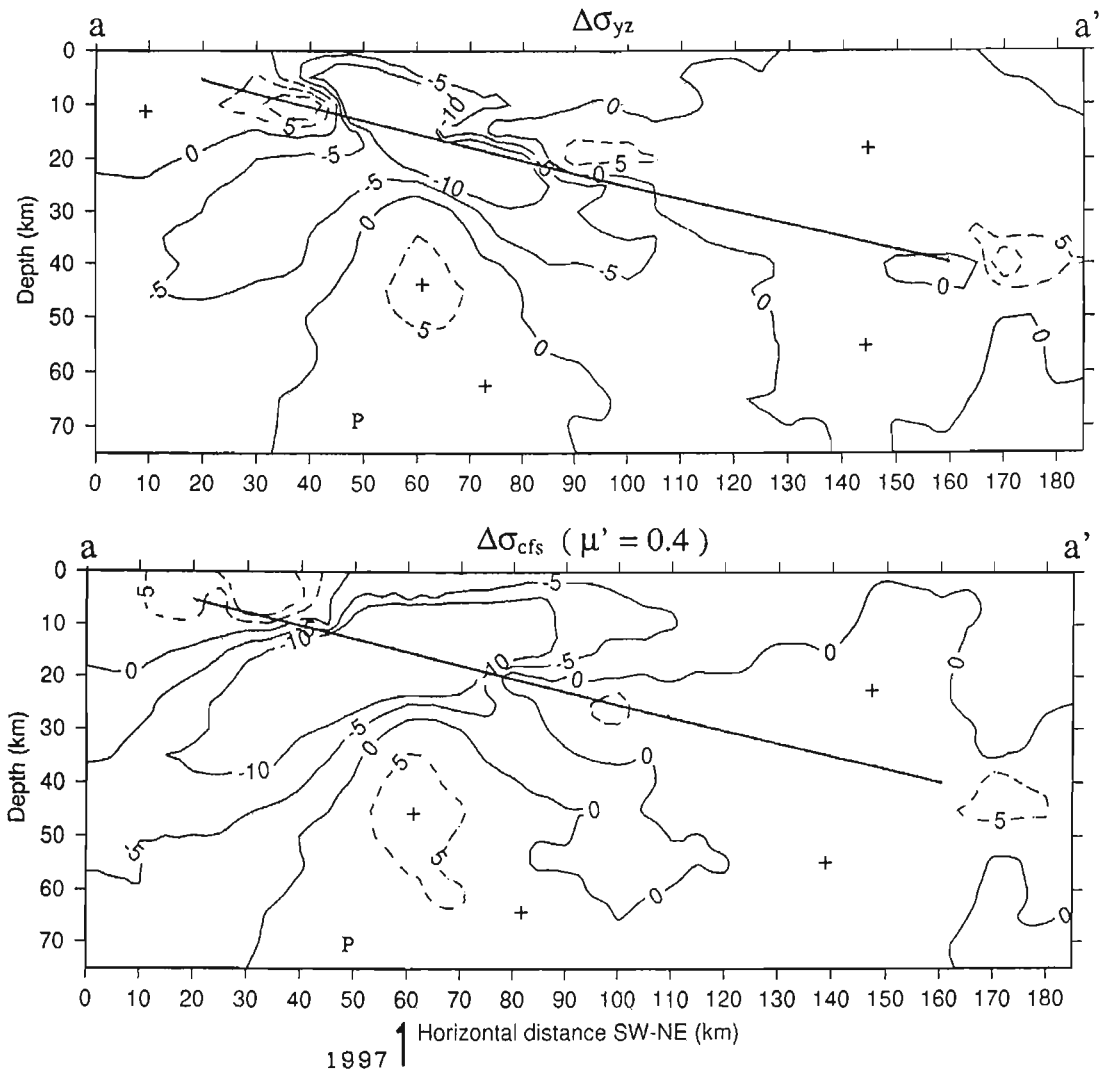


Figure 6. Coseismic changes of the vertical shear stress  $\Delta\sigma_{yz}$  (in bars, top) and the Coulomb failure stress  $\Delta\sigma_{cfs}$  for  $\mu' = 0.4$  (in bars, bottom) due to the 1985 thrust event on two profiles. (a) profile a-a', (b) profile b-b'. An arrow indicates the approximate horizontal location of the 1997 vertical fault. (See also Figure 1b.)

the coseismic, extensional stress change below the updip portion of the thrust plane decreases, and the coseismic, compressional stress change below the downdip portion also decreases with time), but still do not change their sign within the first 15–30% (corresponding to 12 years) of the recurrence time. This implies that the additional extensional stress caused by the 1985 thrust event was still present in the P-zone at the time of the 1997 earthquake. Moreover, the total stress will be dominated by the slab pull due to the subduction process and, hence, would remain extensional at all times (Dmowska *et al.*, 1988; Taylor *et al.*, 1996). Another possible mechanism that could produce tensile stress in such a shallow-dipping, young oceanic lithosphere as in the Mexican subduction zone would be loading of the overriding continental plate decoupled from the subducting plate (Fujita

and Kanamori, 1981; Singh *et al.*, 1985). In any case, this extensional feature would increase  $\Delta\sigma_{yz}$  and  $\Delta\sigma_{cfs}$  in the subducting slab at some depth below the 1985 thrust event.

All the above considerations suggest that the 1985 coseismic-stress increase at some depth below the middle portion of the subducting slab could be enhanced either by the subduction process or by the loading from the continental plate, and also by postseismic slip, if it actually existed.

It is important, however, to mention that the above explanations do not apply to the two normal-faulting events of 1994 that occurred farther downdip of the 1985 thrust zone and near the bottom of the subducting Cocos plate. These events may possibly be related to the unbending of the slab (e.g. Cocco *et al.*, 1997; Gardi *et al.*, 1999). However, the present calculations might give another explanation as to

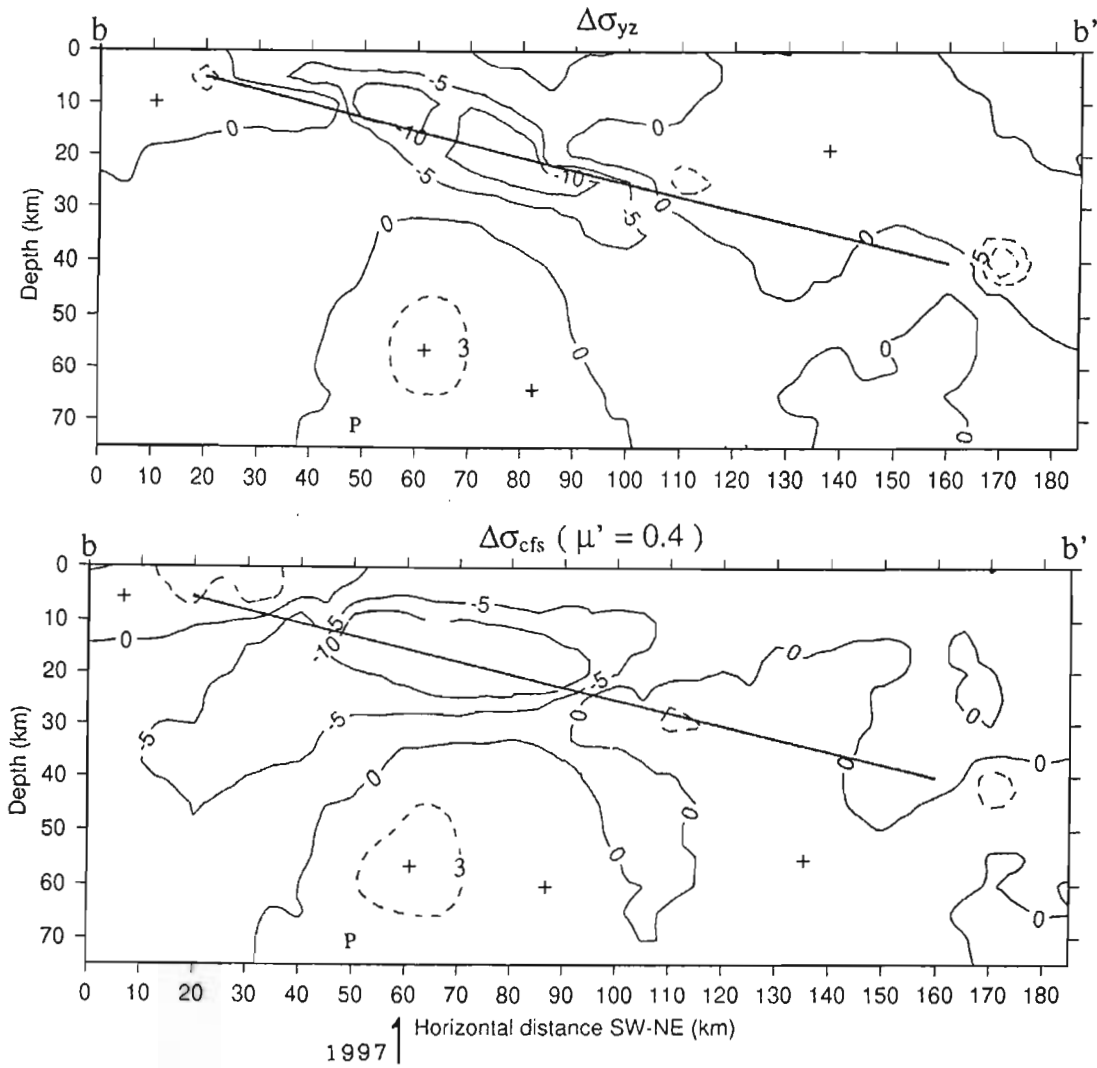


Figure 6. Continued.

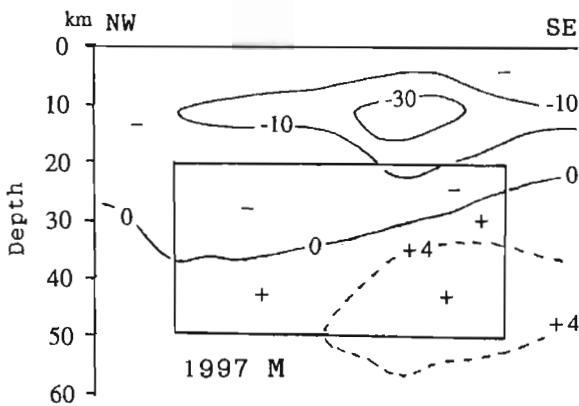


Figure 7. Coseismic changes in the shear stress  $\Delta\sigma_{yz}$  (in bars) due to the 1985 thrust event projected onto the 1997 vertical fault located at depths between 20 and 50 km.

why a normal-faulting earthquake could also take place in some other subduction zones near the trench or some far downdip of the thrust plane following a large-thrust earthquake. It is clear from Figure 6a and b that coseismic-stress increase will also occur in these portions of the slab after a large-thrust earthquake.

### Conclusions

We have calculated coseismic stress changes due to the 1985 Michoacan, Mexico, thrust earthquake ( $M_w = 8.1$ ) in the subducting Cocos plate and in the overlying crust and uppermost mantle to investigate if there is any stress interaction between this thrust earthquake and the 1997 nearly vertical, normal-faulting earthquake that took place just beneath the ruptured fault zone of the 1985 event. The maximum magnitude of stress increase in the vertical-shear stress and in the Coulomb failure stress at depths below 30 km in



the middle portion of the subducting plate ranges between 4 and 8 bars (0.4–0.8 MPa). It was found that the 1997 earthquake took place in the zone of maximum coseismic stress increase due to the 1985 event. The dynamic rupture pattern of the 1997 earthquake also appears consistent with that of the stress increase from the 1985 event. Some qualitative considerations on the postseismic-stress change suggest that they may strengthen the coseismic-stress change. All the aforementioned evidence suggests that the 1997 normal-faulting earthquake occurred under stress transfer from the 1985 earthquake to the interior of the subducting Cocos plate.

### Acknowledgments

We wish to thank Hiroo Kanamori for providing us with some information on lithospheric normal-faulting earthquakes in the subduction zones around the globe. Our thanks are extended to Diane I. Doser (Associate Editor), Martin Reyners, and an anonymous reviewer for their constructive comments in improving the manuscript.

### References

- Abe, K. (1972a). Lithospheric normal faulting beneath the Aleutian trench, *Phys. Earth Planet. Interiors* **5**, 90–98.
- Abe, K. (1972b). Mechanisms and tectonic implications of the 1966 and 1970 Peru earthquakes, *Phys. Earth Planet. Interiors* **5**, 367–379.
- Abe, K. (1977). Tectonic implications of the large Shioya-oki earthquake of 1938, *Tectonophysics*, **41**, 269–289.
- Christensen, D. H., and T. Lay (1988). Large earthquakes in the Tonga region associated with subduction of the Louisville ridge, *J. Geophys. Res.* **93**, 13367–13389.
- Clayton, R., and B. Engquist (1977). Absorbing boundary conditions for acoustic and wave equations, *Bull. Seism. Soc. Am.* **67**, 1529–1540.
- Cocco, M., M. J. Pacheco, S. K. Singh, and F. Courboux (1997). The Zihuatanejo, Mexico, earthquake of 1994 December 10 ( $M = 6.6$ ): source characteristics and tectonic implications, *Geophys. J. Int.* **131**, 135–145.
- Dmowska, R., J. R. Rice, L. C. Lovinson, and D. Josell (1988). Stress transfer and seismic phenomena in coupled subduction zones during the earthquake cycles, *J. Geophys. Res.* **93**, 7869–7884.
- Eissler, H., and H. Kanamori (1982). A large normal-fault earthquake at the junction of the Tonga trench and Louisville ridge, *Phys. Earth Planet. Interiors* **29**, 161–172.
- Freed, A. M., and J. Lin (1998). Time-dependent changes in failure stress following thrust earthquakes, *J. Geophys. Res.* **103**, 24393–24409.
- Fujita, K., and H. Kanamori (1981). Double seismic zones and stresses of intermediate depth earthquakes, *Geophys. J. Int.* **66**, 131–156.
- Gardi, A., M. Cocco, A. M. Negro, R. Sabadini, and S. K. Singh (1999). Dynamic modelling of the subduction zone of central Mexico, *Geophys. J. Int.* (submitted).
- Harris, R. A. (1998). Introduction to special section: stress triggers, stress shadows, and implications for seismic hazard, *J. Geophys. Res.* **103**, 24347–24358.
- Kanamori, H. (1971). Seismological evidence for a lithospheric normal faulting—the Sanriku earthquake of 1933, *Phys. Earth Planet. Interiors* **4**, 289–300.
- Kausel, E., and J. Campos (1992). The  $M_s = 8$  tensional earthquake of 9 December 1950 of northern Chile and its relation to the seismic potential of the region, *Phys. Earth Planet. Interiors* **72**, 220–235.
- King, G. C. P., R. S. Stein, and J. Lin (1994). Static stress changes and the triggering of earthquakes, *Bull. Seism. Soc. Am.* **84**, 935–953.
- Lundgren, P., and E. A. Okal (1988). Slab decoupling in the Tonga arc: the June 22, 1977, earthquake, *J. Geophys. Res.* **93**, 13355–13366.
- Lynnes, C. S., and T. Lay (1988). Source process of the great Sumba earthquake, *J. Geophys. Res.* **93**, 13407–13420.
- Mendoza, C., and S. Hartzell (1989). Slip distribution of the 19 September 1985 Michoacan, Mexico, earthquake: near-source and teleseismic constraints, *Bull. Seism. Soc. Am.* **79**, 655–669.
- Mikumo, T., and T. Miyatake (1993). Dynamic rupture processes on a dipping fault and estimates of stress drop and strength excess from the results of waveform inversion, *Geophys. J. Int.* **112**, 481–496.
- Mikumo, T., T. Miyatake, and M. A. Santoyo (1998). Dynamic rupture of asperities and stress change during a sequence of large interplate earthquakes in the Mexican subduction zone, *Bull. Seism. Soc. Am.* **88**, 686–702.
- Mikumo, T., M. A. Santoyo, and S. K. Singh (1999). Dynamic rupture and stress change in a normal faulting earthquake in the subducted Cocos plate, *Geophys. J. Int.* (in press).
- Pardo, M., and G. Suarez (1995). Shape of the subducted Rivera and Cocos plates in Southern Mexico: seismic and tectonic implications, *J. Geophys. Res.* **100**, 12357–12373.
- Santoyo, M. A., S. K. Singh, and T. Mikumo (1999). Source characteristics of the 11 January, 1997 Michoacan, Mexico, earthquake ( $M_w = 7.1$ ), *Seism. Soc. Am.* (to be submitted).
- Shiono, K., and T. Mikumo (1975). Tectonic implications of subcrustal normal faulting earthquakes in the western Shikoku region, Japan, *J. Phys. Earth* **23**, 257–278.
- Singh, S. K., G. Suarez, and T. Dominguez (1985). The Oaxaca, Mexico, earthquake of 1931: lithospheric normal faulting in the subducted Cocos plate, *Nature* **317**, 56–58.
- Spence, W. (1986). The 1977 Sumba earthquake series: evidence for slab pull force acting at a subduction zone, *J. Geophys. Res.* **91**, 7225–7239.
- Taylor, M. A. J., G. Zheng, J. R. Rice, D. Stewart, and R. Dmowska (1996). Cyclic stressing and seismicity at strongly coupled subduction zones, *J. Geophys. Res.* **101**, 8363–8381.
- UNAM Seismology Group (1986). The September 1985 Michoacan earthquakes: aftershock distribution and history of rupture, *Geophys. Res. Lett.* **13**, 573–576.
- Valdes, C., and R. P. Meyer (1996). Seismic structure between the Pacific coast and Mexico City from the Petatlan earthquake ( $M_s = 7.6$ ) aftershocks, *Geophys. Res. Lett.* **23**, 377–401.
- Yoshida, Y., K. Satake, and K. Abe (1992). The large normal faulting Mariana earthquake of April 5, 1990 in coupled subduction zone, *Geophys. Res. Lett.* **19**, 297–300.

Instituto de Geofísica  
 Universidad Nacional Autónoma de México  
 Ciudad Universitaria, México 04510 D.F., México  
 E-mail: mikumo@ollin.igeofcu.unam.mx  
 (T.M., S.K.S., M.A.S.)

Manuscript received 12 April 1999.

## Capítulo VI

RUPTURA DINÁMICA Y CAMBIO DE ESFUERZOS EN UN SISMO DE FALLA  
NORMAL EN LA PLACA DE COCOS SUBDUCENTE

# Dynamic rupture and stress change in a normal faulting earthquake in the subducting Cocos plate

Takeshi Mikumo, Miguel A. Santoyo and Shri Krishna Singh

Instituto de Geofísica, UNAM, Ciudad Universitaria, Cp 04510, Mexico DF, Mexico. E-mail: mikumo@ollin.igeofcu.unam.mx

Accepted 1999 October 15. Received 1999 September 27; in original form 1999 March 24

## SUMMARY

A large nearly vertical, normal faulting earthquake ( $M_w = 7.1$ ) took place in 1997 in the Cocos plate, just beneath the ruptured fault zone of the great 1985 Michoacan thrust event ( $M_w = 8.1$ ). Dynamic rupture and resultant stress change during the 1997 earthquake have been investigated on the basis of near-source strong-motion records together with a 3-D dynamic model.

Dynamically consistent waveform inversion reveals a highly heterogeneous distribution of stress drop, including patch-like asperities and negative stress-drop zones. Zones of high stress drop are mainly confined to the deeper, southeastern section of the vertical fault, where the maximum dynamic stress drop reaches 280 bars (28 MPa). The dynamically generated source time function varies with location on the fault, and yields a short slip duration, which is caused by a short scalelength of stress-drop heterogeneities. The synthetic seismograms calculated from the dynamic model are generally consistent with the strong-motion velocity records in the frequency range lower than 0.5 Hz.

The pattern of stress-drop distribution appears, in some sense, to be consistent with that of coseismic changes in shear stress resulting from the 1985 thrust event. This consistency suggests that the stress transfer from the 1985 event to the subducting plate could be one of the possible mechanisms that increased the chance of the occurrence of the 1997 earthquake.

**Key words:** dynamics, inversion, normal faulting, rupture propagation, shear stress, synthetic waveforms.

## INTRODUCTION

The south Pacific coastal region of Mexico, where the Cocos plate subducts beneath the North American plate, is one of the world's most seismically active zones. Large thrust earthquakes with low dip angles and shallow depths frequently occur on the upper interface of the subducting plate. In addition to these, large intermediate-depth normal faulting earthquakes also take place in the subducting slab: for example, the 1858 Michoacan ( $M_s = 7.5$ ) (Singh *et al.* 1996), 1931 Oaxaca ( $M_s = 7.8$ ) (Singh *et al.* 1985), 1973 Orizaba ( $M_s = 7.3$ ) (Singh & Wyss 1976), 1980 Huajuapán de León ( $M_s = 7.6$ ) (Yamamoto *et al.* 1984), and 1994 Zihuatanejo ( $M_s = 6.6$ ) (Cocco *et al.* 1997; Quintanar *et al.* 1999) earthquakes. Most intermediate-depth earthquakes take place in the unbending and subhorizontal portion of the subducting plate, while a few occur somewhat closer to the trench.

A large nearly vertical, normal faulting earthquake ( $M_w = 7.1$ ) occurred in the Michoacan segment of the Mexican subduction zone on 1997 January 11, just beneath the extensive ruptured zone of the great Michoacan thrust earthquake ( $M_w = 8.1$ ) of

1985 September 19 (Fig. 1). An inversion of teleseismic *P* and *SH* waves, based on a horizontally propagating line source model, favoured a nearly vertical faulting mechanism (dip = 87°, strike = 105°, and rake = -110°) (Fig. 1a), and a centroid focal depth of 35 km (Santoyo *et al.* 1999). Two other moment tensor inversions (M. Kikuchi, personal communication 1997; Monthly Listing of the USGS 1997) also gave a vertical plane as one of the two nodal planes. Although there are some minor differences in focal mechanism solutions, the 1997 earthquake appears to have a nearly vertical fault at mid-depth in the subducting Cocos plate (Fig. 1b). We may regard it as a normal faulting event in view of the geometry of the subducting plate and the sense of the down-thrown side.

The 1997 earthquake was preceded by the 1985 large thrust event that occurred just above it. From the close proximity of their locations and relatively short time interval of 12 years, a causal relationship between the two events is expected. One possible explanation may be stress transfer (i.e. coseismic stress increase) from the 1985 event to the zone of the 1997 vertical fault in the subducting slab and its possible postseismic increase (Mikumo *et al.* 1999). Another tectonic force to enhance this

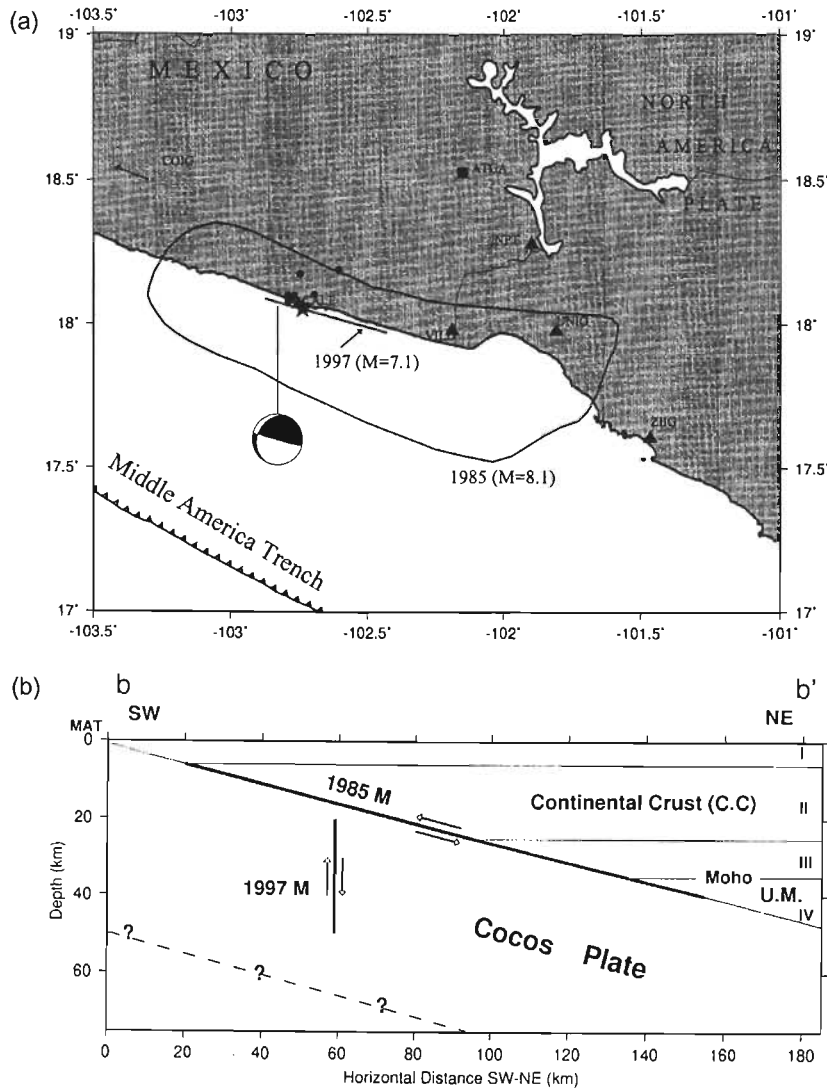


**Figure 1.** (a) Location of the 1997 earthquake (a thick straight line with asterisk near the coast, indicating the horizontal projection of its nearly vertical fault and the epicentre), and the fault plane solution obtained from moment tensor inversion of teleseismic body waves (Santoyo *et al.* 1999). Small solid circles indicate the locations of several aftershocks. A nearly elliptical-shaped curve shows the aftershock zone of the 1985 Michoacan earthquake. Solid triangles indicate strong-motion recording stations in this region. (b) Side-view of the locations of the 1985 thrust event and the 1997 nearly normal faulting earthquake with respect to the subducting Cocos plate and the overlying continental crust and uppermost mantle.

possibility would be the loading of the overriding continental lithosphere temporarily decoupled during the 1985 event from the subducting plate (Singh *et al.* 1985).

Although our previous study (Santoyo *et al.* 1999) revealed the kinematic properties of the fault, including the fault geometry, slip distribution on the fault, average rupture velocity and total source duration of the 1997 event, the fault's dynamic rupture process and the change of stress state have not yet been made clear. In the present study, we develop a 3-D dynamic rupture model for this earthquake in order to clarify its dynamic processes. To accomplish this goal, some of the kinematic fault parameters derived from waveform inversion (Santoyo *et al.* 1999) are used as observational constraints. We derive the rupture pattern and the spatial distribution of

dynamic stress drop over the nearly vertical fault. We also discuss the possible effects of stress interaction between the 1985 thrust event and the 1997 earthquake, by comparing the stress-drop distribution with the pattern of coseismic stress change due to the 1985 earthquake.

#### KINEMATIC FAULT MODEL

Fig. 1(a) shows the horizontal projection of the 1997 earthquake fault, its fault plane solution, and the locations of near-source strong-motion stations in the Michoacan region. The velocity waveforms obtained by integration from the accelerograms recorded at four of these stations (CALE, VILD, INPT

and UNIO) have been used in the kinematic waveform inversion (Santoyo *et al.* 1999). The crust and uppermost mantle structures beneath these stations are slightly different, but in this inversion an average velocity model over the region was used to calculate Green's functions by applying the discrete wavenumber method (Bouchon 1979). The rupture begins at the hypocentre, located at a depth of 35 km and 10 km south-east of the northwestern edge of the fault, and was assumed to propagate circularly at a constant velocity of  $2.8 \text{ km s}^{-1}$ . This velocity gave the best fit between the integrated velocity waveforms and the corresponding synthetic seismograms in the searched range between  $2.6$  and  $3.0 \text{ km s}^{-1}$ . The velocity source time function was assumed to have a triangular shape with a duration of between  $1.0$  and  $2.0 \text{ s}$ , which is the same everywhere on the fault: a duration of  $1.2 \text{ s}$  was finally adopted. The top of the fault is buried  $20 \text{ km}$  from the surface, and the fault width and length were taken as  $30 \text{ km}$  and  $50 \text{ km}$ , respectively (Fig. 2). For one of the inversions, the fault was divided into a  $2 \text{ km} \times 2 \text{ km}$  mesh. Fig. 2 shows the slip distribution on the fault, which has been obtained from the inversion with smoothing and positive slip constraints (Santoyo *et al.* 1999). The seismic moment was found to be  $3.9 \times 10^{26} \text{ dyn cm}$ . It is noticed that major slip ( $> 100 \text{ cm}$ ) is mostly confined to depths between  $25$  and  $45 \text{ km}$  and between  $17$  and  $47 \text{ km}$  in the strike direction. Slip larger than  $200 \text{ cm}$  is concentrated mainly at depths of between  $28$  and  $40 \text{ km}$  in the southeastern fault section, and the maximum slip exceeds  $300 \text{ cm}$ . We derive the dynamic rupture models that follow based on this distribution of kinematic fault slip.

#### METHOD OF DYNAMIC RUPTURE MODELLING

The method of dynamic rupture modelling has been described in a number of previous works (Miyatake 1992; Fukuyama & Mikumo 1993; Mikumo & Miyatake 1993, 1995; Beroza &

Mikumo 1996; Ide & Takeo 1996, 1997; Mikumo *et al.* 1998), but is again summarized here. The first step is to construct a 3-D dynamic model incorporating a vertical fault in the subducting plate, which is embedded in a horizontally layered half-space. The fault geometry and the rupture starting point have been taken to be the same as those in the above kinematic fault model. We assume that the initial shear stress is applied parallel to the vertical fault, generating pure dip-slip motion on the fault, and that dynamic rupture starts at the point where the initial stress exceeds the prescribed level, and propagates at a constant velocity. We also assume that the shear stress at any point on the fault gradually increases due to the approach of the rupture front, and, for simplicity, drops immediately to the level of dynamic friction at the time of the rupture arrival, which may be regarded as a slip-weakening process with an extremely small slip-weakening distance. The rupture time in the modelling is specified by the kinematic model, and the difference between the assumed initial stress and the dynamic stress is taken as the static stress drop. With these assumptions and given stress drop, the rupture propagation and all displacement components at every point on the fault are calculated successively by solving 3-D wave equations at each time step, with a second-order finite difference scheme under appropriate boundary conditions. At the final time step, we obtain the slip distribution over the fault, called here the final dynamic slip. The boundary conditions imposed are as follows: (a) the ground surface is stress-free; (b) the continuity of all stress and displacement components at each of the layer interfaces; and (c) absorbing boundary conditions (Clayton & Engquist 1977) at the side and bottom boundaries of the model space.

The second step is to evaluate the spatial distribution of dynamic and static stress drops over the fault, from that of the fault slip obtained from waveform inversion in the kinematic model. To do this, we use a non-linear, iterative, least-squares technique. Given approximate estimates of static stress drop on the fault as starting values, we calculate the distribution of

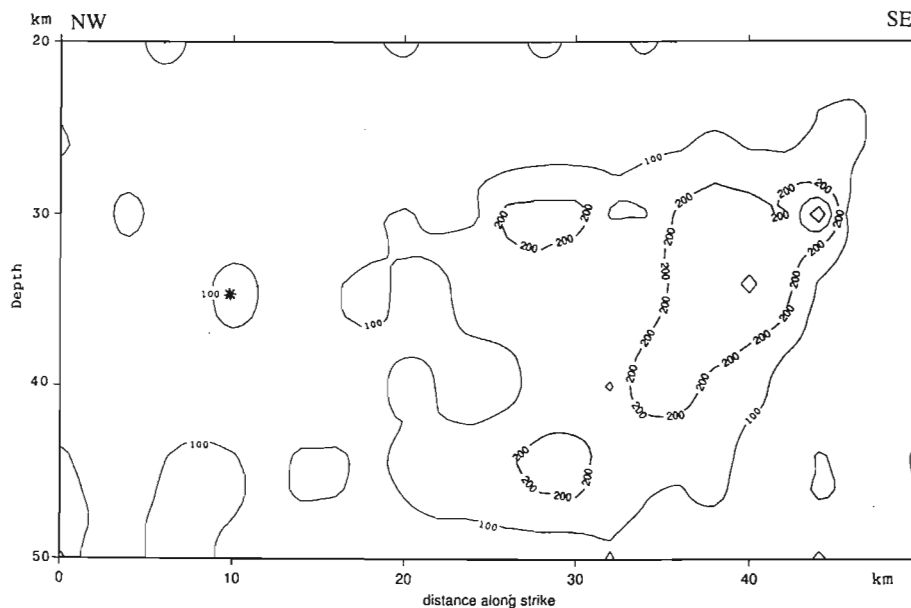


Figure 2. Spatial distribution of fault slip (in cm) obtained from kinematic waveform inversion of strong-motion records (Santoyo *et al.* 1999). The asterisk shows the location of the rupture starting point.

dynamic fault slip in the way described above, and compare this with the already-obtained kinematic slip. The ratio between the kinematic and final dynamic slips at each point on the fault is then multiplied, in the next iteration, to the previously estimated stress drop. This procedure is repeated until the rms difference between the kinematic and dynamic slips over the fault can be minimized within a reasonably small value, which gives a best-fitting model. From the final model, we obtain the distribution of dynamic and static stress drops over the fault.

The crust and uppermost structure assumed here is nearly the same as that used in the kinematic model as the average velocity model (Santoyo *et al.* 1999) over the Michoacan region. However, since a more refined model (Valdes & Meyer 1996) in this region shows slightly higher velocities in the subducting Cocos plate, the velocities and densities in the plate are assumed to be higher by 10 per cent than those in the overlying continental crust and uppermost mantle in the same layer. For numerical calculations we take a grid spacing of 2.0 km and a time increment of 0.1 s, in order to be consistent with those in the kinematic model, keeping the stability conditions for wave propagation in the 3-D space. However, these slightly coarse configuration parameters limit the range of wave frequency that can be discussed. The dimension of the model space is 240 km  $\times$  137 km  $\times$  220 km, and the total number of time steps is taken to be 300 over 30 s.

## DYNAMIC RUPTURE AND STRESS CHANGE

### Model I

Following the method of dynamic rupture modelling described above, we calculate the dynamic slip at each time step at every

point on the fault, for a fixed rupture velocity of 2.8 km s<sup>-1</sup>. After repeating the optimization procedure seven times, we obtain the spatial distribution of stress drop with a reasonably small rms difference of 5.8 cm (1.9 per cent of the maximum slip) between the already-obtained kinematic slip and the calculated dynamic slip at the final time step of 30 s. We call this model Model I. Fig. 3 shows the distribution of static stress drop thus obtained over the vertical fault. Comparing this distribution with Fig. 2, we find that quite a large stress drop, higher than 100 bars and even 200 bars in a few localized zones, generated fault slip larger than 200 cm in the southeastern fault section and also at depths of around 30 km and 42 km in the central section. Another feature to be noted is the negative stress-drop zones, mostly near the upper and lower edges of the fault and also in the lower right (southeast) section and some parts of the lower left (northwest) section.

For the next step, we calculate the slip-velocity source time functions at each point on the fault from this dynamic Model I—the results are shown in Fig. 4. To suppress high-frequency numerical noise, we applied a 0.6-s running mean as a high-cut filter and a taper to its later part. The shape of the source time functions is found to vary with the location on the fault, with the duration of the first sharp pulse ranging between 0.5 and 2.0 s. A smaller second bump at some points may be mainly due to the effects of waves reflected back from adjacent high-stress-drop or negative stress-drop segments, but might still be contaminated by numerical noise coming from the coarse grid used here. Nearly flat lines at several points correspond to very low slip.

Next, we calculate the synthetic seismograms by forward modelling, incorporating the slip-velocity source time functions obtained above, in order to compare them with the observed records. To do this, the Green's functions, which were calculated

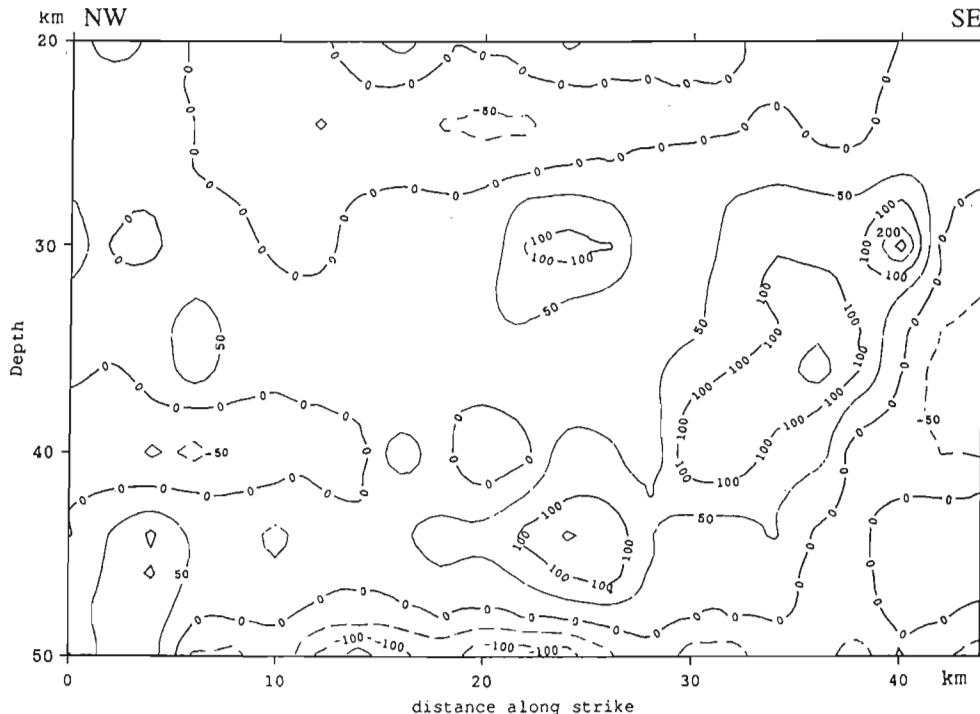


Figure 3. Spatial distribution of static stress drop (in bars) (Model I) calculated from the kinematic fault slip in Fig. 2.

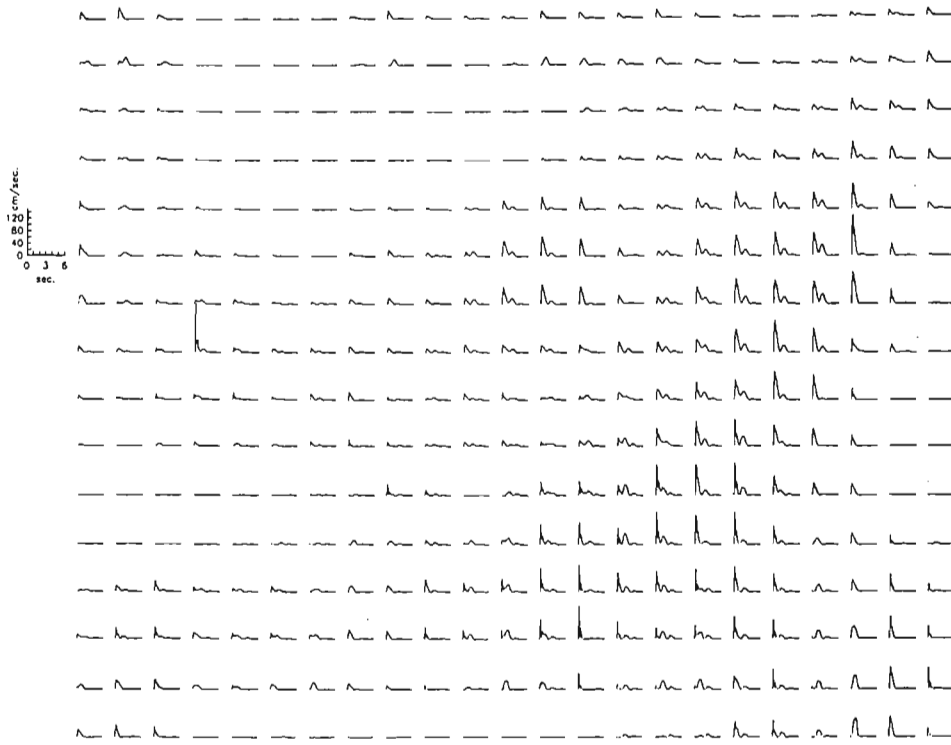


Figure 4. Slip-velocity source time functions at selected points on the fault, calculated from Model I. All the initial times of these time functions are shifted to zero from the arrival time of rupture at these points. Locations are arranged from the top to the bottom and from NW (left) to SE (right) on the vertical fault.

when obtaining the kinematic model, are convolved with the above dynamically generated source time functions, and are integrated over the fault plane. In view of the grid spacing used in the numerical calculations, the minimum wavelength (8 km) needed for wave propagation without grid dispersion means that the reliable upper frequency limit is less than 0.5 Hz. Accordingly, the calculated synthetic seismograms and the observed strong-motion velocity records are low-pass filtered with a cut-off frequency of 0.5 Hz; the results are shown in Fig. 5. The comparison gives quite a good fit between the synthetic and observed waveforms, except for the EW component at the INPT and UNIO stations and the vertical component at CALE. The rms difference between the recorded and synthetic waveforms for each component is given in Table 1.

#### Model II

In order to improve the above model, we perform another waveform inversion using the low-pass filtered velocity records as the observed data, incorporating the dynamically generated slip-velocity time functions shown in Fig. 4, instead of using an *a priori* assumed source time function. In this inversion, again with smoothing and positive slip constraints, only slip is allowed to vary, with a fixed rupture velocity of  $2.8 \text{ km s}^{-1}$ . Fig. 6 gives the spatial distribution of fault slip derived from this dynamically consistent inversion. The pattern of slip distribution is quite different from that in Fig. 2, and appears to be more confined to the lower half of the vertical fault, and also the slip amplitude in some sections is larger than in the original kinematic model. This concentration of slip patterns has been

Table 1. The degree of misfit between the recorded and synthetic waveforms, given by the rms difference ( $\sigma/R_m$ ) between the two types of waveforms.

Comp.	MODEL I				MODEL II			
	CALE	VILE	INPT	UNIO	CALE	VILE	INPT	UNIO
V	0.336	0.199	0.179	0.201	0.333	0.173	0.097	0.122
EW	0.199	0.191	0.278	0.213	0.135	0.137	0.303	0.262
NS	0.198	0.108	0.241	0.166	0.084	0.074	0.272	0.165

$$\sigma = \left\{ \sum_{j=1}^N [R(t_j) - cS(t_j)]^2 / N \right\}^{1/2}; c = R_m / S_m \text{ (a normalization constant) where } R \text{ and } S \text{ denote the recorded and synthetic waveforms}$$

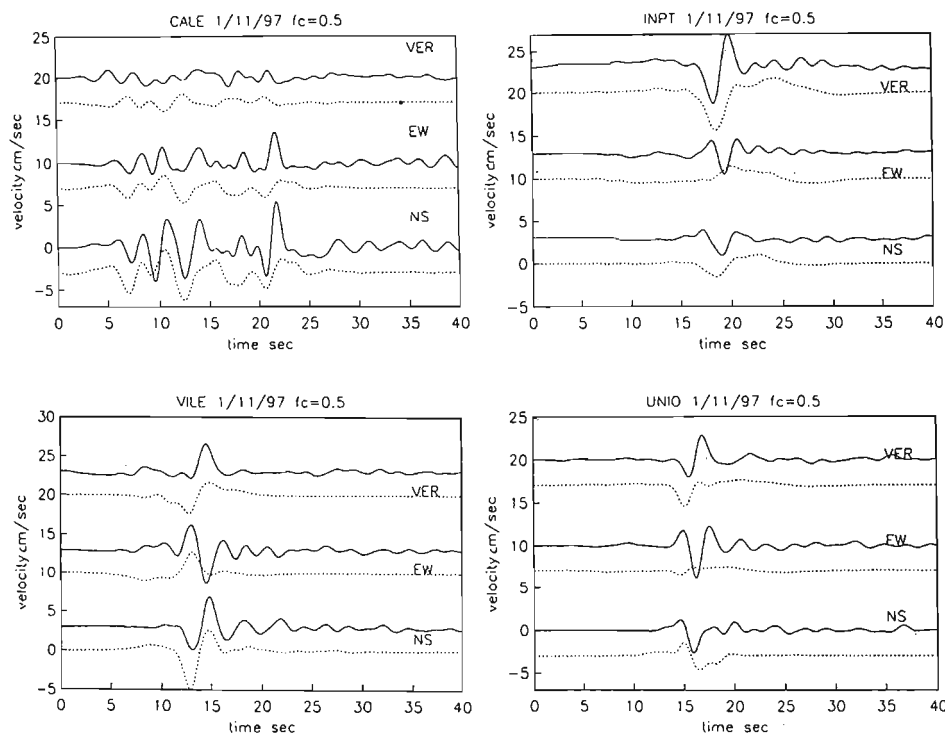


Figure 5. Low-pass filtered ( $<0.5$  Hz) strong-motion velocity records (continuous lines), and the corresponding synthetic seismograms (dotted lines) calculated from Model I by forward modelling with the dynamically generated source time functions.

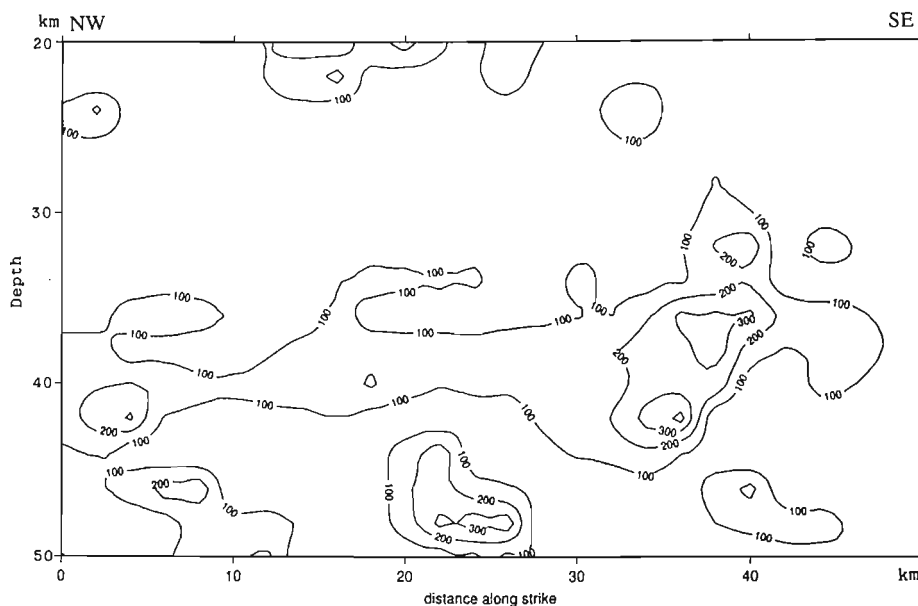


Figure 6. Spatial distribution of fault slip (in cm) derived from waveform inversion of the low-pass filtered strong-motion records, incorporating the dynamically generated slip-velocity source time functions.

noted by Beroza & Mikumo (1996), who also performed a dynamically consistent waveform inversion. The zone of major slip, with the maximum slip exceeding 300 cm, is still located at depths between 30 and 45 km, and between 35 and

40 km in the strike direction. Another high-slip zone, with slip larger than 200 cm, appears in the deepest middle section, and the mid-depth high-slip zone extends to the northwest fault section.



We calculate static stress drop from the above slip distribution given in Fig. 6 through the optimization procedure described above, again with a fixed rupture velocity of  $2.8 \text{ km s}^{-1}$ . The rms difference between the slip given in Fig. 6 and the final dynamic slip is now 4.4 cm (1.4 per cent of the maximum slip), which is slightly better than that in Model I. Fig. 7 shows the distribution of static stress drop in this improved dynamic model, which we call Model II. Again, the zones of high stress drop ( $>100$  bars) are located below 30 km and are mostly confined to certain areas: one is in the southeastern section at depths between 30 and 43 km, and 32 and 42 km in the strike direction, where the maximum stress drop reaches 280 bars; the second, with stress drop exceeding 200 bars, is in the middle section below 45 km; and the other three, having stress drops between 100 and 150 bars, are located in the strike direction between 14 and 20 km, between 5 and 10 km and between 0 and 7 km. These patch-like high-stress-drop zones may be regarded as asperities.

The synthetic seismograms calculated from the above inversion and the corresponding low-pass filtered records are shown in Fig. 8. The fit appears to be slightly improved. The rms differences between the recorded and synthetic waveforms are given in Table 1, along with those for Model I. There still remains, however, a slight phase shift in the EW and NS components at INPT. The EW component at UNIO shows a nearly reverse sense or a considerable phase delay to the observed record. This discrepancy, which was also pointed out in the above kinematic inversion, would not be reconciled by further inversions. The discrepancy might be attributable to possible lateral variations in the upper crustal structure between the two stations (Santoyo *et al.* 1999), which are not included in the theoretical Green's functions.

## DISCUSSION

### Comparison between Model I and Model II

The dynamically consistent waveform inversion of the low-pass filtered velocity records provided the slip distribution (Fig. 6) and stress-drop distribution (Fig. 7) for Model II, while Figs 2 and 3 show the corresponding slip and stress-drop distributions for Model I, respectively. As mentioned above, Model II gives a slightly smaller rms difference between the inverted slip and the final dynamic slip than Model I. Table 1 gives the rms differences between the recorded and synthetic waveforms for three components at each of the four stations in Models I and II. It can be seen from the Table that the fit between the two types of waveforms in Model II has been improved to some extent, as compared with that in Model I, except for the EW and NS components at INPT and the EW component at UNIO. The fairly large rms values for these components are due to the reverse sense and the phase mismatch, as in Model I. From these comparisons, we can regard Model II as the preferred model in this study, although Model I still cannot be totally ruled out.

### Heterogeneous stress-drop distribution

The two models reveal a highly heterogeneous distribution of static stress drop and fault slip over the nearly vertical fault. Zones of high stress drop are mainly concentrated in the southeastern fault section, at depths between 30 and 45 km. Several other patch-like zones of relatively high stress drop can be identified, but a few isolated patches might be spurious,

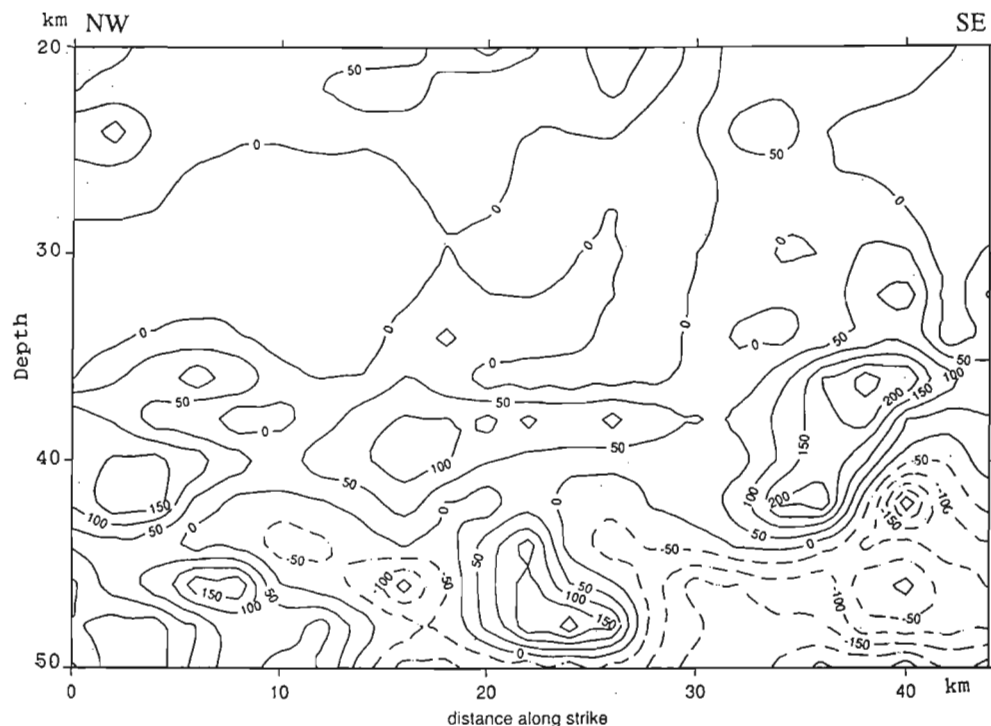


Figure 7. Spatial distribution of static stress drop (in bars) (Model II) calculated from the fault slip (Fig. 6).

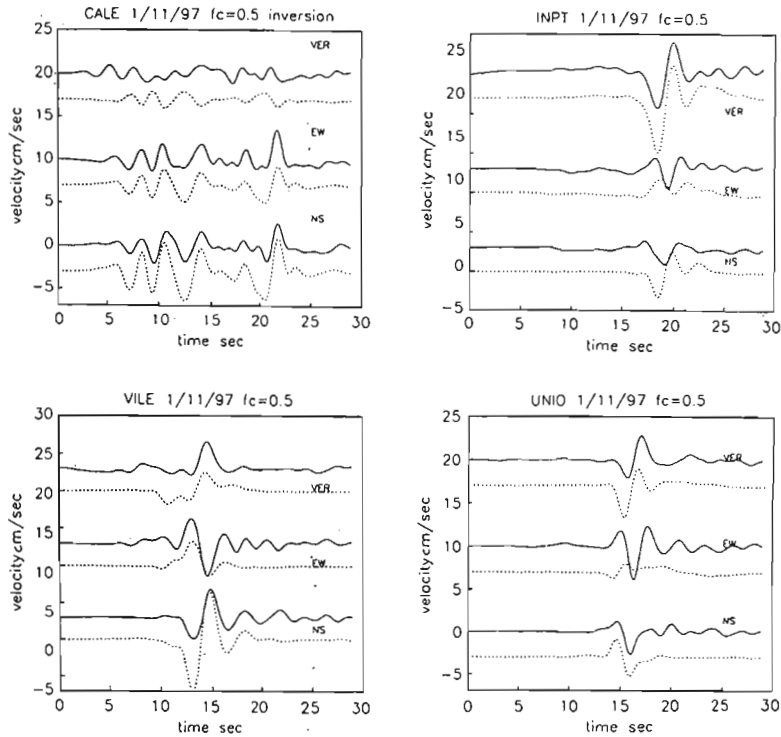


Figure 8. Low-pass filtered ( $<0.5$  Hz) strong-motion velocity records (continuous lines), and the corresponding synthetic seismograms (dotted lines) calculated from Model II by waveform inversion of the filtered records, incorporating the dynamically generated source time functions. (The amplitude of the NS record at CALE has been reduced for convenience by half in this plot).

resulting from numerical noise included in the inversion. Zones of negative stress drop are distributed in between the zones of high stress drop and near the upper and lower edges of the fault. These negative drops (stress increases) are required to account for very low slip, and also partly to compensate the high stress drops (stress decreases). However, the negative values near the fault edges may be due to the edge effect. Some uncertainties and less well-resolved slip on some subfaults that might be included in the inversions, partly because of the somewhat coarse grid used and possible uncertainties in the velocity model, would affect the estimate of dynamic and static stress drop almost linearly. For these reasons, the absolute values of stress drop could involve uncertainties probably much larger than 10 per cent, although it is difficult to give an exact estimate of these uncertainties because of the non-linear properties of the problem. Nevertheless, the maximum stress drop in a localized zone in the southeastern fault section exceeds 280 bars. This is significantly larger than the maximum drop of 130 bars during the 1985 thrust earthquake (Mikumo *et al.* 1998). The difference suggests that the stress resistance to shear fracture in the subducting plate may be considerably higher than that on the upper interface of the plate, although the direction of the applied shear stress is different.

#### Short slip duration

It is found that the slip duration in the velocity source time functions calculated from the dynamic model ranges between

0.5 and 2.0 s, although some of the source time functions are perturbed by subsequent small bumps. The duration is quite short compared with a simple estimate for the time needed for the rupture to travel across half of the shorter dimension of the fault (Day 1982). The short slip duration in the fault can be entirely attributed to the short scalelength of stress-drop heterogeneities, including negative stress-drop zones, making it unnecessary to introduce any specific self-healing mechanism (e.g. Heaton 1990), as has been demonstrated and discussed in some detail in a previous work on the 1984 Morgan Hill, California, earthquake (Beroza & Mikumo 1996). A similar conclusion was reached in the cases of the 1995 Kobe, Japan earthquake (Ide & Takeo 1997), and the 1992 Landers and 1994 Northridge, California, earthquakes (Day *et al.* 1998). A possible interpretation is that negative stress-drop zones in these cases provide geometrical constraints, which preclude further extension of slip and thus will generate healing pulses. Day *et al.* (1998) found further evidence favouring this model, in that a pronounced recovery of shear stress after the passage of a rupture front, which is considered inherent to the self-healing hypothesis, cannot be detected from their inversion analysis. However, the limited spatial and time resolutions in the present kinematic and dynamic models mean that the possible existence of self-healing, frictional fault behaviour cannot be totally ruled out. It is to be emphasized that the present dynamic model with 'velocity-independent' friction and an extremely small slip-weakening distance provided this type of short slip duration, and has been proved to be consistent with the strong-motion data obtained.

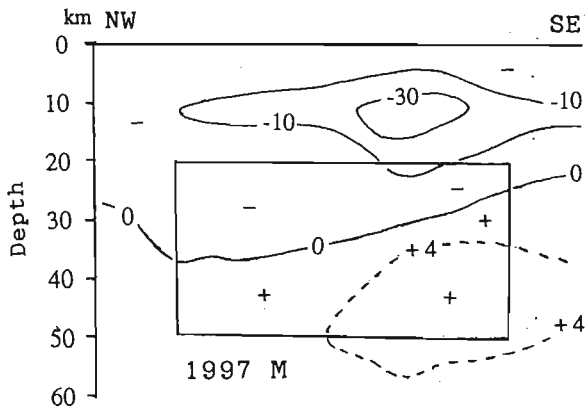


Figure 9. Calculated coseismic changes in the shear stress (in bars) on the 1997 vertical fault due to the 1985 thrust event.

#### Possible stress transfer from the 1985 thrust earthquake

Mikumo *et al.* (1999) estimated the coseismic stress change in the subducting Cocos plate due to the 1985 thrust event. Fig. 9 shows the coseismic change in shear stress along the vertical fault plane of the 1997 earthquake, with the fault zone enclosed by a rectangle. It is clear that the shear stress after the 1985 event dropped in the upper section of the 1997 fault to its minimum below a high-stress-drop zone of the 1985 event. In the lower fault section, on the other hand, the shear stress increased by up to 5 bars. The zone of stress increase appears to be separated from that of stress decrease by an oblique lobe traversing nearly the mid-depth of the fault. Comparing this pattern with the slip (Fig. 6) and stress-drop (Fig. 7) distributions from the 1997 earthquake, we notice that large slip and high stress drop took place in the zone of previous stress increase in the lower fault section, while only small slip and negative stress drop occurred in the zone of previous stress decrease in the upper part. The pattern of coseismic stress change (Fig. 9) due to the 1985 thrust event and that of stress drop (Fig. 7) during the 1997 earthquake have been derived from completely different observations. We are inclined to believe that their similar patterns are not just a coincidence but indicate a physical interaction between them. We may conclude that the 1997 near-vertical, normal faulting earthquake occurred under some stress transfer from the 1985 large thrust event to the subducting plate just beneath it, and possibly with postseismic stress increase up to the time of the 1997 event.

#### CONCLUSIONS

We have investigated the dynamic rupture and resultant stress change in the 1997 nearly vertical, normal faulting earthquake that occurred in the subducting Cocos plate just beneath the ruptured fault zone of the great 1985 Michoacan earthquake, on the basis of near-source strong-motion observations together with a 3-D dynamic model. The main results are summarized below.

(1) A highly heterogeneous stress-drop distribution has been revealed by dynamically consistent waveform inversions. High-stress-drop zones are mainly confined to the deeper part of the southeastern side of the fault, and are surrounded by

negative stress-drop zones. The maximum stress drop reaches 280 bars (28 MPa). This is significantly larger than that experienced during the 1985 thrust earthquake that occurred on the upper interface of the subducting slab, suggesting the existence of higher stress within the slab.

(2) The dynamically generated slip-velocity source time functions have a short slip duration, ranging between 0.5 and 2.0 s. This short duration can be attributed to the short scale-length of stress-drop heterogeneities, particularly including negative stress-drop zones. The synthetic waveforms derived from the dynamic model with these source time functions and heterogeneous stress drop are generally consistent with the strong-motion records in the frequency range lower than 0.5 Hz.

(3) The stress-drop distribution on the vertical fault of the present 1997 earthquake appears to be consistent with the pattern of coseismic stress changes caused over the fault by the 1985 thrust earthquake. This consistency suggests that the stress transfer from the 1985 event down to the interior of the subducting plate could be one possible source that enhanced the chance of occurrence of the 1997 earthquake.

#### ACKNOWLEDGMENTS

We are grateful to the critical reviews and constructive comments given by Raul Madariaga and Steve Day, which greatly improved our original manuscript. We also thank Masayuki Kikuchi for providing us with early information on the moment tensor inversion of the 1997 earthquake.

#### REFERENCES

- Beroza, G. & Mikumo, T., 1996. Short slip duration in dynamic rupture in the presence of heterogeneous fault properties, *J. geophys. Res.*, **101**, 22 449–22 460.
- Bouchon, M., 1979. Discrete wave number representation of elastic wave fields in three-space dimensions, *J. geophys. Res.*, **84**, 3609–3614.
- Clayton, R. & Engquist, B., 1977. Absorbing boundary conditions for acoustic and elastic wave equations, *Bull. seism. Soc. Am.*, **67**, 1529–1540.
- Cocco, M., Pacheco, J., Singh, S.K. & Courbouloux, F., 1997. The Zihuatanejo, Mexico, earthquake of 1994 December 10 ( $M = 6.6$ ): source characteristics and tectonic implications, *Geophys. J. Int.*, **131**, 135–145.
- Day, S.M., 1982. Three-dimensional finite difference simulation of fault dynamics: Rectangular faults with fixed rupture velocity, *Bull. seism. Soc. Am.*, **72**, 705–727.
- Day, S.M., Yu, G. & Wald, D.J., 1998. Dynamic stress change during earthquake rupture, *Bull. seism. Soc. Am.*, **88**, 512–522.
- Fukuyama, E. & Mikumo, T., 1993. Dynamic rupture analysis: inversion for the source process of the 1990 Izu Oshima, Japan earthquake ( $M 6.5$ ), *J. geophys. Res.*, **98**, 6529–6542.
- Heaton, T.H., 1990. Evidence for implications of self-healing pulses of slip in earthquake rupture, *Phys. Earth planet. Inter.*, **64**, 1–29.
- Ide, S. & Takeo, M., 1996. The dynamic rupture process of the 1993 Kushiro-oki earthquake, *J. geophys. Res.*, **101**, 5661–5675.
- Ide, S. & Takeo, M., 1997. Determination of constitutive relations of fault slip based on seismic wave analysis, *J. geophys. Res.*, **102**, 23 379–23 391.
- Mikumo, T. & Miyatake, T., 1993. Dynamic rupture processes on a dipping fault, and estimates of stress drop and strength excess from the results of waveform inversion, *Geophys. J. Int.*, **112**, 481–496.

- Mikumo, T. & Miyatake, T., 1995. Heterogeneous distribution of dynamic stress drop and relative fault strength recovered from the results of waveform inversion: the 1984 Morgan Hill, California, earthquake, *Bull. seism. Soc. Am.*, **85**, 178–193.
- Mikumo, T., Miyatake, T. & Santoyo, M.A., 1998. Dynamic rupture of asperities and stress change during a sequence of large interplate earthquakes in the Mexican subduction zone, *Bull. seism. Soc. Am.*, **88**, 686–702.
- Mikumo, T., Singh, S.K. & Santoyo, M.A., 1999. A possible stress interaction between large thrust and normal faulting earthquakes in the Mexican subduction zone, *Bull. seism. Soc. Am.*, **89**, in press.
- Miyatake, T., 1992. Reconstruction of dynamic rupture process of an earthquake with constraints of kinematic parameters, *Geophys. Res. Lett.*, **19**, 349–352.
- Quintanar, L., Yamamoto, J. & Jimenez, Z., 1999. Source mechanism of two intermediate depth focus earthquakes in Guerrero, Mexico, *Bull. seism. Soc. Am.*, **89**, 845–853.
- Santoyo, M.A., Singh, S.K. & Mikumo, T., 1999. Source characteristics of the 11 January, 1997 Michoacan, Mexico earthquake ( $M_w = 7.1$ ), *Bull. seism. Soc. Am.*, to be submitted.
- Singh, S.K. & Wyss, M., 1976. Source parameters of the Orizaba earthquake of August 28, 1973, *Geof. Int.*, **16**, 165–194.
- Singh, S.K., Suarez, G. & Dominguez, T., 1985. The Oaxaca, Mexico, earthquake of 1931: Lithospheric normal faulting in the subducted Cocos plate, *Nature*, **317**, 56–58.
- Singh, S.K., Ordaz, M. & Perez-Rocha, L.E., 1996. The great Mexican earthquake of 1858: Expected ground motions in Mexico City from a similar future event, *Bull. seism. Soc. Am.*, **86**, 1655–1666.
- Valdes, C. & Meyer, R.P., 1996. Seismic structure between the Pacific coast and Mexico City from the Petatlan earthquake ( $M_S = 7.6$ ) aftershocks, *Geof. Int.*, **35**, 377–401.
- Yamamoto, J., Jimenez, Z. & Mota, R., 1984. El temblor de Huajuapán de León, Oaxaca, Mexico, del 24 de octubre de 1980, *Geof. Int.*, **23**, 83–110.

## CONCLUSIONES

Estudios previos han destacado que tanto el proceso de ruptura, como los cambios de esfuerzos asociados y las interacciones de esfuerzos entre eventos adyacentes, son algunos de los factores más importantes que controlan la ocurrencia y localización de la sismicidad en las diferentes regiones sismogénicas del mundo. En muchos de estos trabajos, los esfuerzos de Coulomb cosísmicos han sido exitosamente utilizados para el análisis de la transferencia e interacción de esfuerzos, tanto dentro como fuera del área de falla.

En el caso de México, diversos autores han obtenido la distribución cinemática de deslizamientos sobre el plano de falla, entre otras propiedades de la fuente, de varios eventos en la zona de subducción del Pacífico mexicano, sin embargo, existen aún pocos trabajos sobre los cambios que estos producen en el estado de esfuerzos, así como sobre los procesos dinámicos de ruptura y sus efectos tanto en las regiones vecinas como en el ciclo sísmico.

Con el fin de alcanzar un mejor entendimiento sobre los procesos de ruptura de los sismos mexicanos, los cambios en el estado de esfuerzos tectónico y sus efectos en el ciclo sísmico en la zona de subducción mexicana, en esta tesis se estudiaron las propiedades cinemáticas y dinámicas de la fuente sísmica de algunos grandes sismos importantes en la zona de subducción, así como los cambios de esfuerzos durante grandes eventos inversos de subducción y normales dentro de la placa subducente, sus posibles relaciones debido a la transferencia de esfuerzos, sus efectos espacio-temporales y las posibles implicaciones de estas anteriores en el ciclo sísmico.

Primeramente se señala que la transferencia de esfuerzos debido a grandes sismos interplaca, puede efectivamente conducir a agrupamientos en el espacio-tiempo en la zona de subducción mexicana. En el intervalo entre 0 y 5 años a partir de la ruptura de un gran evento, se muestra que la probabilidad de ocurrencia de otro gran sismo en la región circundante es de alrededor de 30%, que es aproximadamente el doble del esperado por un modelo de Poisson. Así mismo, se hace ver que este agrupamiento de corto plazo puede explicarse mediante la transferencia de esfuerzos cosísmicos sobre el plano de falla. Por

otra parte, los intervalos de largo plazo observados, pueden estar asociados a los procesos de recarga tectónica debido al régimen convergente en la región. Por las implicaciones que estos resultados pueden tener en el análisis del ciclo sísmico en México, es importante considerar tomarlos en cuenta en las futuras estimaciones de pronóstico y peligro sísmico.

Otra conclusión importante, es que las interacciones laterales de esfuerzos de Coulomb entre grandes sismos de interplaca a lo largo de la zona de subducción, juegan un papel importante en el disparo o aceleración del tiempo de ocurrencia de los grandes sismos subsecuentes. Por otra parte, se ha encontrado en este trabajo que los efectos debidos a la relajación viscoelásticos de esfuerzos, resultan muy pequeños debido a los cortos intervalos de tiempo estudiados, y no conducen a una difusión de esfuerzos laterales significativos a lo largo de la frontera entre placas. Estos resultados, junto con la evidencia sobre los efectos de la transferencia de esfuerzos en el agrupamiento espacio-temporal de grandes sismos muestran que los cambios en los esfuerzos de Coulomb cosísmicos, son factores importantes que deben ser tomados en cuenta en futuros estudios sobre interacción de sismos y el peligro sísmico en la región.

Hemos mostrado también que debido a las inherentes variaciones espaciales de los esfuerzos y la fricción en la interfaz entre la placa cabalgante de NorteAmérica y las placas oceánicas subducentes de Cocos y Rivera, la distribución de deslizamientos y los cambios de esfuerzos asociados dentro y fuera de las áreas de ruptura de los sismos aquí estudiados, son bastante heterogéneas. Los resultados obtenidos de la inversión cinemática de formas de onda del sismo de subducción del 30/01/73, muestran que la ruptura tiene una distribución espacial de deslizamientos con varias asperezas, así como un patrón espacial de esfuerzos altamente variable dentro del área de falla. Por otra parte, los incrementos generados en los esfuerzos en las regiones circundantes del área de ruptura, podrían aumentar la posibilidad de falla en estas zonas, y que debido a esto pudieron haberse generado efectos de disparo en la sismicidad subsecuente.

Del trabajo sobre el proceso de ruptura del sismo de fallamiento normal intraplaca del 11/01/97, los cálculos estáticos, cinemáticos y dinámicos muestran algunos importantes

resultados: primero que los grandes eventos de falla normal intraplaca en México pueden tener patrones de deslizamientos complejos, reflejando que las heterogeneidades espaciales en los esfuerzos y las resistencias de fricción sobre el plano de ruptura, también están presentes dentro de la placa subducente. Segundo, que estos eventos muestran efectos de una fuerte directividad horizontal probablemente debidos a su confinamiento en la placa subducida. Finalmente, que este tipo de eventos pueden ocurrir no sólo en la zona cercana a la trinchera o en la zona del desdoblamiento de la placa subducente, sino también bajo la porción acoplada de la zona de subducción.

En este mismo estudio, se muestra que las regiones con esfuerzos de Coulomb positivos pueden generar una mayor tasa de actividad postsísmica que las regiones con esfuerzos negativos. También apuntamos que para detallar la posible correlación entre las réplicas y los esfuerzos asociados al evento principal, es necesario contar con información tanto de la localización como del mecanismo focal de las réplicas. Así, se ha visto que las caídas de esfuerzos en los esfuerzos de Coulomb provocados por el fallamiento normal del evento principal, en realidad vienen a actuar como incrementos en los esfuerzos para un fallamiento inverso. Por otra parte, es importante mencionar que en este caso, la distribución de réplicas en realidad no está definiendo el plano de falla, sino más bien planos de debilidad secundarios dentro de la placa subducente, donde la sismicidad subsecuente probablemente fue inducida por el evento principal.

Se observa también, que el disparo por transferencia de esfuerzos puede ser extendido a la interacción entre eventos con diferentes mecanismos sismogénicos y localizaciones. Este es el caso del posible disparo del sismo de falla normal del 11/01/1997 debido a los esfuerzos transferidos por el macrosismo de subducción del 19/09/1985. Aquí concluimos que el evento de 1997 tuvo lugar en la zona de máximo incremento en los esfuerzos cosísmicos debidos al evento interplaca. Se sugiere también que los posibles cambios en los esfuerzos cosísmicos debidos al proceso de subducción o a la carga tectónica de la litosfera continental cabalgante, así como a los deslizamientos asísmicos, pueden incrementar el estado general de esfuerzos y por lo tanto la posibilidad de ocurrencia de un sismo de falla normal en la placa subducente. Un trabajo reciente de *Mikumo et. al., (2002)* muestra la

posible interacción de esfuerzos entre el sismo de subducción del 29/11/1978 y el sismo de falla normal del 30/09/1999 en Oaxaca, los cuales ocurrieron en una situación y geometría muy similar al caso aquí presentado. Estos dos ejemplos sugieren que este tipo de relación entre eventos con diferentes mecanismos sismogénicos puede ser más común de lo que previamente se pensaba.

De los cálculos dinámicos basados en la distribución de deslizamientos del sismo del 11/01/1997, encontramos que las funciones de tiempo de la fuente generadas dinámicamente, varían con la posición dentro de la falla y tienen una duración relativamente corta (0.5 a 2.0 seg). Estas duraciones pueden ser atribuidas en cierta forma a heterogeneidades de pequeña escala en las caídas de esfuerzos locales. También encontramos que las caídas de esfuerzos obtenidas a partir de las distribuciones de deslizamientos dinámicamente consistentes, sugieren la existencia de un estado de esfuerzos mayor dentro de la placa subducente que los observados durante el sismo de 1985. Observamos en este sentido, que las caídas de esfuerzos estáticos obtenidas a partir del análisis dinámico pueden ser ligeramente mayores que aquellas obtenidas con técnicas directas de cálculo. Por otra parte, se muestra que la distribución de deslizamientos dinámicamente consistentes tiene un confinamiento mayor entre los 30 y 45 km de profundidad, los cuales resultan consistentes con el patrón de esfuerzos transmitidos a este sismo por el evento de 1985.

Los resultados aquí presentados, tratan únicamente sobre algunos de los grandes eventos en la porción noroccidental de la zona de subducción, así como con los efectos de la transmisión de esfuerzos en el tiempo de ocurrencia y la localización de los eventos estudiados. Sin embargo, es necesario investigar no solo en otras regiones tectónicas diferentes sino también sobre otros posibles factores que pudieran también tener importantes efectos en la generación de sismos, como pueden ser la presión de poro y en general el papel que juegan los fluidos en la resistencia de fricción en la interfaz, los cambios en el estado de esfuerzos por esfuerzos dinámicos transitorios y la difusión de esfuerzos viscoelásticos.



## CONCLUSIONS

It has been shown by several works that the fault rupture process of earthquakes, its associated stress changes, and also the stress interactions among adjacent seismic events, are some of the most important factors that control the timing and location of the seismicity in different seismogenic regions around the world. In many of these works, the Coulomb failure stress function has been used extensively to account for these stress changes, both inside and outside the fault area, mostly with positive results.

In Mexico, several authors have published studies on the slip distribution on the fault, among other source properties, of various earthquakes on the Mexican subduction zone. Unfortunately, there are still few works about the changes on the stress field associated with them, and also a few results about the source process from the dynamic point of view and their effects on the neighborhood regions and on the seismic cycle in Mexico.

In order to account for a better understanding on the rupture process of Mexican earthquakes, on the changes of the stress field, and on its effects in the seismic cycle in the Mexican subduction zone, we study in this thesis the rupture process of some earthquakes with different driving mechanisms (thrust interplate and normal intraplate), and also we explore the possibility of stress interaction among these earthquakes of different types and its possible spatio-temporal effects.

One of the main results from this work is that we have shown that stress transfer from large and great thrust earthquakes, can effectively lead to a space-time clustering of events in the Mexican subduction zone. During the interval of 0 to 5 years after a large earthquake, the probability of occurrence of another large event in the neighboring region is estimated to be about 30%, which is about twice that expected from a Poisson model. Although previous works have explained some of the long term recurrence intervals for different regions in the Mexican subduction zone (e.g. Singh et al 1983, etc.), a more complete understanding of the space-time behavior of earthquakes remains unsolved. Our results show that the short-term clustering effect observed for large earthquakes in the Mexican subduction zone can be mainly explained by the coseismic static stress transfer. Due to the inherent implications

on the understanding of these cycles, our results should be taken into account in earthquake forecast and seismic hazard estimation in Mexico. These results should help to draw a more complete picture of the earthquake cycle in the Mexican subduction zone

Another important conclusion here is that lateral Coulomb stress interaction among large and great interplate earthquakes will play an important role on the triggering or acceleration of the occurrence of some large thrust earthquakes on the Mexican subduction zone. On the other hand, the effects from viscoelastic stress relaxation were found to be quite small during short time intervals and did not yield significant lateral stress diffusion along the plate boundary. These results together with the evidence of the effects of stress transfer on the space time clustering of large events, show that coseismic Coulomb failure stress changes are important factors that should be taken into account in future studies on earthquake interaction and seismic hazard on the region.

We have also shown that due to the inherent spatial variations of the frictional and stress properties on the interface between the overriding North America plate and the subducting Cocos and Rivera oceanic plates, the slip distribution and its associated stress changes inside and outside the fault areas of the earthquakes studied here, are very heterogeneous yielding a complicated spatio-temporal behavior of these earthquakes; The results obtained from the kinematic waveform inversion of the 30/01/73 interplate thrust event show that the rupture yields heterogeneous spatial distribution of slips, and also a highly variable spatial stress pattern inside the fault area. On the other hand, the additional effects on the neighboring regions around the fault area shows that possible positive effects towards thrust failure is enhanced, and that possible triggering effects could have taken place in the subsequent seismicity.

From our study on the source process of the in-slab normal faulting event of the 11/1/97 event, static, kinematic and dynamic computations lead to some important results: First, large in-slab normal faulting events in Mexico can have complex slip patterns, reflecting that spatial heterogeneities on the frictional and tectonic stress properties over a seismic fault plane are also present inside the subducting slab. Second, these events show highly

directivity effects maybe due to their confinement in the subducting slab. Finally, this type of events may occur not only on the near trench zone of the slab or near the unbending zone, but also may occur below the coupled portion of the subducting zone.

Here, stress changes results show that regions with positive Coulomb failure stress can generate a higher ratio of aftershocks than the regions with negative stress. We also point out that, in order to see a possible correlation between the location of the aftershocks and the regions of different stress change associated to the mainshock, it is necessary to have information about both of the location and the faulting mechanism of the aftershocks.

The Coulomb failure stress drops due to normal faulting of the mainshock, in turn becomes stress increases for an inverse faulting. It is to be noted in this case that the location of aftershocks will not define the fault plane, but perhaps weak secondary fault planes inside the subducting slab, where the subsequent seismicity probably was induced by the previous mainshock.

We show that the stress triggering can be extended to the interaction between events with different mechanisms, locations and types. This is the case in the possible triggering of the 11/1/97 inslab normal event by the stress transferred from the large thrust interplate 1985 earthquake. Here we conclude that the 11/1/97 event took place in the zone of maximum coseismic stress increase up to several bars due to the interslab event. We also suggest that possible postseismic stress changes due to the subduction process or to the loading of the overriding continental lithosphere and from aseismic slip would enhance the coseismic stress change and hence the possibility of occurrence of a normal faulting earthquake in the subducting slab. A recent paper by *Mikumo et al, (2002)* also shows the possible stress interaction between the 1978 thrust inter-slab and the 1999 normal-faulting inslab Oaxaca earthquakes, which occurred in a very similar situation and geometry to the case presented here. These two examples suggest that this type of relation between events with different mechanisms could be more common than we previously thought.

From the dynamic calculations based on the slip distribution of the 11/01/97 earthquake, we found that the dynamically generated source time functions vary with the location on the fault and have relatively short slip durations (0.5 to 2.0 sec). These durations can be attributed in some sense to a short scale-length of the stress drop heterogeneities. We also found that the stress drops obtained from the dynamically consistent slips, suggests the existence of higher stresses within the subducting slab than those observed during the 19/09/85 earthquake. We observed in this sense that the static stress drops obtained from the dynamic analysis, can be slightly higher than those obtained from direct computation techniques. On the other hand, the dynamically consistent distribution of slips obtained here show a greater confinement between 30 and 45 km depth, which are consistent with respect to the stresses transferred from the 1985 event to the 1997 fault plane.

Our results presented here deal only with some events that in fact took place in this complicated tectonic region. As we have seen, our results show that earthquake stress transfer can be an important factor on the timing and location of future earthquakes in Mexico. However, it is necessary to investigate not only on different tectonic regions but also on other possible factors that could have strong effects on the earthquake occurrence. Some of these could be the pore pressure and in general the role of fluids, the dynamic and transient stress changes, the viscoelastic stress diffusion on the earthquake triggering and in general on earthquake interaction and earthquake suppression in Mexico.

## REFERENCIAS ADICIONALES.

Astiz, L. and H. Kanamori (1984). An earthquake doublet in Ometepec, Guerrero, Mexico, *Phys. Earth Planet. Interiors* **34**, 24-45.

Archuleta, R. (1984). A faulting model for the 1979 Imperial Valley earthquake. *J. Geophys. Res.*, **89**, 4559-4585.

Bouchon, M. (1999). The state of stress on some faults of the San Andreas system as inferred from near field strong motion data. *J. Geophys. Res.*, **102**, 11,731-11,744

Chael, E.P. and G.S. Stewart (1982). Recent large earthquakes along the Middle American trench and their implications for the subduction process, *J. Geophys. Res.* **87**, 329-338.

Courboux, F., M.A. Santoyo, J. Pacheco, and S.K. Singh (1997). The 14 September 1995 (M=7.3) Copala, México earthquake : A Source study using teleseismic, regional, and local data, *Bull. Seism. Soc. Am.* **87**, pp. 999-101.

Cocco, M., J. Pacheco, S.K. Singh, and F. Courboux (1997): The Zihuatanejo, Mexico earthquake of December 10, 1994 (M=6.6): Source characteristics and tectonic implications, *Geophys. J. Int.*, **131**, 135-145.

Das, S. & Scholz, C. H. Off-fault aftershock clusters caused by shear stress increase? *Bull. Seismol. Soc. Amer.* **71**, 1669-1675 (1981).

Deng J, y L.R. Sykes (1997a). Stress evolution in southern California and triggering of moderate-, small-, and micro-size earthquakes *J. Geophys. Res.*, **102**, 24411-24435

Deng J, y L.R. Sykes (1997b). Evolution of the stress field in southern California and triggering of moderate-size earthquakes: A 200-year perspective, *J. Geophys. Res.*, **102**, 9859-9886.

DeMets, C. and S. Stein (1990). Present-day Kinematics of the Rivera Plate and Implications for Tectonics in Southwestern Mexico. *J. Geophys. Res.*, **95**, 21931-21948.

Goes, S.D.B. (1996). Irregular recurrence of large earthquakes: An análisis of historic and paleoseismic catalogs. *J. Geophys. Res.*, **101**, 5739-5749

Hardebeck, J., J. Nazareth y E. Hauksson (1998). The static stress change triggering model: Constraints from two southern California aftershock sequences, *J. Geophys. Res.* **103**, 24,427-24,437.

Harris, R. y R.W. Simpson (1992). Changes in static stress in southern California faults alter the 1992 Landers earthquake. *Nature*, **360**, 251-254.

Harris, R. y R.W. Simpson (1996). In the shadow of 1857-effect of the great Ft. Tejon earthquake on subsequent earthquakes in southern California. *Geophys. Res. Lett.*, **23**, 229-232.

Harris, R. y R.W. Simpson (1998). Supression of large earthquakes by stress shadows--Implication of rate and state friction laws – two examples. *J. Geophys. Res.*, **103**, 24439-24451

Hudnut, K. W., L. Seeber y J. Pacheco (1989). Cross-fault triggering in the November 1987, Superstition Hills earthquake sequence, southern California, *Geophys. Res. Lett.* **16**, 199-202.

Jaumé, S.C. y L.R. Sykes (1992). Change in the state of stress on the southern San Andreas Fault resulting from the California earthquake sequence of April to June 1992, *Science* **258**, 1325-1328.

Kelleher, J. A., L. R. Sykes and J. Oliver (1973). Possible criteria for predicting earthquake locations and their applications to major plate boundaries of the Pacific and Caribbean, *J. Geophys. Res.*, **78**, 2547-2585.

King, G.C.P., R.S. Stein, y J.Lin (1994). Static stress changes and the triggering of earthquakes, *Bull. Seism. Soc. Am.* **84**, 935-953,.

Klitgord, K y J. Mammerickx (1982). East pacific rise: Magnetic anomaly and bathymetric framework. *J. Geophys. Res.*, **87**, 6725-6750.

Kostoglodov V. and W. Bandy, (1995). Seismotectonic *constraints on the convergence rate between the Rivera and North American plates*, *J. Geophys. Res.*, **100**, 17,977-17,989.

Lomnitz, C. (1977). A procedure for eliminating the indeterminacy in focal depth determination. *Bull. Seism. Soc. Am.*, **67**, 533-535.

Mendoza, C. (1993). Coseismic slip of two large Mexican earthquakes from teleseismic body waveforms: Implications for asperity interaction in the Michoacan plate boundary segment. *J. Geophys. Res.*, **98**, 8197-8210.

Mendoza, C. (1995). Finite fault analysis of the 1979 March 14, Petatlan, Mexico earthquake using teleseismic P waveforms. *Geophys. J. Int.*, **121**, 675-683.

Mendoza C. y S. H. Hartzell (1989). Inversion for slip distribution using teleseismic P waveforms: North Palm Springs, Borah Peak and Michoacan earthquakes. *Bull. Seism. Soc. Am.*, **78**, 1092-1111.

Mendoza C. y S. H. Hartzell (1989). Slip distribution of the 19 september 1985 Michoacan, Mexico, earthquake: Near source and teleseismic constraints. *Bull. Seism. Soc. Am.* **79**, 655-669.

Mendoza C. y S. H. Hartzell (1999). Fault slip distribution of the 1995 Colima-Jalisco, Mexico, earthquake. *Bull. Seism. Soc. Am.*, 89, 1338-1344.

Mikumo, T. and T. Miyatake (1993). Dynamic rupture processes on a dipping fault, and estimates of stress drop and strength excess from the results of waveform inversion, *Geophys. J. Int.*, 112, 481-496.

Mikumo, T. And T. Miyatake (1995). Heterogeneous distribution of dynamic stress drop and relative fault strength recovered from the results of waveform inversion: The 1984 Morgan Hill, California Earthquake, *Bull, Seism. Soc. Am.*, 85, 178-193.

Mikumo, T., Y. Yagi, S.K. Singh, and M.A. Santoyo (2002). Coseismic and postseismic stress changes in a subducting plate: Possible stress interactions between large interplate thrust and intraplate normal faulting earthquakes, *J. Geophys. Res.*, 107, B1, ESE5-1-ESE5-12.

Mikumo, T., T. Miyatake and M.A. Santoyo (1998). Dynamic rupture of asperities and stress change during a sequence of large interplate earthquakes in the Mexican subduction zone. *Bull. Seism. Soc. Am.* 88, 686-702.

Nishenko, S.P. and S.K. Singh (1987). Conditional probabilities for the recurrence of large and great interplate earthquakes along the Mexican subduction zone, *Bull. Seism. Soc. Am.* 77, 2095-2114.

Perfettini, H., R. S. Stein, R. W. Simpson and M. Cocco, (1999). Stress Transfer by the 1988-89 M=5.3, 5.4 Lake Elsmar Foreshocks to the Loma Prieta Fault: Unclamping at the Site of Peak Mainshock Slip, *J. Geophys. Res.*, 104, pp. 20,169-20,182,.

Pardo, M. and G. Suarez (1993). Shape of the subducted Rivera and Cocos plates in southern Mexico: Seismic and tectonic implications. *J. Geophys. Res.*, 100, 12357-12373.

Quintanar L. (1991). Tomographie de la source sismique par inversion des ondes P télésismiques. *PhD. dissertation, Université Paris 7*, Paris, France.

Reasenber P.A. y R.W. Simpson (1992). Response of regional seismicity to the static stress change produced by the Loma Prieta Earthquake, *Science* 255, 1687-1690.

Reyes, A., J.N. Brune, and C. Lomnitz (1979). Source mechanism and aftershock study of the Colima, Mexico earthquake of January 10, 1973, *Bull. Seism. Soc. Am.*, 69, 1819-1840.

Rybicki, K. (1971). The elastic residual field of a very long strike-slip fault in the presence of a discontinuity. *Bull. Seism. Soc. Am.*, 61, 79-82.

Rybicki, K. (1973). Analysis of aftershocks on the basis of dislocation theory. *Phys. Earth Planet. Inter.* 7, 409-422.

- Smith, S.W. y W. Van de Lindt (1969). Strain adjustments asociated with earthquakes in southern California. *Bull. Seism. Soc. Am.*, 59, 1569,1589.
- Stein, R. S., King, G. C. P., y Lin, J. (1992). Change in failure stress on the southern San Andreas fault system caused by the 1992 Magnitude = 7.4 Landers earthquake, *Science*, 258, 1328-1332.
- Stein, R.S., G.C.P. King, y J. Lin (1994). Stress triggering of the 1994 M=6.7 Northridge, California earthquake by its predecesors, *Science*, 265, 1432-1435.
- Stein, S. (1999). The role of stress transfer in earthquake occurrence, *Nature*, 402, 605-609.
- Singh, S. K., J. Havskov, K. McNally, L. Ponce, T. Hearn, and M. Vassiliou (1979). The Oaxaca, Mexico, Earthquake of 29 November 1978: A preliminary report on aftershocks. *Science*, v 207, 1211-1213.
- Singh, S. K., L. Astiz, and J. Havskov (1981). Seismic gaps and recurrence periods of large earthquakes along the Mexican subduction zone: A reexamination. *Bulletin of the Seismological Society of America*, v 71, 827-843.
- Singh, S.K., G. Suárez y T. Domínguez, (1985). The great Oaxaca earthquake of 15 January 1931: Lithosphere normal faulting in the subducted Cocos plate, *Nature*, 317, 56-58.
- Singh, S. K. and F. Mortera (1991), Source-time functions of large Mexican subduction earthquakes, morphology of the Benioff zone, and the extent of the Guerrero gap, *J. Geophys. Res.* 96, 21487-21502.
- Singh, S.K, J.G. Anderson and M. Rodríguez (1998). Triggered seismicity in the Valley of Mexico from major mexican earthquakes. *Geofis. Int.*, 37, 3-15.
- Singh, S.K., M. Ordaz, J.F. Pacheco, R. Quaas, L. Alcántara, S. Alcocer, C. Gutierrez, R. Meli and E. Ovando (1999). A preliminary report on the Tehuacán, México earthquake of June 15, 1999 (Mw=7.0). *Seism. Res. Lett.*, 70, 489-504.
- Singh, S.K, J. Pacheco, T. Mikumo and V. Kostoglodov (2000). Intraplate earthquakes in central Mexico and their relationship with large/great interplate thrust earthquakes. *presented at the annual meeting of the S.S.A.*, San Diego, California.
- Toda S., R. S. Stein, P. A. Reasenberg, J. H. Dieterich, y A. Yoshida (1998). Stress transferred by the 1995 Mw=6.9 Kobe, Japan, shock: Effect on aftershocks and future earthquake probabilities, *J. Geophys. Res.* 103, 24543-24565.
- Ward S.N. (1992) An application of synthetic seismicity calculations in earthquake statistics: The middle America trench, *J.Geophys.Res.*, 97,6675-6682.



Yagi, Y, T. Mikumo, J. Pacheco y G. Reyes (2004). Source Rupture Process of the Tecomán, Colima, Mexico Earthquake of 22 January 2003, Determined by Joint Inversion of Teleseismic Body-Wave and Near-Source Data. *Bull. Seism. Soc. Am.*, **94**, 1795-1807.

## AGRADECIMIENTOS

Deseo agradecer de manera especial al Dr. Takeshi Mikumo por sus invaluables sugerencias y comentarios, así como por el interés y el tiempo que dedicó a este trabajo como director de tesis. Así mismo, agradezco a los doctores Shri Krishna Singh, Carlos Mendoza, Mario Ordaz, Luis Quintanar, Francisco J. Sánchez-Sesma, y Carlos Valdés por sus comentarios y sugerencias a esta tesis. Gracias también a los doctores Vladimir Kostoglodov, Javier Pacheco y Raúl Valenzuela quienes siempre ayudaron a resolver mis dudas durante el trabajo doctoral.

A Sara Ivonne Franco y Arturo Iglesias gracias por su sincera amistad y por haber compartido conmigo este largo, sinuoso, a menudo accidentado pero sin duda gratificante camino hacia el doctorado. Así también, a mis amigos Víctor Cruz, Jaime Domínguez, David Escobedo, Daniel García, Mario Islas, Lucy Mora, Xyoli Pérez, Teresa Scolamachia, y muchos más del Instituto de Geofísica. Araceli Chaman y Mónica Salgado, mil gracias por su valiosa ayuda en el Posgrado en Ciencias de la Tierra. Gracias a Julián Bunster por sus sugerencias, en algunas traducciones.

A David Díaz, Carlos Dávila, Margarita Salomón-Atala, Alberto Rojas, Alejandro Méndez, Gabriela López, Lucia López y Ariadne Bello por su invaluable amistad.

A Paul, Ana y María Bambrick-Santoyo, Sandra Esparza, Julieta Amada, Yuriko y Álvaro Leo-Lozano por ser parte de mi familia, y por apoyarme y motivarme para continuar en este camino.

Finalmente mi eterno agradecimiento a mis hermanos Gabriela y Julián por creer siempre en mí, y por su incondicional apoyo ante las múltiples adversidades por las que hemos caminado juntos. Cuenten conmigo siempre.

POR MI RAZA HABLARÁ EL ESPÍRITU

Ciudad Universitaria, Agosto de 2005.